The Synthesis and Photophysical Properties of New Polymetallic Complexes Designed for Use in Photoinitiated Electron Collection

Sumner Weston Jones

Dissertation submitted to the Faculty of the
Virginia Polytechnic Institute and State University
in partial fulfillment of the requirements for the degree of

Doctor of Philosophy
in
Chemistry

Prof. Karen J Brewer, Chair
Prof. Mark R. Anderson
Prof. Brian E. Hanson
Prof. Joseph M. Merola
Prof. Brian M. Tissue

March 12, 1998
Blacksburg, VA

Keywords: Photoinitiated electron collection, supramolecular, ruthenium, osmium, solar energy conversion.

The Synthesis and Photophysical Properties of New Polymetallic Complexes Designed for Use in Photoinitiated Electron Collection

Sumner Weston Jones

(Abstract)

The goal of this research was to develop stereochemically defined multimetallic systems for use as light absorbers and electron donor / light absorber dyads in photoinitiated electron transfer and electron collection. The basis for the stereochemical control was provided by the symmetric bridging ligands 2,3,5,6-tetra(pyridyl)pyrazine (tpp) and 2,2′-bipyrimidine (bpm). The symmetric bidentate ligand 4N-perylene was designed and the majority of the synthesis was completed.

The bimetallic complexes $[(tpy)M(tpp)Ru(LLL)]^{n+}$, where M = Ru or Os and LLL = Cl_3, $(CH_3CN)_3$, tpp, or (dpq)Cl, and the model monometallic complexes $[(tpy)M(tpp)]^{2+}$, where M = Ru or Os, and $[(tpy)Ru(CH_3CN)_3]^{2+}$ were synthesized and characterized using electrochemistry, UV-vis spectroscopy, and UV-vis spectroelectrochemistry. The bimetallic complexes were investigated as potential light-absorber / electron-donor complexes to be used in larger supramolecular devices for photoinitiated electron collection and electron transfer. The electrochemistry showed that the relative energy of the metal orbitals is suitable for the metal in the (tpy)M(tpp) coordination environment to act as an electron donor. These bimetallic complexes possess extremely complicated UV-vis spectroscopy due to the number of possible transitions. The assignment of the UV-vis spectroscopy and the electrochemistry of these complexes was greatly facilitated by the UV-vis spectroelectrochemistry. The metal-to-metal charge transfer spectra

of the mixed-valence species of the bimetallic complexes were obtained using NIR spectroelectrochemistry and indicate a significant degree of metal-metal communication through the bridging tpp. The bimetallic complexes $[(tpy)Ru(tpp)Ru(tpy)]^{4+}$, $[(tpy)Ru(tpp)Ru(tpp)]^{4+}$, $[(tpy)Os(tpp)Ru(tpp)]^{4+}$, and $[(tpy)Ru(tpp)Ru(CH_3CN)_3]^{4+}$ were found to have emission lifetimes on the order of 100 ns.

The complexes $[(bpy)_2Ru(bpm)]^{2+}$, $[(bpy)_2Ru(bpm)Ru(bpy)_2]^{4+}$, $[(bpm)_2IrCl_2]^{+}$, and $\{[(bpy)_2Ru(bpm)]_2IrCl_2\}^{5+}$ were synthesized and characterized using electrochemistry, UV-vis spectroscopy, and UV-vis spectroelectrochemistry. The complex $\{[(bpy)_2Ru(bpm)]_2IrCl_2\}^{5+}$ is a LA-EC-LA device for photoinitiated electron collection. The UV-vis spectroelectrochemistry of these complexes facilitated the assignment of the UV-vis spectroscopy as well as the electrochemistry. The UV-vis spectrum of the electrochemically generated two electron reduced form of $\{[(bpy)_2Ru(bpm)]_2IrCl_2\}^{5+}$ was obtained. This spectrum is critical in the understanding of future studies of the photochemically generated two electron reduced species.

The symmetric, planar, bidentate bridging ligand 4N-perylene was designed. This ligand would eliminate some of the isomers associated with multimetallic complexes bridged by unsymmetric bidentate bridging ligands. The large π system of 4N-perylene would likely result in a low energy π^* orbital compared to dpp, dpq, or bpm. The ligand 4N-perylene would hold bridged metals at a greater distance than 2,2′-bipyrimidine and should facilitate the formation of multimetallic complexes. The synthesis of 1,8-dichloro-2,7-naphthyridine has been completed. 1,8-dichloro-2,7-naphthyridine is a possible reactant in the homo-coupling reaction of a substituted 2,7-naphthyridine to form 4N-perylene.

The stereochemically defined molecular systems developed in this work show great promise for use in larger supramolecular complexes designed for photoinitiated electron transfer and electron collection.

Table of Contents

List of Figures

List of Tables

Abbreviations

bco	bicylco[2.2.2]octane
bpm	2,2′-bipyrimidine
bpy	2,2′-bipyridine
CT	charge transfer
dpb	1,3-bis(2-pyridyl)benzene
dpb	2,3-bis(2-pyridyl)benzoquinoxaline
dpp	2,3-bis(2-pyridyl)pyrazine
dpq	2,3-bis(2-pyridyl)quinoxaline
EC	electron collector
ED	electron donor
eth	ethyne
GS	ground state
HOMO	highest occupied molecular orbital
LA	light absorber
LC	ligand centered
LF	ligand field
LMCT	ligand to metal charge transfer
LUMO	lowest unoccupied molecular orbital
MC	metal centered
MLCT	metal to ligand charge transfer
MMCT	metal to metal charge transfer
ph	phenyl
4N-perylene	1,6,7,12-tetraazaperylene
tpp	2,3,5,6-tetra(2-pyridyl)pyrazine
tpy	2,2′:6′,2′′-terpyridine

Acknowledgements

I would like to thank my parents, Del Jones and Charlotte Means, and my brother, Nathan Jones, for my upbringing. The values and character that they helped to foster have been the greatest gift I could ever hope for.

I would also like to thank Professor Karen J. Brewer for her mentoring throughout my undergraduate and graduate education. Her guidance and encouragement were instrumental in my success in graduate school.

National Science Foundation has been very generous in their financial support of this research (CHE-9313642 and CHE-9632713). Virginia Tech also provided much appreciated financial support throughout this work.

Chapter 1 Introduction

Light absorbers and electronic excited states

When a light absorber molecule (LA) absorbs a photon of light, the molecule goes into an electronically excited state (see equation 1). The energy of the electronic excited state of

$$\text{LA} + h\nu \xrightarrow{\textit{Absorption of Light}} \text{LA}^* \qquad (1)$$

the molecule can be used to do work. This is the basis of photosynthesis and, in fact, is the source of energy for all life on earth. The design of a molecular system that would be able to efficiently harness the energy of the sun is currently the focus of a number of research groups worldwide.[1]

A simple two orbital picture of a light absorber molecule (LA) would consist of one filled orbital and one higher energy, unfilled orbital. Absorption of a photon of light of the proper energy results in the promotion of an electron from the lower energy orbital to the higher energy orbital producing an excited state of the light absorber (see Figure 1.1). The chemical properties of the excited state of a light absorber are much different than those of the ground state giving rise to unique reactivity. For example, the excited state of a light absorber is both a better oxidizing and a better reducing agent than the ground state of a light absorber. The difference in reactivity between the ground state and the excited state of a light absorber allows the excited state to participate in reactions that would not be accessible to the ground state molecule.

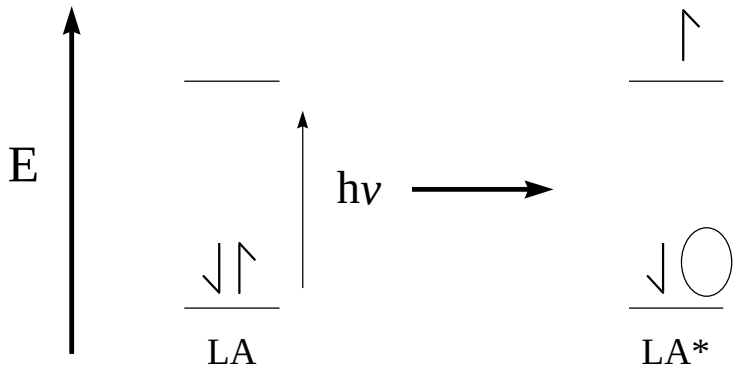

Figure 1.1 Absorption of light by a light absorber (LA).

One class of molecules that has received a lot of attention as light absorbers for use in solar energy conversion schemes has been octahedral d^6 transition metal complexes with polypyridyl ligands.[2] The reasons for the interest in these complexes as light absorbers are that they absorb strongly throughout much of the ultraviolet and visible spectrum, are generally photostable, and in many cases are able to undergo excited state electron or electron transfer. The preeminent d^6 transition metal chromophore that has been studied is $[Ru(bpy)_3]^{2+}$, where bpy = 2,2'-bipyridine.[3]

Molecular orbital picture of octahedral complexes

In order to understand the light-absorbing properties of a molecule, it is necessary to understand the nature of the orbitals involved in the absorption of light. One method of describing the molecular orbitals of a pseudo octahedral d^6 transition metal complex is by the linear combination of atomic orbitals (LCAO) description (see Figure 1.2). In this picture, each molecular orbital is a combination of one or more atomic orbitals. The shaded boxes represent filled sets of orbitals and the empty boxes represent unfilled sets of orbitals. For an octahedral d^6 transition metal complex, the highest occupied molecular orbital (HOMO) is predominantly metal $d\pi$ orbital based and the lowest unoccupied molecular orbital (LUMO) is often predominantly ligand π^* orbital based. The nature and energy of the HOMO and

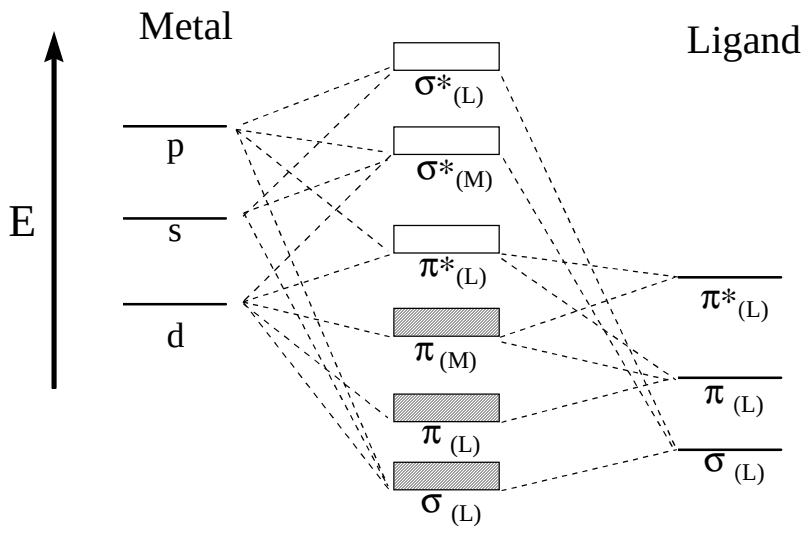

Figure 1.2 Block molecular orbital diagram for a d^6 octahedral metal complex.

LUMO are especially important in understanding the excited state properties of a light absorber molecule since they are the orbitals involved in the lowest energy excited state.

Cyclic voltammetry

One method that is used to characterize the electronic properties of molecules is cyclic voltammetry.[4] Cyclic voltammetry measures the potential at which a molecule is either oxidized or reduced. For a simple two orbital model of a molecule with one filled lower-energy orbital and one empty higher-energy orbital, oxidation is the transfer of an electron from the lower energy filled orbital to the electrode and reduction is the transfer of an electron from the electrode to the higher energy empty orbital of the compound in solution. Figure 1.3 shows the reduction of a compound in solution. As the voltage of the electrode is scanned and the electrons in the electrode become higher in energy than the empty orbital of the compound, electrons are transferred from the electrode to the species in solution. Figure 1.4

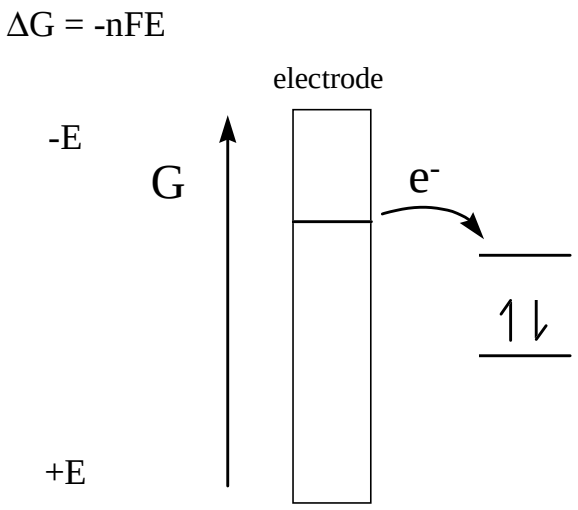

Figure 1.3 Electrochemical reduction of a species at an electrode surface.

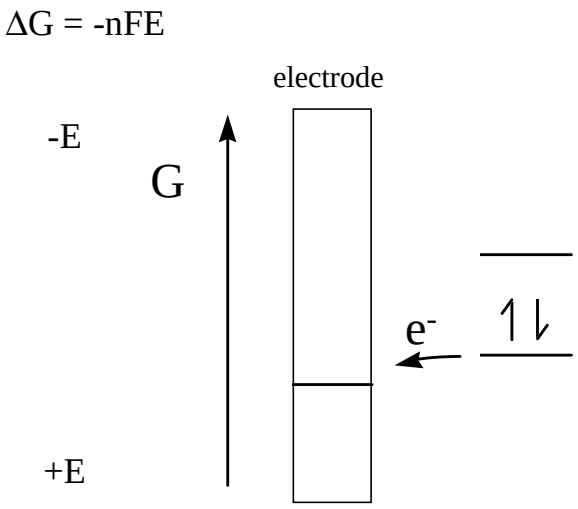

Figure 1.4 Electrochemical oxidation of a species at an electrode surface.

shows the oxidation of a compound in solution. As the energy of the electrons in the electrode becomes lower than the energy of the electrons in the occupied orbital of the compound, electrons are transferred from the compound to the electrode. Since the potential of electrons in the electrode are related to the energy of the electrons by the equation

$\Delta G = - nFE$, where ΔG is the Gibbs free energy, n is the number of electrons transferred, F is Faraday's constant, and E is the potential, it is possible to determine the energy of the orbitals of a compound by measuring the potential of the electrons in the electrode as the oxidation and reduction processes occur. In cyclic voltammetry, the potential of the electrode is cycled through the region where oxidations and reductions of the compound in solution occur and the current is measured as electrons flow to or from the electrode. The cyclic voltammogram of ferrocene in acetonitrile is shown in Figure 1.5. As the potential is scanned from zero to the positive, ferrocene is oxidized. As the majority of the ferrocene at the surface of the electrode is oxidized, the current reaches a maximum. This is called the anodic peak current, i_p^a, and occurs at the anodic peak potential, E_p^a. After the majority of the ferrocene at the surface of the electrode is oxidized, the current is determined by the mass transport of unoxidized

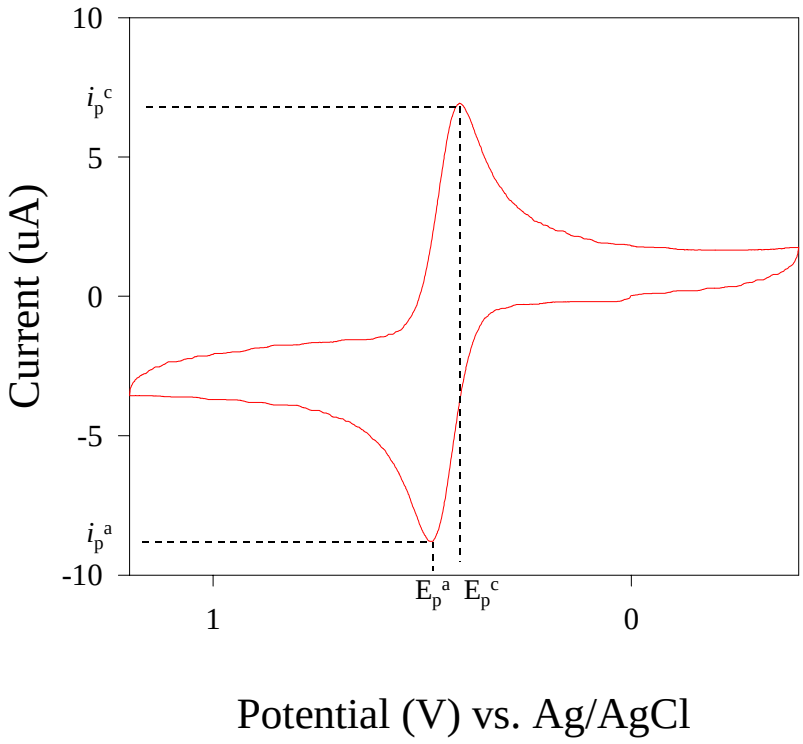

Figure 1.5 Cyclic voltammogram of ferrocene, $Fe(C_5H_5)_2$.

ferrocene from the bulk solution to the electrode surface. As the potential is cycled back in the negative direction toward zero volts, the current reaches a maximum as the majority of the $FeCp^+$ is reduced back to FeCp. This maximum current is called the cathodic peak current, i_p^c, and occurs at the cathodic peak potential, E_p^c. A reversible redox reaction is one in which there is no chemical step after the oxidation or reduction. The theoretical peak separation for a reversible reaction, $\Delta E_p = E_p^a - E_p^c$, is 59 mV / n where n is the number of electrons in the redox process. For a reversible reaction, the half potential, $E_{1/2}$, is defined as $(E_p^a + E_p^c)/2$. In a reversible reaction, $i_p^c / i_p^a = 1$.

Light absorption by octahedral complexes and electronic absorption spectroscopy

When a light-absorbing molecule absorbs a photon of light, an electron can be promoted from any occupied orbital to any unfilled orbital. Symmetry considerations and the amount of orbital overlap between the two orbitals determines the strength of a particular transition. The major electronic transitions that occur in ruthenium and osmium pseudo octahedral d^6 complexes of polyazine ligands are ligand based $n \rightarrow \pi^*$ and $\pi \rightarrow \pi^*$ transitions, metal to ligand charge transfer (MLCT) transitions, and ligand field transitions (see Figure 1.6). The boxes in the molecular orbital diagram of Figure 1.6 represent not one orbital but in many cases a set of orbitals varying slightly in energy. The intensity of a transition is determined by selection rules. In order for a transition to be fully allowed, the transition must be both Laporte and spin allowed.

In octahedral complexes of ruthenium and osmium, transitions that are both spin and Laporte allowed, such as ligand based $\pi \rightarrow \pi^*$ transitions and MLCT transitions, usually have molar extinction coefficients between 10^3 and 10^5 M^{-1} cm^{-1}. Transitions that are spin allowed but Laporte forbidden, such as ligand field transitions, typically have extinction coefficients between 100 and 1,000 M^{-1} cm^{-1}.

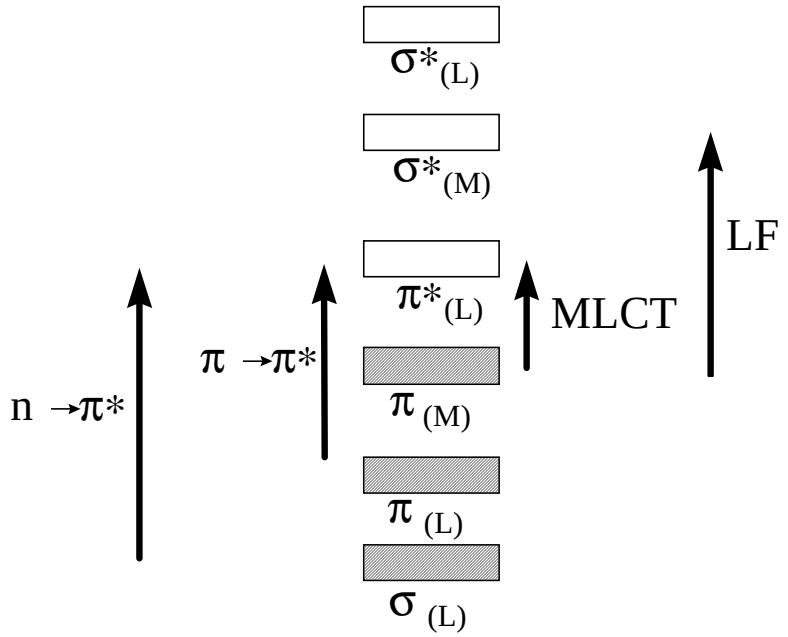

Figure 1.6 Some possible electronic transitions in an octahedral d^6 complex.

Electronic absorption spectroscopy is a technique that is used to determine the energy and intensity of the electronic transitions of a molecule. A UV-vis spectrophotometer consists of a UV-vis light source, a wavelength dispersing element, and a detector. The analyte is placed in the light path and the absorbance of light by the analyte is determined. The absorbance by the sample at each wavelength is defined by the equation $A = \log(I_0/I)$, where I_0 is the incident light intensity and I is the transmitted light intensity. The molar absorptivity (ε) of the sample at a particular wavelength is defined by the equation $\varepsilon = A/(b\ c)$, where b is the cell pathlength and c is the concentration of the sample in moles/liter. The electronic absorption spectrum is plotted as absorbance or molar absorptivity verses wavelength. The electronic absorption spectrum of $[Ru(bpy)_3](PF_6)_2$ in acetonitrile at room temperature is shown in Figure 1.7.[2,3] As is characteristic for octahedral d^6 metal complexes, the electronic absorption spectrum of $[Ru(bpy)_3]^{2+}$ shows $n \rightarrow \pi^*$ and $\pi \rightarrow \pi^*$ transitions in the UV region and a manifold of MLCT transitions in the visible region. The MLCT transition centered at 450 nm is actually a manifold of transitions arising from several electronic absorption transitions differing slightly in energy.

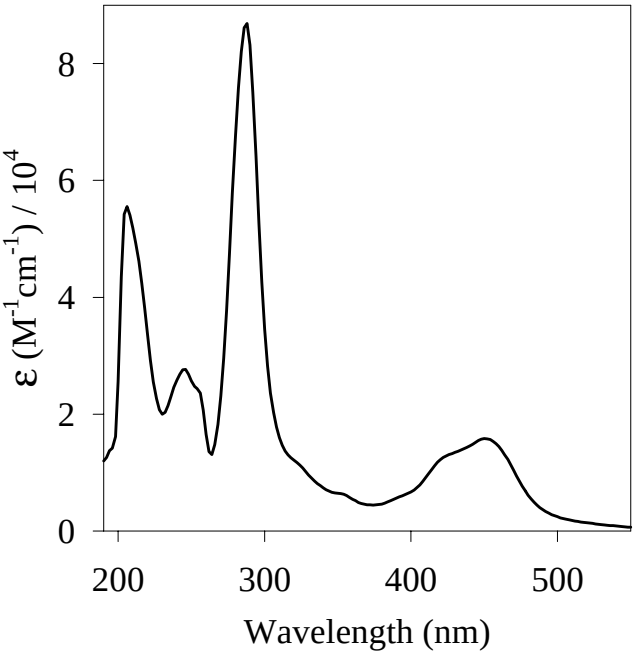

Figure 1.7 Electronic absorption spectrum of $[Ru(bpy)_3](PF_6)_2$ in acetonitrile.

Excited states

Once a light absorber molecule absorbs a photon of light, there are a number of possible pathways for deactivation. Figure 1.8 shows the Jablonski diagram for a typical d^6 octahedral metal complex. Upon absorption of a photon, the molecule is excited from the ground state (GS) to an excited state which quickly decays to the lowest energy singlet excited state, a ^{1}MLCT state. It is possible for the molecule to fluoresce, emitting a photon of light from the ^{1}MLCT state and returning to the ground state (not shown in Figure 1.8). More commonly for octahedral d^6 transition metal complexes, however, the molecule undergoes an intersystem crossing (k_{isc}) quantitatively to the ^{3}MLCT state. From the ^{3}MLCT state, the molecule can decay to the ground state either radiatively (k_{rad}) or non-radiatively (k_{nr}). Radiative decay

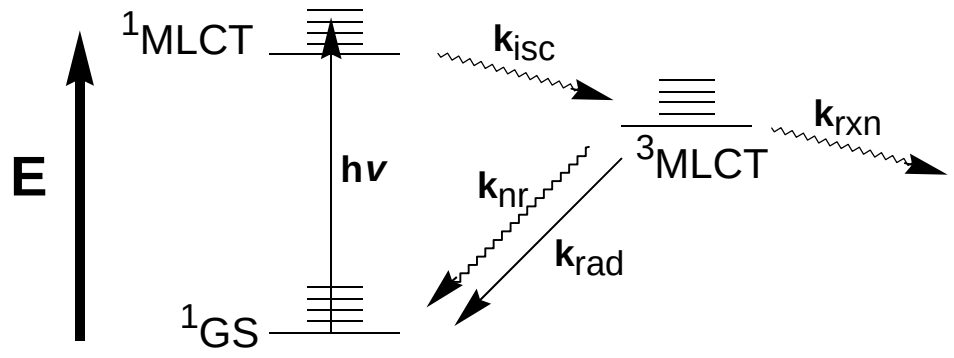

Figure 1.8 Jablonski diagram of a typical d^6 octahedral complex.

from the ^{3}MLCT state to the ground state is called phosphorescence and is formally spin forbidden since there is a change in the spin of the electron during the decay process. For an excited state molecule that is only deactivated by radiative or non-radiative relaxation, the lifetime of the ^{3}MLCT state, $\tau_{(3MLCT)}$, is defined as $1/(k_{rad} + k_{nr})$. The quantum yield for phosphorescence is defined as $k_{rad}/(k_{rad} + k_{nr})$. From the ^{3}MLCT state, the excited light absorber can also be deactivated by energy or electron transfer (k_{rxn}). Energy transfer involves transfer of the excited state energy of the light absorber to a quencher molecule (Q), Equation 2, resulting in the regeneration of the ground state of the light absorber and a quencher in the

Energy Transfer Quenching

$$LA^* + Q \rightarrow LA + Q^* \qquad (2)$$

excited state. Electron transfer involves the transfer of an electron between the excited light absorber and an electron donor or electron acceptor. The excited state of the light absorber is both a better oxidizing agent and a better reducing agent than the ground state. The excited light absorber can undergo oxidative quenching involving an electron acceptor, EA, (equation 3) or reductive quenching involving an electron donor, ED, (equation 4). Oxidative quenching results in the oxidized form of the ground state of the light absorber while reductive quenching results in the reduced form of the ground state of the light absorber.

Oxidative Electron Transfer Quenching

$$LA^* + EA \rightarrow LA^+ + EA^- \quad (3)$$

Reductive Electron Transfer Quenching

$$LA^* + ED \rightarrow LA^- + ED^+ \quad (4)$$

Photophysical properties of $[Ru(bpy)_3]^{2+}$

Since the discovery of the photophysical properties of $[Ru(bpy)_3]^{2+}$, there has been a vast amount of research focused on the use of this chromophore for photoinitiated energy and electron transfer.[3] It was discovered that this complex is photostable, has a long emission lifetime at room temperature (τ = 640 ns in acetonitrile), and has a relatively high emission quantum yield (Φ = 0.062 in acetonitrile). The room temperature emission of this chromophore facilitates excited state studies. At 77 K, the emission lifetime is significantly longer (τ = 5 μs) and the emission quantum yield is 0.4. It was found that $[Ru(bpy)_3]^{2+}$ could undergo both energy and electron transfer from the excited state. For example, upon excitation (equation 5), the excited state, $*[Ru(bpy)_3]^{2+}$, undergoes energy transfer quenching by $[Cr(CN)_6]^{3-}$ which subsequently phosphoresces as in equations 6 and 7.[2] $*[Ru(bpy)_3]^{2+}$

$$[Ru(bpy)_3]^{2+} + h\nu \rightarrow *[Ru(bpy)_3]^{2+} \quad (5)$$

$$*[Ru(bpy)_3]^{2+} + [Cr(CN)_6]^{3-} \rightarrow [Ru(bpy)_3]^{2+} + *[Cr(CN)_6]^{3-} \quad (6)$$

$$*[Cr(CN)_6]^{3-} \rightarrow [Cr(CN)_6]^{3-} + h\nu \quad (7)$$

was also shown to undergo oxidative electron transfer quenching by $[Cr(bpy)_3]^{3+}$ as in equation 8.[2] In all of the bimolecular quenching processes of $*[Ru^{II}(bpy)_3]^{2+}$, the efficiency of

$$*[Ru^{II}(bpy)_3]^{2+} + [Cr^{III}(bpy)_3]^{3+} \rightarrow [Ru^{III}(bpy)_3]^{3+} + [Cr^{II}(bpy)_3]^{2+} \quad (8)$$

quenching is largely determined by the dependence on diffusion in the bimolecular reaction. The light absorber must come into contact with the quencher molecule during the excited state lifetime of the light absorber. In electron transfer, the final quantum efficiency is also limited by back electron transfer. When $*[Ru^{II}(bpy)_3]^{2+}$ is oxidatively quenched by $[Cr^{III}(bpy)_3]^{3+}$, the products of the electron transfer are in close proximity and back electron transfer is energetically favorable, equation 9.

$$[Ru^{III}(bpy)_3]^{3+} + [Cr^{II}(bpy)_3]^{2+} \rightarrow [Ru^{II}(bpy)_3]^{2+} + [Cr^{III}(bpy)_3]^{3+} \quad (9)$$

Molecular devices for photoinitiated electron collection

Some time ago, Balzani wrote an intriguing report on the possible use of supramolecular species as molecular devices for various photoinitiated processes including energy and electron transfer.[5] A molecular device is defined as "an assembly of molecular components (i.e., a supramolecular device) designed to achieve specific functions". The components can be either organic or inorganic moieties. The individual acts of the components add together to give the overall function of the supramolecular species. By carefully choosing the components, a supramolecular species can be designed to carry out complex functions. Since the components of a supramolecular system are chemically bonded to each other, there is no dependence on a bimolecular reaction for energy or electron transfer to occur. This has the potential of greatly increasing the efficiency of energy or electron transfer.

In a supramolecular complex designed for photoinitiated electron collection, multiple chromophores absorb light and intramolecular electron transfer results in multiple electrons collected at an electron collector. The electrons are then available for use in a subsequent

multi-electron chemical process. A simple device for photoinitiated electron collection would consist of an electron collector covalently attached to two light absorbers which would themselves be attached to two electron donors (Figure 1.9). Absorption of a photon of light

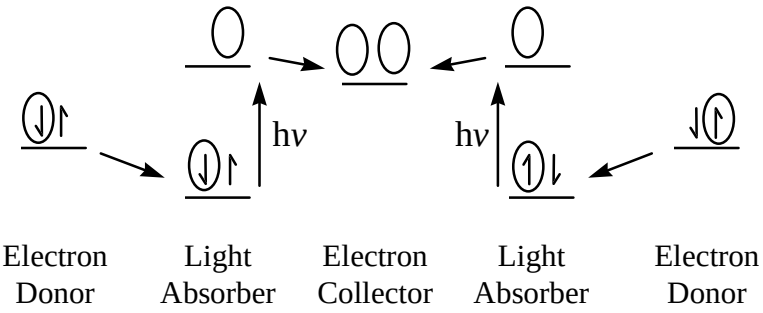

Figure 1.9 Supramolecular device for photoinitiated electron collection.

by a light absorber would produce an excited state of the light absorber which would then be reductively quenched by an electron donor. This would prevent decay of the light absorber back to the ground state. The light absorber would then transfer an electron to the electron collector. The same three step process would then occur with the other light absorber resulting in two electrons being collected on the electron collector and two electron holes on the electron donors (see Figure 1.10). Once the electrons are collected at the electron collector, they are available for some useful chemical reduction.

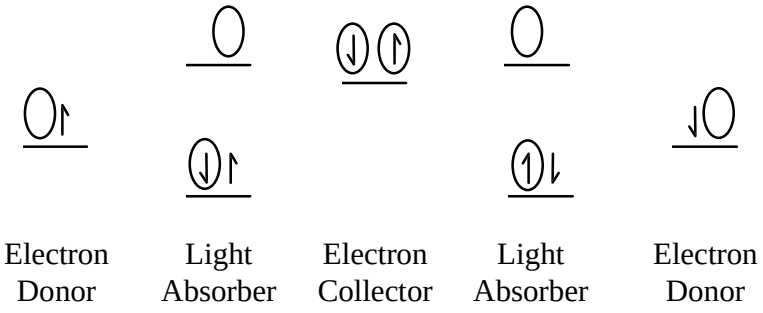

Figure 1.10 Completed photoinitiated electron collection.

The first device for photoinitiated electron collection

The first device for photoinitiated electron collection was synthesized and characterized by our group.[6a-c] In the presence of dimethylaniline, a sacrificial electron donor, the complex $\{[(bpy)_2Ru(dpb)]_2IrCl_2\}(PF_6)_5$, where dpb = 2,3-bis(2-pyridyl)benzoquinoxaline, (see Figure 1.11), undergoes photoinitiated electron collection resulting in two electrons collected at the central $(dpb)Ir^{III}Cl_2(dpb)$ electron collector to give the complex

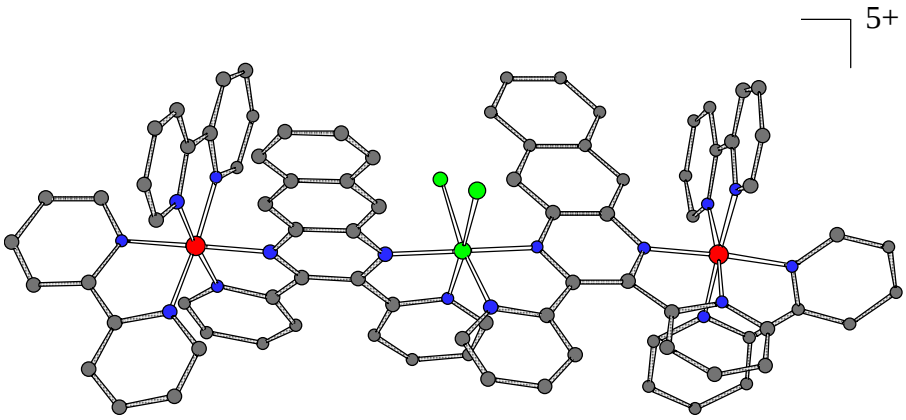

Figure 1.11 $[(bpy)_2Ru(dpb)IrCl_2(dpb)Ru(bpy)_2]^{5+}$.

$[(bpy)_2Ru(dpb^-)IrCl_2(dpb^-)Ru(bpy)_2]^{3+}$. Figure 1.12 shows the proposed catalytic scheme for this complex. Absorption of two photons of light and reaction with two electron donors (ED) results in the doubly reduced species, $[(bpy)_2Ru(dpb^-)IrCl_2(dpb^-)Ru(bpy)_2]^{3+}$, which could then reduce a substrate (S) by two electrons. We have shown that the central $(dpb)Ir^{III}Cl_2(dpb)$ core is an electrocatalyst for reduction of CO_2.[6d] Although this complex was the first to demonstrate photoinitiated electron collection, the quantum yield for generation of the doubly reduced species was low. This may be due in part to the inherently inefficient bimolecular process between the excited state of the complex and the electron donor. The electron donor and the complex must come into contact during the excited state of the

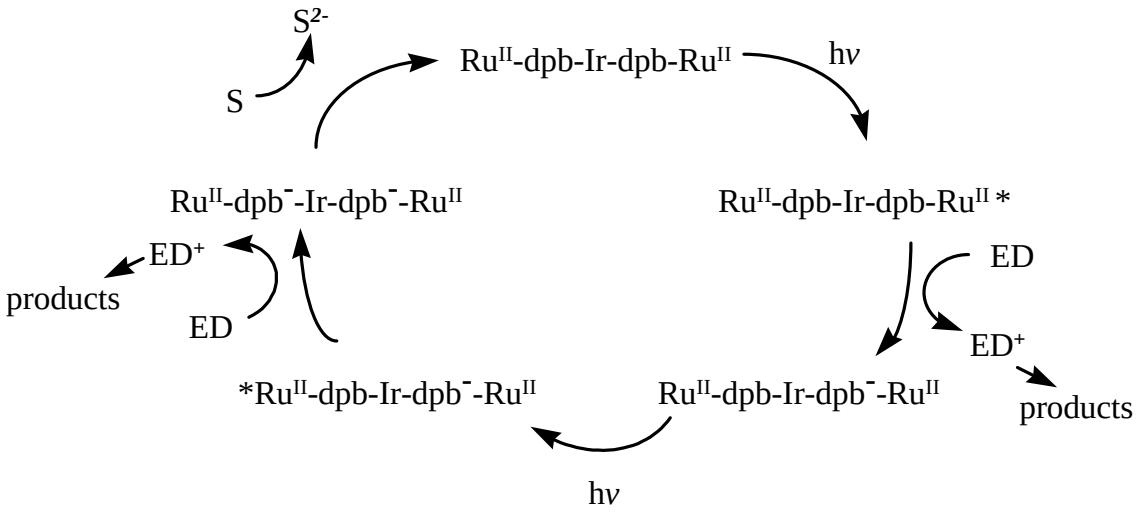

Figure 1.12 Functioning of $[(bpy)_2Ru(dpb)IrCl_2(dpb)Ru(bpy)_2]^{5+}$ as a molecular device for photoinitiated electron collection.

complex which was estimated as having a lifetime of < 4.5 ns.[6] One way to increase the quantum yield of photoinitiated electron collection with this device would be to covalently attach electron donors to the device. This would eliminate the inefficient bimolecular electron transfer process.

Tridentate ligands tpp and tpy in multimetallic systems

In the construction of a polymetallic supramolecular species, bridging ligands covalently connect the different metal centers but also determine many characteristics of the complex. Bidentate polyazine bridging ligands have been used extensively in the construction of polymetallic complexes. Some of the most widely used bidentate bridging ligands are dpp (2,3-bis(2-pyridyl)pyrazine), 2,3-bis(2-pyidyl)quinoxaline (dpq), and 2,3-bis(2-pyridyl)benzoquinoxaline (dpb) (see Figure 1.13).[1,6,7,8]

One disadvantage of using dpp, dpq, or dpb as a bridging ligand is the difficulty in controlling

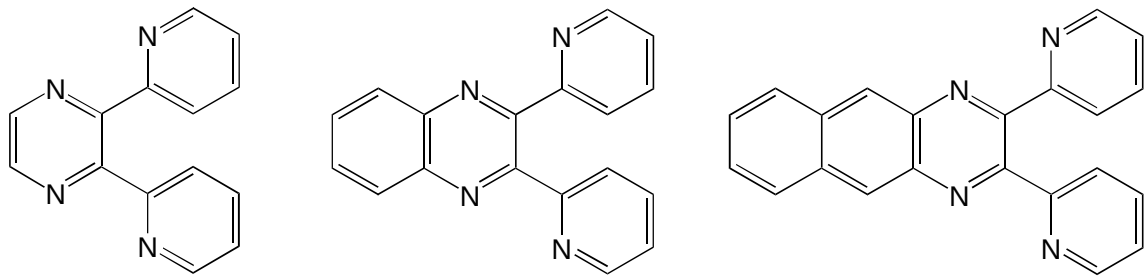

Figure 1.13 2,3-bis(2-pyridyl)pyrazine (dpp), 2,3-bis(2-pyridyl)quinoxaline (dpq), and 2,3-bis(2-pyridyl)benzoquinoxaline (dpb).

the stereochemistry of the resulting polymetallic complexes. Each is an A-B type ligand: the two nitrogens coordinated to a metal center are not equivalent. In a polymetallic complex, this gives rise to a number of possible isomers. For example, in the trimetallic $\{[(bpy)_2Ru(dpb)]_2IrCl_2\}(PF_6)_5$ there are two isomers that can occur from the coordination of the dpb ligands around the central Ir metal if the chlorides are cis to each other (see Figure 1.14). In one isomer the pyrazine rings of the two dpb ligands are trans to each other and the molecule has a more linear shape while in the other isomer the pyrazine rings are cis to each other and the molecule has a more bent shape. In both of these isomers, the central Ir metal center can be either Δ or Λ. Additionally, each tris bidentate $[(bpy)_2Ru(dpq)]$ center can exist

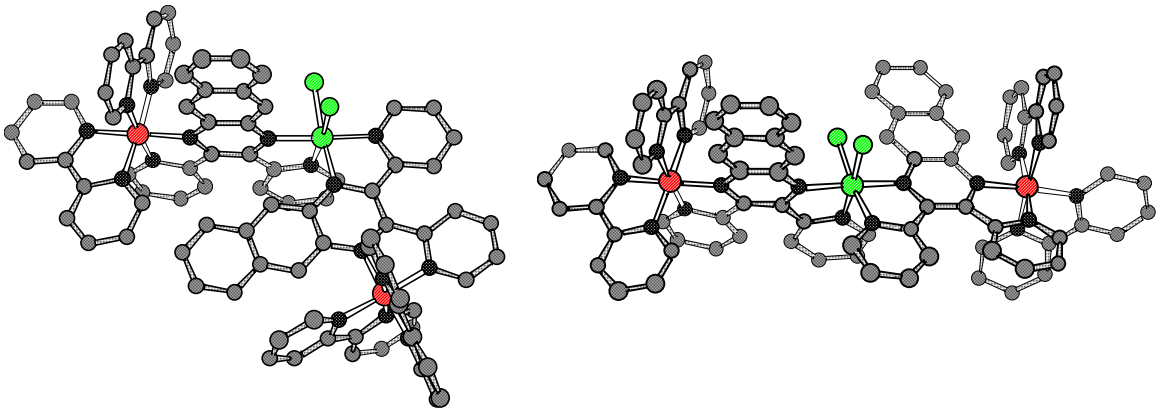

Figure 1.14 Two isomers of $\{[(bpy)_2Ru(dpb)]_2IrCl_2\}(PF_6)_5$.

as either the Δ and Λ isomer.[9] For the trimetallic $\{[(bpy)_2Ru(dpb)]_2IrCl_2\}(PF_6)_5$, these factors combine to give a large number of possible isomers which can have different electrochemical and photophysical properties. For the complex $\{[(bpy)_2Ru(dpb)]_2IrCl_2\}(PF_6)_5$, it is also possible to have two isomers where the two chlorides bound to the central iridium metal center are trans to each other, not considering the ruthenium Δ and Λ isomers. These two differ in that the pyrazine rings of the two dpb ligands coordinated to the iridium center can be trans or cis to each other.

An A-A type polyazine bridging ligand has equivalent nitrogens bound to a metal center and dramatically reduces the number of possible isomers. 2,2'-Bipyrimidine (bpm) is one A-A type bridging ligand that has been used to build multimetallic systems (Figure 1.15).[1,7,10,11,12,13] The trimetallic complexes $\{[(bpy)_2Ru(bpm)]_2IrCl_2\}(PF_6)_5$ and $\{[(bpy)_2Ru(bpm)]_2RhCl_2\}(PF_6)_5$ have been synthesized and characterized by our group.[14]

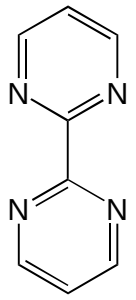

bpm

Figure 1.15 An A-A type bridging ligand, 2,2'-bipyrimidine.

The electrochemistry of these complexes shows more well defined ligand based reductions than in dpb and dpq bridged analog systems. This has been attributed to the defined stereochemistry around the central metal. Although bpm has been used to build some multimetallic complexes, there are some disadvantages. First of all, bpm holds the two

bridged metals fairly close together and this can sometimes prevent the synthesis of multimetallic complexes. Secondly, when designing multimetallic complexes for photoinitiated electron collection, it is desirable to have a bridging ligand with a tunable electronic structure. It would be fairly difficult to add any electron withdrawing or donating groups to bpm and would probably interfere sterically with the synthesis of multimetallic complexes even more.

Tridentate Ligands tpp and tpy

Tridentate ligands offer the possibility of controlling the stereochemistry of octahedral metal complexes. When two symmetric tridentate ligands are coordinated to a metal, there is only one possible stereoisomer. If symmetric tridentate bridging ligands are used in the construction of multimetallic systems, there is only one possible isomer for the whole multimetallic system. Furthermore, the whole complex is a linear, rod-like, system. This fixes the metal-metal distance which is essential in understanding energy and electron transfer. Tridentate bridged systems therefore offer many advantages over bidentate bridging ligand bridged systems where the metal-metal distance and photophysical properties can vary depending on the coordination of the ligands.

Even though tridentate ligands offer advantages in transition metal complexes, there has been less work done with tridentate ligands than with bidentate ligands.[1] Compared to the large amount of work done with bipyridine complexes, there has been relatively little interest in complexes utilizing the analogous tridentate ligand, 2,2',6',2"-terpyridine (tpy) (see Figure 1.16). This is due to the nonemissive nature of $[Ru(tpy)_2]^{2+}$ and its short excited state lifetime, 0.25 ns at RT.[15,16] Given the short excited state lifetime of $[Ru(tpy)_2]^{2+}$, it was believed that tridentate complexes of this type could not be used effectively in any sort of energy or electron transfer scheme. It has been shown, however, that the short lifetime of the ^{3}MLCT state of

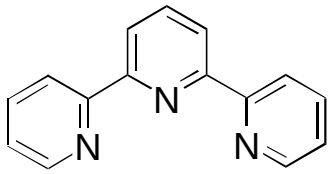

Figure 1.16 A tridentate ligand, 2,2',6',2"-terpyridine (tpy).

$[Ru(tpy)_2]^{2+}$ is due to a ligand field (LF) state that is thermally accessible at RT (Figure 1.17). The ligand field state quickly decays non-radiatively to the ground state, k'_{nr}. The accessibility of the ligand field state is attributed to the non-ideal bite angle of tpy for an octahedral complex which lowers the energy of the ligand field state relative to the ^{3}MLCT state.[17] The bite angles are defined as the N-Ru-N angles involving the nitrogens of a single tpy ligand. The ideal bite angles for a tridentate ligand in an octahedral environment would be 90° and 180°. The tpy-Ru bite angles are somewhat less than the ideal angles at approximately 79° and 158°[18,19,20].

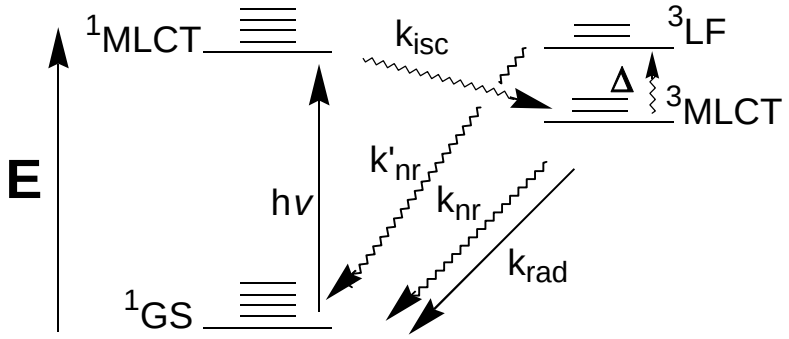

Figure 1.17 Jablonski diagram of $[Ru(tpy)_2]^{2+}$.

The first polyazine tridentate bridging ligand reported for ruthenium systems was tpp, 2,3,5,6-tetrakis(2-pyridyl)pyrazine.[21] Petersen et al.[22] and Thummel et al.[23] independently showed that tpp could function as a bridging ligand in the complex $[(tpy)Ru(tpp)Ru(tpy)](PF_6)_4$.[22, 23] This is a linear, rigid complex with interesting electrochemical and photophysical properties.

The two ruthenium centers give rise to two oxidation couples at 1.43 and 1.72 V vs. SCE even though the two metal centers have identical coordination environments. The oxidation of one of the metal centers affects the oxidation potential of the second metal center and is indicative of significant metal-metal communication. The first reduction in both the monometallic and the bimetallic occurs at the tpp based π^* orbital. The tpp in $[Ru(tpp)(tpy)]^{2+}$ reduces at -0.94 V while the bridging tpp in $[(tpy)Ru(tpp)Ru(tpy)]^{4+}$ reduces at a less negative potential of -0.34 V. The second electron deficient metal center pulls electron density away from the bridging tpp making the reduction occur at a lower energy in the bimetallic complex. The lowering in energy of the tpp π^* orbital in the bimetallic system is also evident in the electronic absorption spectrum. The lowest energy transition in $[(tpy)Ru(tpp)Ru(tpy)]^{4+}$ is a Ru ($d\pi$) $\rightarrow$ tpp (π^*) CT transition at 548 nm, red shifted from the same Ru ($d\pi$) $\rightarrow$ tpp (π^*) CT transition for $[Ru(tpp)(tpy)]^{2+}$ at 470 nm. Interestingly, even though $[Ru(tpy)_2]^{2+}$ is non-emissive at room temperature, both $[Ru(tpp)(tpy)]^{2+}$ and $[(tpy)Ru(tpp)Ru(tpy)]^{4+}$ are emissive at room temperature. $[Ru(tpp)(tpy)]^{2+}$ has an emission lifetime of 30 ns[24] while $[(tpy)Ru(tpp)Ru(tpy)]^{4+}$ has a lifetime of 100 ns.[22] We have postulated that the lower energy π^* orbital of tpp compared to that of tpy lowers the energy of the ^{3}MLCT state and reduces the thermal population of the ligand field state in $[Ru(tpp)(tpy)]^{2+}$ compared to $[Ru(tpy)_2]^{2+}$. Formation of the bimetallic $[(tpy)Ru(tpp)Ru(tpy)]^{4+}$ results in a lowering in the energy of the tpp π^* orbital and the corresponding ^{3}MLCT state, further reducing thermal accessibility of the ligand field state (see Figure 1.18). This postulate is consistent with the RT lifetime data as well as the 77 K studies. At 77 K, where thermal accessibility of the ligand field state would be significantly limited, $[Ru(tpy)(tpp)]^{2+}$ has a lifetime of 7100 ns and $[(tpy)Ru(tpp)Ru(tpy)]^{4+}$ has an emission lifetime of 480 ns. When this thermal population of the ligand field state is eliminated, the monometallic has a longer lifetime than the bimetallic, as expected by energy gap considerations.[25,26]

Recent work in the Brewer group has focused on the development of tpp bridged bimetallic complexes where one of the metal centers could function as a light absorber and the other

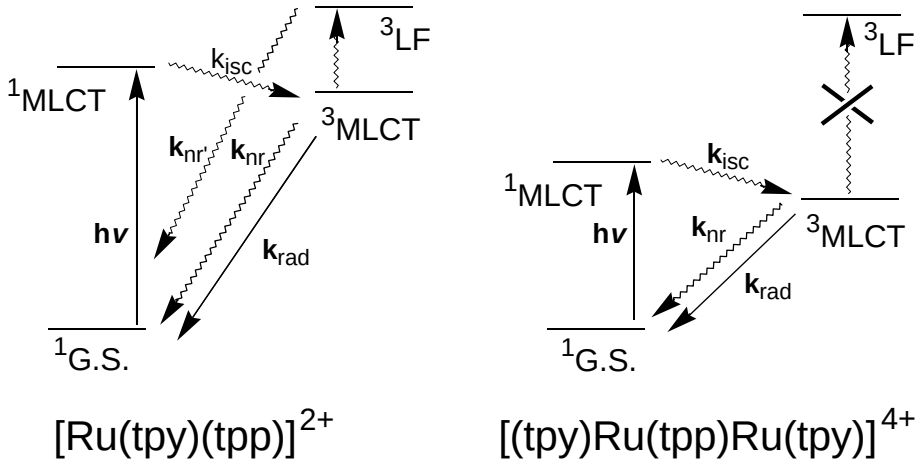

Figure 1.18 Jablonski diagram of $[Ru(tpp)(tpy)]^{2+}$ and $[(tpy)Ru(tpp)Ru(tpy)]^{4+}$.

metal center could function as an electron donor.[27] These light absorber - electron donor bimetallics could be incorporated into larger multimetallic systems through a bridging ligand. For example, attaching two of these light absorber - electron donor complexes to an electron collector would complete a molecular device for photoinitiated electron collection.[5]

The light absorber - electron donor complexes that have been previously designed and investigated in the Brewer group have the general formula $[(tpy)M(tpp)Ru(LLL)]^{n+}$ where M = Ru^{II} or Os^{II}, and LLL = Cl_3 or tpp.[27] When the bridging ligand tpp is incorporated as the terminal ligand in this LA-ED dyad, it allows the covalent attachment of an electron collector or some other component in a supramolecular device.

The synthesis of these complexes follows a building block approach where ruthenium or osmium is coordinated to tpy followed by the attachment of the bridging tpp followed by the coordination of ruthenium followed by the attachment of the terminal ligands. In this way, exact control of every component in the complex is achieved.

In all of the above tpp bridged complexes the lowest unoccupied molecular orbital is μ-tpp based and the localization of the highest occupied molecular orbital is dependent on the components. For the complexes $[(tpy)M(tpp)RuCl_3]^+$, the ruthenium is the site of the HOMO due to the electron donating character of the three chlorides while in the complexes $[(tpy)M(tpp)Ru(tpp)]^{4+}$ the HOMO is based on the metal, M, whether it is ruthenium or osmium.

In all of these complexes, the lowest energy transition in the electron absorption spectrum is either M $\rightarrow$ μ-tpp CT or Ru $\rightarrow$ μ-tpp CT. In the complexes $[(tpy)M(tpp)RuCl_3]^+$, the lowest energy transition involves the ruthenium bound to three chlorides while for the $[(tpy)M(tpp)Ru(tpp)]^{4+}$ complexes, the lowest energy transition involves the ruthenium or osmium that is bound to tpp and tpy.

As with $[(tpy)Ru(tpp)Ru(tpy)]^{4+}$, the complexes $[(tpy)M(tpp)Ru(tpp)]^{4+}$, where M = Ru or Os, both exhibit excited state emission lifetimes of approximately 100 ns.[27b] This is critically important for the use of these LA-ED dyads in electron transfer since the lifetime of the dyad must be long enough to have electron transfer to an electron collector. A 100 ns lifetime is sufficient to allow efficient electron transfer to an attached electron collector. An emission was not detected from the $[(tpy)M(tpp)RuCl_3]^+$ complexes. Given the low energy of the lowest energy electronic absorbance transition for $[(tpy)M(tpp)RuCl_3]^+$, the emission would be expected to be beyond the detection limits of our system.

The tpp bridged bimetallic complex $[(tpy)Ru(tpp)IrCl_3](PF_6)_2$ has also been previously studied in our group.[24] This was the first example of a bimetallic tpp bridged system incorporating a light absorber and a catalytic site. In this ruthenium / iridium complex, the ruthenium portion serves as the light absorber while the iridium center is a potential catalytic site. Electrochemically, the first oxidation of this complex is ruthenium based and the second oxidation is iridium based. The first two reductions in this complex are tpp based and the third reduction is tpy based. The $Ir^{III/I}$ couple seen in monometallic iridium complex

[(tpp)$IrCl_3$] was not seen for the bimetallic complex in the solvent window. This is due to the electron rich nature of the doubly reduced tpp ligand and the singly reduced tpy, increasing the electron density on the iridium.

The electronic absorption spectroscopy of [(tpy)Ru(tpp)$IrCl_3$]$(PF_6)_2$ was found to be quite complicated due to the many possible transitions. It is possible to have tpy and tpp $\pi \rightarrow \pi^*$ and n $\rightarrow \pi^*$ transitions as well as Ru $\rightarrow$ tpy, Ru $\rightarrow$ tpp, and Ir $\rightarrow$ tpp CT transitions.

Spectroelectrochemistry

Spectroelectrochemistry is a powerful tool for probing the electronic transitions and electrochemical processes of metal complexes with polyazine ligands.[27c, 28, 29, 30, 31, 32, 33] These complexes are typically described using a localized molecular orbital approach. The electrochemical oxidations are metal based and the reductions are ligand based. These same orbitals are involved in the electronic transitions. In an electronic absorption spectroelectrochemical experiment, the compound is chemically or electrochemically either oxidized or reduced and the changes in the electronic absorption spectrum are monitored. When a compound is oxidized or reduced, the energy of any transition involving the orbital involved in the redox process is altered so drastically that the transition is typically no longer seen in the UV-vis region. Oxidation of a metal center is expected to cause the dramatic shift of any MLCT transitions involving that metal. The more positive nature of the metal will also lower the energy of π^* orbitals of coordinated ligands and cause a small red shift in the ligand $\pi \rightarrow \pi^*$ transitions. When a compound is reduced and an electron is formally put in a ligand π^* orbital, any transition involving that orbital will shift out of the UV-vis region. Ligand based $\pi \rightarrow \pi^*$ transitions of that ligand and MLCT transitions to that ligand will no longer be seen in the same spectral region. The greater electron density on the ligand can also donate electron density to the metal and lower the energy of MLCT transitions involving other

ligands. Upon reduction, the ligand can also exhibit new $\pi^* \rightarrow \pi^*$ transitions which are typically seen in the visible region.

Spectroelectrochemistry has been used to elucidate many properties of ruthenium complexes with bpy ligands.[28, 29, 33] Berger used electronic absorption spectroelectrochemistry to confirm electrochemical assignments of $[(bpy)_2Ru(dpp)]^{2+}$ and $\{[(bpy)_2Ru]_2(dpp)\}^{4+}$ and to help make assignments in the excited state electronic absorption spectra of these complexes.[28] Wertz et al. used electronic absorption spectroelectrochemistry along with resonance Raman and ESR to investigate the difference in the behavior of $[(bpy)_2Ru(BL)Ru(bpy)_2]^{4+}$ (BL = dpp and dpq).[29] These two pioneering studies by Berger and Wertz showed the power of spectroelectrochemistry in probing the spectroscopic and electrochemical properties of polyazine bridged polymetallic complexes. Our group has studied the spectroelectrochemistry of many bidentate bridged polyazine systems.[6c,14,34] Although the spectroelectrochemical behavior of metal complexes containing a number of bidentate bridging ligands such as dpp has been investigated, the complex $[(tpy)Ru(tpp)IrCl_3](PF_6)_2$ was the first tpp bridged system studied by spectroelectrochemistry.[24]

Metal-to-metal charge transfer transitions

In multimetallic systems designed for energy or electron transfer, it is desirable to know the degree of metal-metal communication. One of the most reliable and direct methods of determining the amount of intercomponent electronic communication in bimetallic systems is by the study of the intervalence charge transfer (IT) band.[35, 36] In a symmetric mixed valence bimetallic system, M^{II}-M^{III}, the degree of coupling between the metal centers determines the characteristics of the transition M^{II}-$M^{III} + h\nu \rightarrow M^{III}$-$M^{II*}$. For a symmetric system, Hush related the energy, intensity, and halfwidth at maximum intensity of this intervalence charge transfer transition to the degree of electronic coupling as in equations 10 through 12 where

$$E_{op} = \lambda + \Delta G° \qquad (10)$$

$$\Delta\overline{\nu}_{1/2} = 48.06(E_{op} - \Delta G°)^{½}(cm^{-1}) \qquad (11)$$

$$H = 0.0205(\varepsilon_{max}\Delta\overline{\nu}_{1/2}E_{op})^{½} / r \qquad (12)$$

E_{op}, $\Delta\overline{\nu}_{1/2}$, and ε_{max} are the energy, halfwidth at half height in cm^{-1}, and extinction coefficient at the absorption maximum of the IT band, λ is the reorganization energy of M^{III}-M^{II*}, $\Delta G°$ is the free energy change of the electron transfer reaction, H is the electronic coupling parameter, and r is the metal-metal distance in Angstroms.[35] For a symmetric system where the coordination sphere of the two metals are identical, $\Delta G° = 0$ for electron transfer and equation 11 simplifies to equation 13.

$$\Delta\overline{\nu}_{1/2} = 48.06\,\overline{\nu}_{max}^{½}\ (cm^{-1}) \qquad (13)$$

For mixed valence bimetallic systems, Robin and Day distinguished three classes depending on the amount of metal to metal interaction.[37] Figure 1.19 is a plot of nuclear configuration vs. energy for the three classes of mixed valence compounds. If there is essentially no interaction between the metal centers, it is classified as a Class I system. Compounds of this type have properties that are a simple combination of the properties of the two independent metal centers. Class I compounds do not exhibit an IT transition. Mixed valence compounds that have some limited degree of interaction between the metal centers are classified as Class II. Class II systems still have a localized valency and can be described as M^{II}-M^{III} but have some new properties that can be attributed to the mixed valence species. Class II compounds typically have IT transitions that can be characterized using the Hush theory. Class III systems are compounds that have such strong electronic communication between the metal centers that they are completely delocalized systems. The oxidation state of the metal centers in a Class

III system can best be described as $M^{2.5}/ M^{2.5}$. Class III complexes typically do not have properties that can be attributed to the M^{II} or M^{III} metal center.

To differentiate between Class II and Class III compounds, the peak width at half height of the IT band, $\Delta\overline{\nu}_{1/2}$, is measured. If $\Delta\overline{\nu}_{1/2} \geq 48.06(E_{op} - \Delta G°)^{½}$, the compound can be classified as Class II. If $\Delta\overline{\nu}_{1/2} < 48.06(E_{op} - \Delta G°)^{½}$, the compound is classified as Class III.

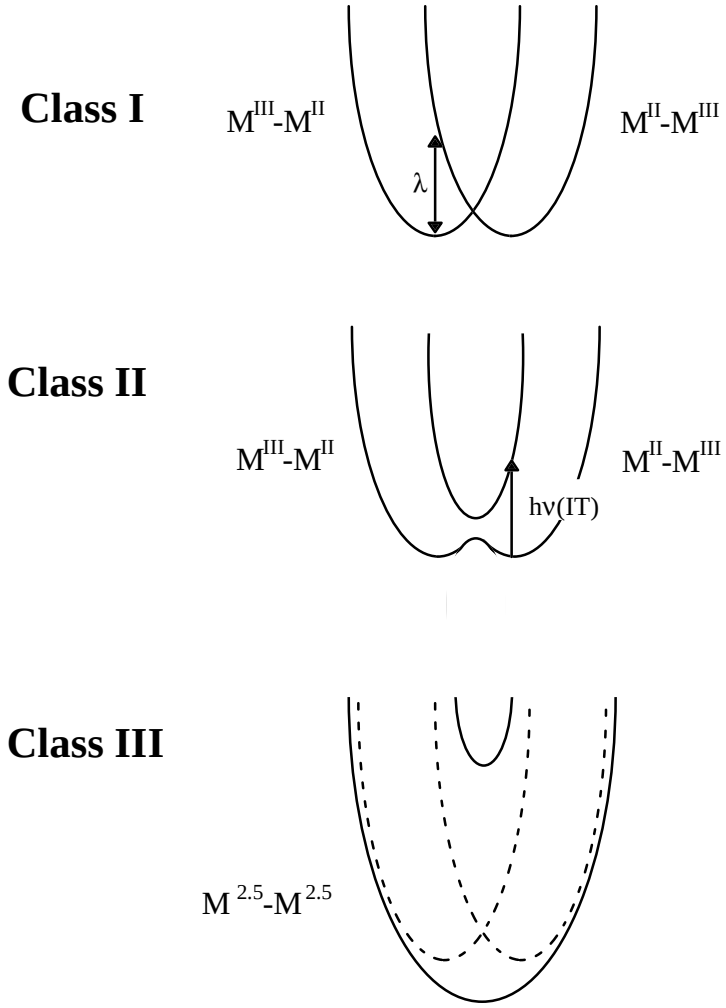

Figure 1.19 Classes of metal-metal interaction in ruthenium bimetallic systems bridged by polyazine bridging ligands.

The solvent dependence of the IT band can also be used as an indication of the extent of delocalization. Since Class III compounds do not have a change in dipole upon intervalence charge transfer, the IT bands of Class III compounds do not exhibit a strong solvent dependence. A third method of determining the class of a compound is by the intensity of the IT band. Class II compound typically have moderately intense bands ($\varepsilon < 1{,}000\ M^{-1}\ cm^{-1}$) while Class III compounds can have IT bands with molar extinction coefficients as high as $10{,}000\ M^{-1}\ cm^{-1}$.[35]

The electronic coupling parameter for a Class II complex is calculated as

$$H = 0.0205(\varepsilon_{max}\Delta\overline{\nu}_{1/2}E_{op})^{1/2} / r$$

while the electronic coupling parameter for a Class III complex is calculated as

$$H = (E_{op})/2 .$$

Tridentate bridging ligands in polymetallic systems

Many different types of polyazine tridentate bridging ligands have been investigated. Figure 1.20 shows some of the tridentate ligands that have been used in the synthesis of polymetallic complexes.

One of the main types of tridentate bridging ligands studied has been two coordinating tpy "ends" held back to back by a spacer at the 4′ position. The spacer that is used affects both the metal to metal distance as well as the amount of electronic coupling through the ligand. Sauvage, Constable, et al. have reported on a series of ruthenium and osmium complexes using the bridging ligand tpy-spacer-tpy where phenyl groups serve as the spacer.[38,39a-d,40] The complexes have the form $[(ttpy)Ru(tpy\text{-}ph_n\text{-}tpy)M(ttpy)]^{4+}$ where n = 0, 1, or 2, M = Ru

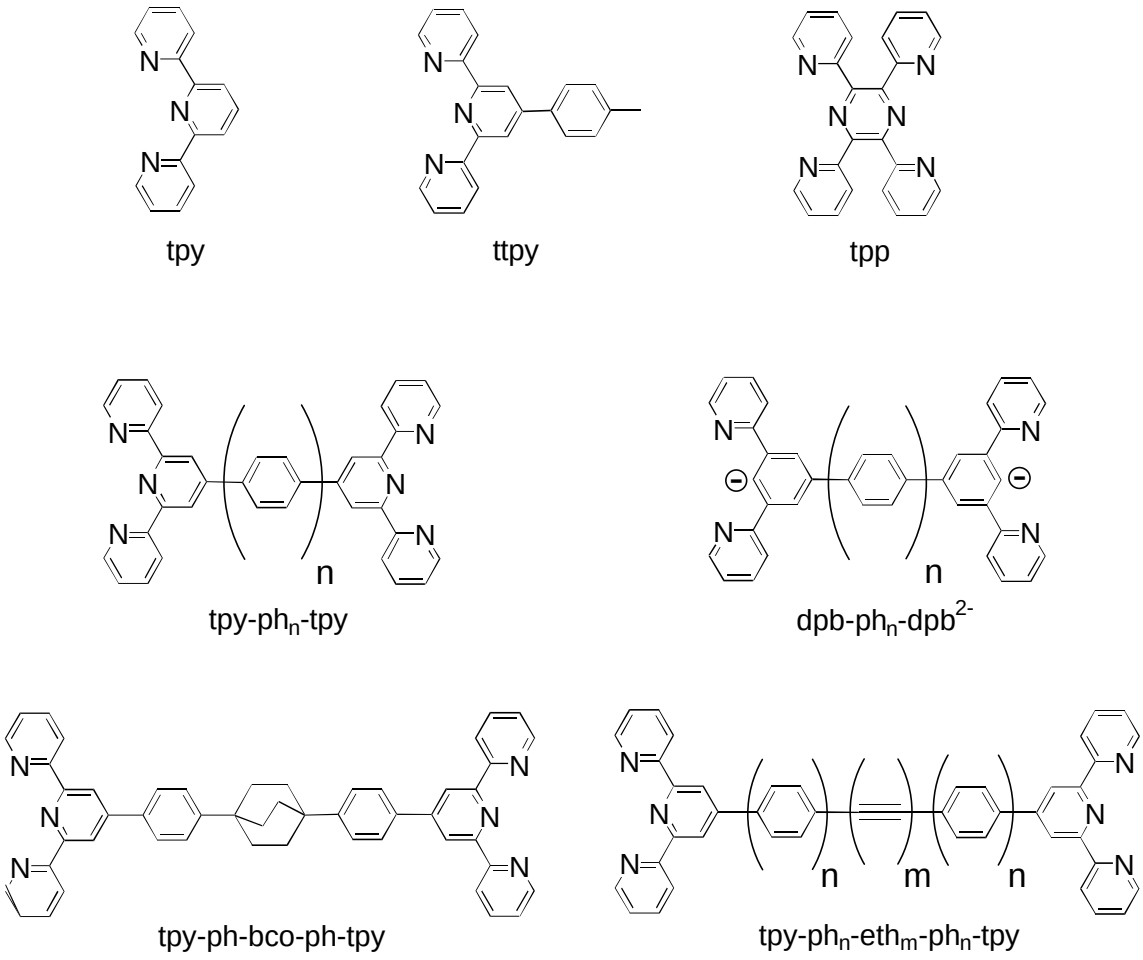

Figure 1.20 Polyazine tridentate ligands

or Os, and ttpy = p-tolyl-2,2′,6′,2′′-terpyridine. This series of stereochemically defined complexes is held in a rigid, linear fashion with well defined metal-metal distances ranging from 11 to 20 Å. The electrochemistry of the ruthenium-ruthenium bimetallic complex $[(ttpy)Ru(tpy\text{-}tpy)Ru(ttpy)]^{4+}$ showed that the two ruthenium centers have the same oxidation potential. This is in marked contrast to the tpp bridged system, $[(tpy)Ru(tpp)Ru(tpy)]^{4+}$, where the oxidation potentials of the two ruthenium centers are split by 300 mV. This seems to indicate that there is significantly less metal-metal communication in the tpy-tpy bridged system. The reduction potential of the bridging tpy-tpy is less negative than the reduction potential of tpy in the model monometallic $[Ru(tpy)_2]^{2+}$, indicating that there is at least some

interaction of the two tpy "ends" of tpy-tpy. This interaction stabilizes the bridging ligand π* orbital and makes the reduction potential less negative. In both the homometallic Ru/Ru complexes, $[(ttpy)Ru(tpy\text{-}ph_n\text{-}tpy)Ru(ttpy)]^{4+}$, and the Os/Ru mixed metal complexes, $[(ttpy)Ru(tpy\text{-}ph_n\text{-}tpy)Os(ttpy)]^{4+}$, the lowest energy electronic transition in the UV-vis region is a $M(d\pi) \rightarrow BL(\pi^*)$ CT transition, where BL = bridging ligand, Table 1. When two phenyl spacers are used, the $M(d\pi) \rightarrow tpy\text{-}ph_n\text{-}tpy(\pi^*)$ charge transfer transition is only slightly lower in energy than the $M \rightarrow ttpy$ CT for the model monometallic, $[M(ttpy)_2]^{2+}$. As the number of phenyl spacers is decreased, the $M(d\pi) \rightarrow tpy\text{-}ph_n\text{-}tpy(\pi^*)$ CT transition decreases in energy. This is due to the increasing interaction of the two tpy ends of the bridging ligand which lowers the energy of the bridging ligand π* orbital. The lowering in energy of the $M(d\pi) \rightarrow tpy\text{-}ph_n\text{-}tpy(\pi^*)$ CT transition is a possible indication of increased electronic

Table 1. Photophysical Data for a Series of Complexes Using the Bridging Ligand $tpy\text{-}ph_n\text{-}tpy$ and Model Compounds.[a,b]

Compound	λ_{max}^{abs} (nm)[c]	ε x 10^{-4} (M^{-1} cm^{-1})	λ_{max}^{em} (nm)	τ (ns)	ref.
$[Ru(ttpy)_2]^{2+}$	490	2.8	640[d]	0.95[d]	39b,c
$[Os(ttpy)_2]^{2+}$	490	2.6	734[d]	230[d]	39b,c
$[(ttpy)Ru(tpy\text{-}tpy)Ru(ttpy)]^{4+}$	520	5.8	720	570[e]	39a,j
$[(ttpy)Ru(tpy\text{-}ph\text{-}tpy)Ru(ttpy)]^{4+}$	499	6.3	656	4.0[e]	39a,j
$[(ttpy)Ru(tpy\text{-}ph_2\text{-}tpy)Ru(ttpy)]^{4+}$	495	7.4	[g]	[g]	39a
$[(ttpy)Ru(tpy\text{-}tpy)Os(ttpy)]^{4+}$	522	6.2	800[d]	110[d]	39b
$[(ttpy)Ru(tpy\text{-}ph\text{-}tpy)Os(ttpy)]^{4+}$	500	6.6	746[d]	190[d]	39b
$[(ttpy)Ru(tpy\text{-}ph_2\text{-}tpy)Os(ttpy)]^{4+}$	496	6.6	738[d]	200[d]	39b
$[(ttpy)Ru(tpy\text{-}tpy)Rh(ttpy)]^{5+}$	520	[g]	720[f]	<0.[f]	39e
$[(ttpy)Ru(tpy\text{-}ph\text{-}tpy)Rh(ttpy)]^{5+}$	499	[g]	655[f]	3.0[f]	39e
$[(ttpy)Ru(tpy\text{-}ph_2\text{-}tpy)Rh(ttpy)]^{5+}$	495	[g]	648[f]	3.5[f]	39e
$[(ttpy)Ru(tpp)Ru(ttpy)]^{4+}$	553	6.5	[g]	[g]	39a

[a] Measured at room temperature in acetonitrile unless noted
[b] tpy = 2,2',2"-terpyridine, ttpy = 4'-p-tolyl-2,2',2"-terpyridine, and ph = phenyl
[c] The lowest energy ^{1}MLCT reported
[d] Measured at room temperature in deoxygenated butyronitrile
[e] Measured at room temperature in deoxygenated acetonitrile
[f] Measured at 150 K in aerated 4:1 methanol:ethanol
[g] Not reported

communication between the two metal centers. The analogous Ru/Ru tpp bridged complex, which has a much lower MLCT transition, is included for comparison. While the complex $[(ttpy)Ru(ttpy)]^{2+}$ has an excited state lifetime of 0.9 ns at RT, the bimetallic complex $[(ttpy)Ru(tpy\text{-}tpy)Ru(ttpy)]^{4+}$ has a lifetime of 570 ns at RT.[39j] This has been attributed to a delocalization of the tpy-tpy π^* orbital which lowers the energy of the bridging ligand π^* orbital and decreases deactivation through the metal centered state.

In the series of complexes $[(ttpy)Ru(tpy\text{-}ph_n\text{-}tpy)Os(ttpy)]^{4+}$, where n = 0, 1, or 2, energy transfer between metal centers was studied by luminescence.[39b] For all three of the Ru/Os complexes, it was found that there was quantitative energy transfer from the ruthenium center to the osmium center and the rate of energy transfer for all three complexes was extremely

Table 2. Electrochemical Data for a Series of Complexes Using the Bridging Ligand tpy-ph_n-tpy and Model Compounds.[a,b]

Complex	$E_{1/2}$ ox	$E_{1/2}$ red	ref
$[Ru(ttpy)_2]^{2+}$	+1.25 $Ru^{II/III}$	-1.24 $ttpy^{0/-}$	39b,c
$[Os(ttpy)_2]^{2+}$	+0.97 $Os^{II/III}$	-1.23 $ttpy^{0/-}$	39b,c
$[(ttpy)Ru(tpy\text{-}tpy)Ru(ttpy)]^{4+}$	+1.31 $Ru^{II/III}$	-0.93 $tpy\text{-}tpy^{0/-}$	39a
$[(ttpy)Ru(tpy\text{-}ph\text{-}tpy)Ru(ttpy)]^{4+}$	+1.27 $Ru^{II/III}$	-1.18 $tpy\text{-}ph\text{-}tpy^{0/-}$	39a
$[(ttpy)Ru(tpy\text{-}ph_2\text{-}tpy)Ru(ttpy)]^{4+}$	+1.26 $Ru^{II/III}$	-0.93 $tpy\text{-}ph_2\text{-}tpy0^{/-}$	39a
$[(ttpy)Ru(tpy\text{-}tpy)Os(ttpy)]^{4+}$	+0.94 $Os^{II/III}$	-0.97 $tpy\text{-}tpy^{0/-}$	39b
	+1.31 $Ru^{II/III}$		
$[(ttpy)Ru(tpy\text{-}ph\text{-}tpy)Os(ttpy)]^{4+}$	+0.94 $Os^{II/III}$	-1.16 $tpy\text{-}ph\text{-}tpy^{0/-}$	39b
	+1.29 $Ru^{II/III}$		
$[(ttpy)Ru(tpy\text{-}ph_2\text{-}tpy)Os(ttpy)]^{4+}$	+0.94 $Os^{II/III}$	-1.18 $tpy\text{-}ph_2\text{-}tpy^{0/-}$	39b
	+1.28 $Ru^{II/III}$		
$[(ttpy)Ru(tpp)Ru(ttpy)]^{4+}$	+1.40 $Ru^{II/III}$	-0.35 $tpp^{0/-}$	39a
	+1.70 $Ru^{II/III}$	-0.85 $tpp^{-/2-}$	
$[(ttpy)Ru(tpy\text{-}tpy)Rh(ttpy)]^{5+}$	+1.31 $Ru^{II/III}$	-0.54 $Rh^{III/I}$	39e
		-1.22 $tpy\text{-}tpy^{0/-}$	
$[(ttpy)Ru(tpy\text{-}ph\text{-}tpy)Rh(ttpy)]^{5+}$	+1.29 $Ru^{II/III}$	-0.56 $Rh^{III/I}$	39e
		-1.18 $tpy\text{-}tpy^{0/-}$	
$[(ttpy)Ru(tpy\text{-}ph_2\text{-}tpy)Rh(ttpy)]^{5+}$	+1.27 $Ru^{II/III}$	-0.56 $Rh^{III/I}$	39e
		-1.20 $tpy\text{-}tpy^{0/-}$	

[a] tpy = 2,2',2"-terpyridine, ttpy = 4'-p-tolyl-2,2',2"-terpyridine, and ph = phenyl
[b] Potentials reported in acetonitrile solution with 0.1 M Bu_4NBF_4 versus SCE

fast, $k_{en} > 10^{10}$ s^{-1} at room temperature.[39b] No emission could be detected from the ruthenium center at 293 or 77 K. By comparison, the rate of energy transfer between $Ru^{II}(bpy)_3$ and $Os^{II}(bpy)_3$ separated by a rigid nonconjugated bridging ligand with a Ru-Os distance of 17 Å was 1000 times less.[41] This seems to indicate that the phenyl spacers are good bridges for efficient energy transfer even for tpy-ph_2-tpy where the Ru-Os distance is 20 Å.

The intervalence charge transfer transitions of the (tpy-ph_n-tpy) bridged mixed valence Ru^{II}/Ru^{III} complexes were studied to further characterize the degree of electronic coupling between metal centers in these systems.[39a] All the complexes showed IT bands in the 1150 to 1580 nm region, Table 3. From the electronic coupling parameter, H_{ab}, it can be seen that the phenyl groups only slightly attenuate the amount of intercomponent coupling, as also indicated from the luminescence studies of the Ru/Os systems. All three of the tpy-ph_n-tpy systems were classified as Class II mixed valence compounds that have localized valences with some intercomponent electronic coupling. By comparison, the analogous tpp bridged system, $[(ttpy)Ru(tpp)Ru(ttpy)]^{4+}$, was shown to have an IT transition at 1520 nm with a

Table 3. Metal to Metal Charge Transfer Transition Data for Mixed Valence Compounds with Tridentate Bridging Ligands.[a,b]

Compound	λ_{max}^{abs} (nm)	ε (M^{-1} cm^{-1})	$\Delta\nu_{1/2}$ (cm^{-1})	H_{ab} (eV)	ref.
$[(ttpy)Ru(tpy\text{-}ph_2\text{-}tpy)Ru(ttpy)]^{5+}$	1150	709	4008	0.022[c]	39a
$[(ttpy)Ru(tpy\text{-}ph\text{-}tpy)Ru(ttpy)]^{5+}$	1295	729	6036	0.030[c]	39a
$[(ttpy)Ru(tpy\text{-}tpy)Ru(ttpy)]^{5+}$	1580	1618	4008	0.047[c]	39a
$[(ttpy)Ru(tpp)Ru(ttpy)]^{5+}$	1520	5,132	1159	0.40[d]	39a

[a] tpy = 2,2',2"-terpyridine, ttpy = 4'-p-tolyl-2,2',2"-terpyridine, tpp = 2,3,5,6-tetra(2-pyridyl)pyrazine, and ph = phenyl

[b] Measured at room temperature in deoxygenated acetonitrile

[c] Calculated as a Class II complex

[d] Calculated as a Class III complex

electronic coupling parameter of 0.40 eV.[39a] This tpp bridged system was therefore classified as a Class III delocalized compound.

The mixed metal Ru/Rh $[(ttpy)Ru(tpy\text{-}ph_n\text{-}tpy)Rh(ttpy)]^{5+}$ complexes, where n = 0, 1, and 2, were studied by Sauvage et al. to investigate electron transfer from the excited ruthenium center to the rhodium center. For n = 1, it was found that electron transfer was efficient at room temperature with a rate $\geq 3.0 \times 10^9\ s^{-1}$. For n = 2, the rate of electron transfer was determined to be $\leq 5 \times 10^8\ s^{-1}$.[39g] The rate of electron transfer in the complex with n = 0 was not able to be determined due to the lack of a suitable model monometallic ruthenium complex.

To further investigate the ability of the phenyl spacers to electronically couple two metal centers, Sauvage et al. studied a system where an insulating, saturated hydrocarbon was used as part of the spacer between the tpy ends of the tpy-ph_n-tpy bridging ligand. Bicylco[2.2.2]octane (bco) was used between two phenyl rings as the spacer in the complex $[(ttpy)Ru(tpy\text{-}ph\text{-}bco\text{-}ph\text{-}tpy)Os(ttpy)]^{4+}$ (see Figure 1.21).[42] This complex has a Ru-Os distance of 24 Å. It was found that there was a large decrease in the rate of energy transfer from the excited state of the ruthenium component to the osmium component. At room temperature, the excited state lifetime of the ruthenium component was 1.1 ns, comparable to

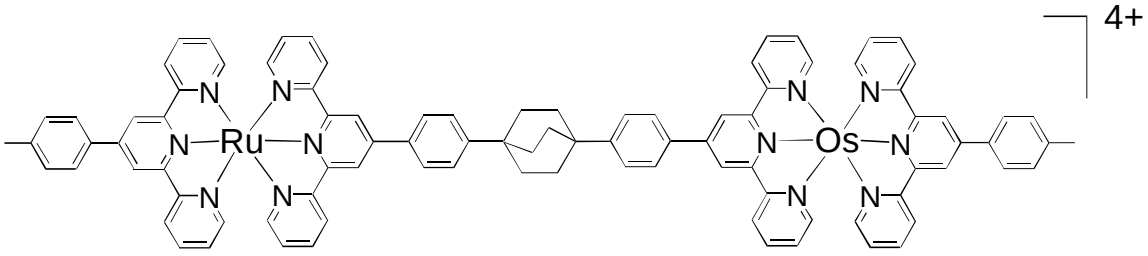

Figure 1.21 $[(ttpy)Ru(tpy\text{-}ph\text{-}bco\text{-}ph\text{-}tpy)Os(ttpy)]^{4+}$, bco = bicylco[2.2.2]octane, ttpy = 4'-p-tolyl-2,2',2"-terpyridine, ph = phenyl.

the 0.7 ns lifetime of the monometallic model compound, $[Ru(ttpy)_2]^{2+}$. There was no energy transfer from the ruthenium to the osmium component at room temperature. At 77 K, the lifetime of the excited state of the ruthenium component was 10.5 μs. This is long enough to allow energy transfer to the osmium component and the rate of energy transfer at 77 K was found to be 4.4×10^6 s^{-1}. This can be compared to $[(ttpy)Ru(tpy\text{-}ph_2\text{-}tpy)Os(ttpy)]^{4+}$ where although the Ru - Os distance is only 20 Å, the rate of energy transfer is at least 1,000 times greater. This demonstrates that the saturated bco spacer has a large insulating effect between the metal components and emphasizes the energy transfer ability of the tpy-ph_n-tpy bridge.

Ziessel et al. have used ethyne units as spacers in the tpy-spacer-tpy framework to yield the bridging ligands tpy-eth_n-tpy, where eth = ethyne.[43] As in the tpy-ph_n-tpy ligands, the ethyne units generate linear, rigid bridging ligands. The ethyne units also serve to lower the energy of the tpy-eth_n-tpy π^* orbital. This lowers the energy of the $Ru(d\pi) \rightarrow$ tpy-eth_n-tpy(π^*) CT enough in $[(tpy)Ru(tpy\text{-}eth\text{-}tpy)]^{2+}$ that it appears to limit deactivation of the MLCT excited state through the ligand field state in polymetallic systems. $[(tpy)Ru(tpy\text{-}eth\text{-}tpy)]^{2+}$ is reported to have a emission centered at 690 nm with a lifetime of 55 ns at room temperature, Table 4. A second ethynyl spacer lowers the energy of the MLCT which lowers the energy of the emission to 710 nm with a lifetime of 170 ns in $[(tpy)Ru(tpy\text{-}eth_2\text{-}tpy)]^{2+}$. When bimetallic complexes are formed, the tpy-eth_n-tpy π^* orbital is further stabilized resulting in even longer lifetimes. This gives $[(tpy)Ru(tpy\text{-}eth\text{-}tpy)Ru(tpy)]^{4+}$ an emission centered at 722 nm with a lifetime of 565 ns at room temperature and $[(tpy)Ru(tpy\text{-}eth_2\text{-}tpy)Ru(tpy)]^{4+}$ an emission centered at 735 nm with a lifetime of 720 ns.[43a] The lowering in energy of the tpy-eth_n-tpy π^* orbital compared to tpy can also be seen in the electrochemical data, Table 5. In $[(ttpy)Ru(tpy\text{-}eth\text{-}tpy)Ru(ttpy)]^{4+}$, the metal based oxidation is more positive and the bridging ligand based reduction is more negative compared to the same redox processes in $[(ttpy)Ru(tpy\text{-}tpy)Ru(ttpy)]^{4+}$.

Table 4. Photophysical Data for a Series of Complexes Using the Bridging Ligand tpy-eth$_n$-tpy and Model Compounds.[a,b]

Compound	λ_{max}^{abs} (nm) [c]	$\varepsilon \times 10^{-4}$ (M^{-1} cm^{-1})	λ_{max}^{em} (nm)	τ (ns)	ref.
$[Ru(ttpy)_2]^{2+}$	490	2.8	640[d]	0.95[d]	39b,c
$[Os(ttpy)_2]^{2+}$	490	2.6	734[d]	230[d]	39b,c
$[(tpy)Ru(tpy\text{-}eth\text{-}tpy)]^{2+}$	490	1.9	690[e]	55[e]	43a
$[(tpy)Ru(tpy\text{-}eth_2\text{-}tpy)]^{2+}$	490	2.3	710[e]	170[e]	43a
$[(tpy)Ru(tpy\text{-}eth\text{-}tpy)Ru(tpy)]^{4+}$	515	3.9	722[e]	565[e]	43a
$[(tpy)Ru(tpy\text{-}eth_2\text{-}tpy)Ru(tpy)]^{4+}$	512	3.3	735[e]	720[e]	43a
$[(tpy)Ru(tpy\text{-}eth\text{-}tpy)Os(tpy)]^{4+}$	[f]	[f]	746[e]	225[e]	43f
$[(tpy)Ru(tpy\text{-}eth_2\text{-}tpy)Os(tpy)]^{4+}$	ca. 480	[f]	760[e]	200[e]	43f

[a] Measured at room temperature in acetonitrile unless noted.
[b] tpy = 2,2',2"-terpyridine, ttpy = 4'-p-tolyl-2,2',2"-terpyridine, and eth = ethyne
[c] The lowest energy ^{1}MLCT reported.
[d] Measured at room temperature in deoxygenated butyronitrile.
[e] Measured at room temperature in deoxygenated acetonitrile.
[f] Not reported

Table 5. Electrochemical Data for a Series of Complexes Using the Bridging Ligand tpy-eth$_n$-tpy and Model Compounds[a,b].

Complex	$E_{1/2}$ ox		$E_{1/2}$ red	ref
$[Ru(ttpy)_2]^{2+}$	+1.25	$Ru^{II/III}$	-1.24 $ttpy^{0/-}$	39b
$[Os(ttpy)_2]^{2+}$	+0.97	$Os^{II/III}$	-1.23 $ttpy^{0/-}$	39b
$[(ttpy)Ru(tpy\text{-}tpy)Ru(ttpy)]^{4+}$	+1.31	$Ru^{II/III}$	-0.93 $tpy\text{-}tpy^{0/-}$	39a
$[(tpy)Ru(tpy\text{-}eth\text{-}tpy)Ru(tpy)]^{4+}$	+1.42	$Ru^{II/III}$	-0.97 $tpy\text{-}eth\text{-}tpy^{0/-}$	43g
			-1.19 $tpy\text{-}eth\text{-}tpy^{-/2-}$	
$[(tpy)Ru(tpy\text{-}eth_2\text{-}tpy)Ru(tpy)]^{4+}$	+1.41	$Ru^{II/III}$	-0.92 $tpy\text{-}eth_2\text{-}tpy^{0/-}$	43g
			-1.15 $tpy\text{-}eth_2\text{-}tpy^{-/2-}$	
$[(ttpy)Ru(tpy\text{-}tpy)Os(ttpy)]^{4+}$	+0.94	$Os^{II/III}$	-0.97 $tpy\text{-}tpy^{0/-}$	39b
	+1.31	$Ru^{II/III}$		
$[(tpy)Ru(tpy\text{-}eth_2\text{-}tpy)Os(tpy)]^{4+}$	+0.95	$Os^{II/III}$	-1.04 $tpy\text{-}eth_2\text{-}tpy^{0/-}$	43h
	+1.39	$Ru^{II/III}$	-1.34 $tpy\text{-}eth_2\text{-}tpy^{-/2-}$	

[a] tpy = 2,2',2"-terpyridine, ttpy = 4'-p-tolyl-2,2',2"-terpyridine, and eth = ethyne
[b] Potentials reported in acetonitrile solution with 0.1 M Bu_4NBF_4 versus SCE

Interesting ruthenium, cobalt, zinc, and iron containing mixed metal trimetallic systems were studied that use the tpy-eth$_n$-tpy bridging ligands (Figure 1.22).[43b] The Fe^{II} and Co^{II} systems were found to have emission lifetimes of less than 0.1 ns, significantly less than the 55 ns lifetime of the monometallic $[(tpy)Ru(tpy\text{-}eth\text{-}tpy)]^{2+}$. This is attributed to energy transfer in the case of the Ru/Fe/Ru trimetallic and electron transfer in the case of the Ru/Co/Ru trimetallic. Transient absorption studies showed that when the iron containing complex was irradiated with a laser pulse to generate the Ru $\rightarrow$ BL CT excited state, there was energy transfer within ca. 10 ps to the $Fe(tpy)_2$ fragment. In the case of the cobalt complex, irradiation with a laser pulse to generate the Ru $\rightarrow$ BL CT excited state, there was reductive quenching by the cobalt to produce the $Co^{III}(tpy)_2$ center that lasted for ca. 130 ps.

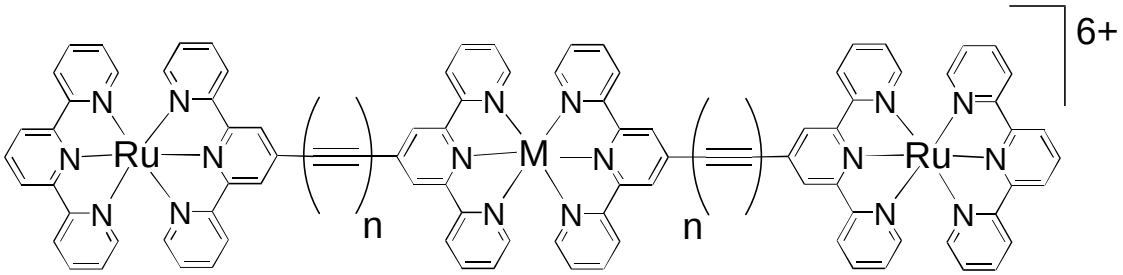

Figure 1.22 $[(tpy)Ru(tpy\text{-}eth_n\text{-}tpy)M(tpy\text{-}eth_n\text{-}tpy)Ru(tpy)]^{6+}$ where n = 1 or 2, M = Co^{2+}, Fe^{2+}, or Zn^{2+}, eth = ethyne, and tpy = 2,2',2"-terpyridine

A set of Ru/Os bimetallics containing the bridging ligand tpy-eth$_n$-tpy, were also investigated for energy transfer (Figure 1.23).[43f] It was found that upon generation of the $Ru(tpy)_2$ based MLCT excited state, there was efficient energy transfer to the osmium portion of the molecule within 20 ps. For both of these complexes the rate of energy transfer at 295 K was greater than $1x10^{10}$ s^{-1}. Based on these and other studies, it was proposed that it should be possible to have electron transfer in ethyne bridged systems with 50% efficiency over a distance of 250 angstroms.[43e]

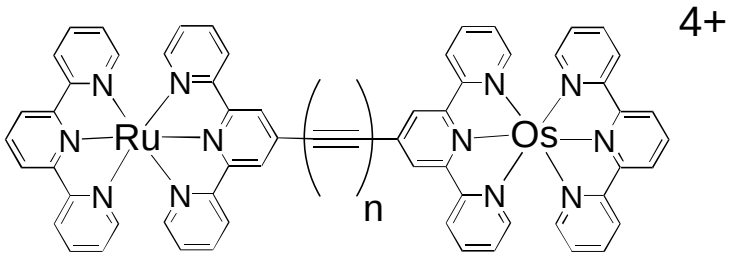

Figure 1.23 $[(tpy)Ru(tpy\text{-}eth_n\text{-}tpy)Os(tpy)]^{4+}$ where n = 1 or 2, tpy = 2,2',2"-terpyridine, and eth = ethyne.

A series of bridging ligands has been studied by Sauvage et al. that uses a cyclometallating benzene ring in place of the central pyridyl ring of tpy and is bridged through the 4 position of the benzene, dpb-ph_n-dpb, where dpb = 3,5-(dipyridyl)benzene and n = 0, 1, 2 (see Figure 1.24).[39f, 44] The Ru/Ru, Os/Os, and Ru/Os complexes, $[(ttpy)M(dpb\text{-}ph_n\text{-}dpb)M(ttpy)]^{2+}$, where M = Ru or Os and n = 0, 1, 2, were synthesized and characterized. In the Ru/Ru system, the metal oxidations are split by 0.15 V and in the Os/Os system the metal oxidations are split by 0.12 V.[44c] This indicates a large degree of metal-metal communication, in contrast to the noncyclometallated analog, $[(ttpy)Ru(tpy\text{-}tpy)Ru(ttpy)]^{4+}$, no split in the oxidation potential of the ruthenium centers. The mixed valence compounds were generated and the IT bands were characterized to aid in the determination of the amount of electronic

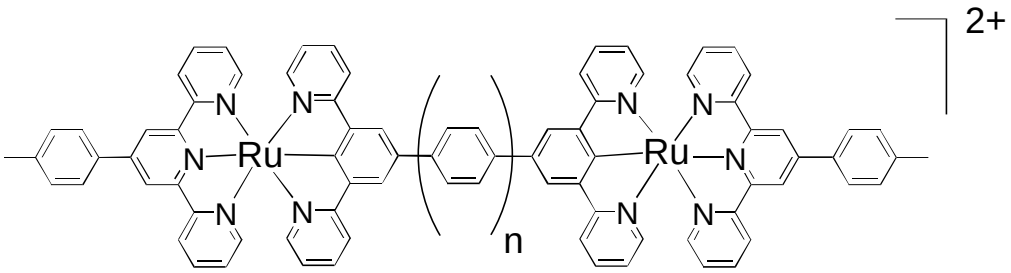

Figure 1.24 $[(ttpy)Ru(dpb\text{-}ph_n\text{-}dpb)Ru(ttpy)]^{2+}$, where dpb = dipyridyl benzene, ttpy = 4'-p-tolyl-2,2',2"-terpyridine, ph = phenyl, and n = 0, 1, 2.

Table 6. Electrochemical Data for a Series of Complexes Using the Bridging Ligand dpb-ph_n-dpb and Model Compounds.[a,b]

Complex	$E_{1/2}$ ox	$E_{1/2}$ red	ref
$[Ru(ttpy)_2]^{2+}$	+1.25 $Ru^{II/III}$	-1.24 $ttpy^{0/-}$	39b
$[Os(ttpy)_2]^{2+}$	+0.97 $Os^{II/III}$	-1.23 $ttpy^{0/-}$	39b
$[(ttpy)Ru(dpb)]^{+}$	+0.48 $Ru^{II/III}$	-1.61	44c
$[(ttpy)Os(dpb)]^{+}$	+0.33 $Os^{II/III}$	-1.60	44c
$[(ttpy)Ru(dpb\text{-}dpb)Ru(ttpy)]^{2+}$	+0.34 $Ru^{II/III}$	-1.55	44c
	+0.51 $Ru^{II/III}$		
$[(ttpy)Ru(dpb\text{-}ph\text{-}dpb)Ru(ttpy)]^{2+}$	+0.51 $Ru^{II/III}$	< -1.5	44
	+1.39[c]		
$[(ttpy)Ru(dpb\text{-}ph_2\text{-}dpb)Ru(ttpy)]^{2+}$	+0.51 $Ru^{II/III}$	< -1.5	44
	+1.39[c]		
$[(ttpy)Os(dpb\text{-}dpb)Os(ttpy)]^{2+}$	+0.22 $Os^{II/III}$	-1.53	44c
	+0.34 $Os^{II/III}$		
$[(ttpy)Os(dpb\text{-}dpb)Ru(ttpy)]^{2+}$	+0.29 $Os^{II/III}$	-1.48	44d
	+0.51 $Ru^{II/III}$		
$[(ttpy)Os(dpb\text{-}ph\text{-}dpb)Ru(ttpy)]^{2+}$	+0.33 $Os^{II/III}$	-1.50	44d
	+0.53 $Ru^{II/III}$		
$[(ttpy)Os(dpb\text{-}ph_2\text{-}dpb)Ru(ttpy)]^{2+}$	+0.33 $Os^{II/III}$	-1.50	44d
	+0.52 $Ru^{II/III}$		

[a] dpb = dipyridylbenzene, ttpy = 4'-p-tolyl-2,2',2"-terpyridine, and ph = phenyl
[b] Potentials reported in acetonitrile solution with 0.1 M Bu_4NBF_4 versus SCE.
[c] Irreversible Ru^{III}, Ru^{III}/Ru^{IV},Ru^{IV} two electron oxidation

communication between the metal centers, Table 8. The Ru/Ru complex was found to have a coupling parameter of 0.15 eV while the Os/Os complex was found to have a coupling parameter of 0.12 eV. This is significantly greater than the 0.022 to 0.047 eV coupling parameter found in the analogous tpy-ph_n-tpy bridged systems. In fact, characteristics of the intervalence charge transfer band suggested that these mixed valence dpb-dpb bridged systems are completely delocalized Class III systems. The strong coupling through the dpb-dpb^{2-} ligand is attributed to the highly covalent, electron donating nature of the bond between the cyclometallating benzene ring and the metal center. This raises the energy of the metal $d\pi$ orbitals which can be seen in the less positive oxidation potentials of the metals compared to those in analogous systems using non-cyclometallating ligands. The higher energy metal $d\pi$

Table 7. Photophysical Data for a Series of Complexes Using the Bridging Ligand dpb-ph$_n$-dpb and Model Compounds.[a,b]

Compound	λ_{max}^{abs} (nm)[c]	ε x 10^{-4} (M^{-1} cm^{-1})	λ_{max}^{em} (nm)	τ (ns)	ref.
$[(ttpy)Ru(dpb)]^{+}$	506	1.3	784[d]	4.5	44d
$[(ttpy)Os(dpb)]^{+}$	531	1.3	920[d]	[e]	44d
$[(ttpy)Ru(dpb\text{-}dpb)Ru(ttpy)]^{4+}$	543	3.1	798	4.0	44
$[(ttpy)Ru(dpb\text{-}ph\text{-}dpb)Ru(ttpy)]^{4+}$	513	3.5	[f]	[f]	44d
$[(ttpy)Ru(dpb\text{-}ph_2\text{-}dpb)Ru(ttpy)]^{4+}$	511	3.5	[f]	[f]	44d
$[(ttpy)Os(dpb\text{-}dpb)Os(ttpy)]^{2+}$	540	3.5	820	[e]	44
$[(ttpy)Os(dpb\text{-}dpb)Ru(ttpy)]^{2+}$	542	3.6	816[d]	0.35[g]	44d
$[(ttpy)Os(dpb\text{-}ph\text{-}dpb)Ru(ttpy)]^{2+}$	534	4.0	800[d]	3.5[g]	44d
$[(ttpy)Os(dpb\text{-}ph_2\text{-}dpb)Ru(ttpy)]^{2+}$	532	3.7	792[d]	4.9[g]	44d

[a] dpb = dipyridylbenzene, ttpy = 4'-p-tolyl-2,2',2"-terpyridine, and ph = phenyl
[b] Measured at room temperature in acetonitrile.
[c] The lowest energy ^{1}MLCT reported.
[d] Measured at room temperature in deoxygenated butyronitrile.
[e] Not detected.
[f] Not reported.
[g] Lifetime of the ruthenium based emission.

Table 8. Metal to Metal Charge Transfer Transition Data for Mixed Valence Compounds Using the Bridging Ligand dpb-ph$_n$-dpb.[a,b]

Compound	λ_{max} (nm)	ε (M^{-1} cm^{-1})	$\Delta\nu_{1/2}$ (cm^{-1})	H_{ab} (eV)	ref.
$[(ttpy)Ru(dpb\text{-}ph_2\text{-}dpb)Ru(ttpy)]^{3+}$	1214	574	2200	0.041[c]	44b
$[(ttpy)Ru(dpb\text{-}ph\text{-}dpb)Ru(ttpy)]^{3+}$	1650	6,600	5112	0.074[c]	44b
$[(ttpy)Ru(dpb\text{-}dpb)Ru(ttpy)]^{3+}$	1936	22,000	2660	0.127[c]	44b
$[(ttpy)Os(dpb\text{-}dpb)Os(ttpy)]^{3+}$	1410	18,000	3360	0.12[d]	44c
	1800	8,000			
$[(ttpy)Ru(dpb\text{-}dpb)Ru(ttpy)]^{3+}$	1820	27,000	2820	0.15[d]	44a

[a] dpb = dipyridylbenzene, ttpy = 4'-p-tolyl-2,2',2"-terpyridine, and ph = phenyl
[b] Measured at room temperature in deoxygenated acetonitrile.
[c] Calculated as a Class II complex
[d] Calculated as a Class III complex

orbitals have a large degree of overlap with the dpb-dpb^{2-} π^* orbital, resulting in a large electronic coupling parameter. The complex (ttpy)Os(dpb-dpb)Os(ttpy)]$^{3+}$ showed a second MMCT transition at 1800 nm and is attributed to the presence of strong spin-orbit coupling.

In luminescence studies of the mixed metal complexes, [(ttpy)Ru(dpb-ph$_n$-dpb)Os(ttpy)]$^{2+}$, it was found that the rate of energy transfer from the ruthenium center to the osmium center was orders of magnitude slower than in tpy-ph$_n$-tpy systems.[44d] For [(ttpy)Ru(dpb-dpb)Os(ttpy)]$^{2+}$ the energy transfer rate was found to be 2.6 x 10^9 s^{-1} while that of [(ttpy)Ru(dpb-ph$_2$-dpb)Os(ttpy)]$^{2+}$ was found to be < 2.2 x 10^7 s^{-1}. For the complex with two phenyl spacers, this is three orders of magnitude slower than in the analogous tpy-ph$_n$-tpy bridged system even though the cyclometallating complex has a much great electronic coupling parameter. These results are explained by considering the nature of the lowest energy excited state of the two series. In the tpy-ph$_n$-tpy bridged series, the lowest energy excited state is a M(dπ) $\rightarrow$ tpy-ph$_n$-tpy(π^*) CT state. This puts the excited electron on the bridging ligand and close to the other metal, facilitating energy transfer. In the dpb-ph$_n$-dpb^{2-} bridged series, it was determined that the π^* orbital of the bridging dpb-ph$_n$-dpb is higher in energy than the π^* orbital of the terminal ttpy. This may make the lowest energy excited state a Ru(dπ) $\rightarrow$ ttpy(π^*) CT state, putting the excited electron a long distance from the other metal and inhibiting energy transfer. While these dpb-ph$_n$-dpb bridging ligands did not prove advantageous for energy transfer in these systems, they do offer the ability to control electron and energy transfer in polymetallic systems. By carefully choosing cyclometallating and non-cyclometallating ligands, the rate and direction of energy and electron transfer should be able to be controlled.

Recently, Balzani et al. have investigated two trimetallic systems using three 2,2'2"-terpyridine ligands linked together with -CH_2-CH_2- or -CH=CH- groups, Figure 1.25.[45] The -CH_2-CH_2- bridged system was found to behave almost identically to [Ru(tpy)$_2$]$^{2+}$ with no emission at room temperature and a lifetime of 9.4 μs at 77 K. The -CH_2=CH_2- bridged

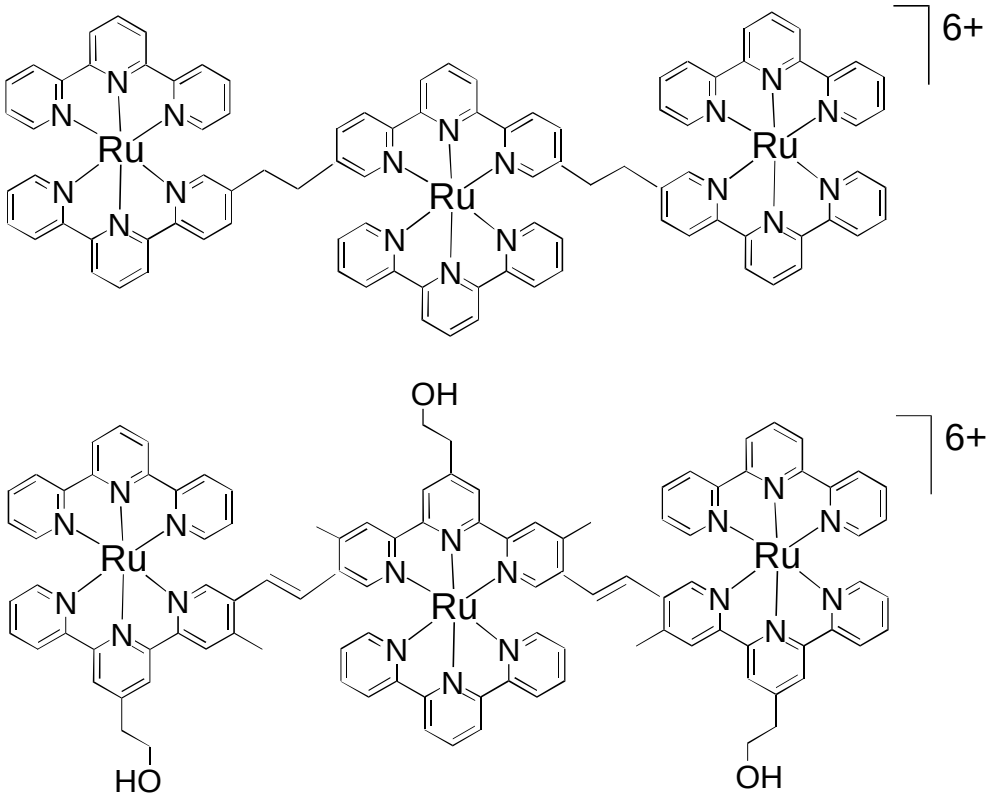

Figure 1.25 Trimetallic complexes bridged by -CH_2-CH_2- and -CH=CH-linked terpyridines

trimetallic system had a detectable emission at room temperature with a lifetime of 11 ns. At 77 K, the emission had a lifetime of 1.6 μs. These results are explained in terms of the nature of the lowest energy excited state. In the -CH_2-CH_2- bridged system the lowest energy MLCT excited state involves a tpy ligand while in the-CH=CH- system, the lowest energy excited state involves the bridging ligand. This lowers the energy of the MLCT and gives rise to a slightly lower degree of thermal activation of the deactivating LF excited state.

Constable et al. have investigated a tri-nucleating tridentate ligand formed by three tpy ligands bound to a benzene ring through the 4′ position of each tpy (see Figure 1.26).[46] This

trinucleating ligand forms the complex $\{[(tpy)Ru]_3(tris\text{-}tpy)\}^{6+}$ when reacted with $Ru(tpy)Cl_3$. This compound displays only one ruthenium based oxidation suggesting weak metal-metal interaction.

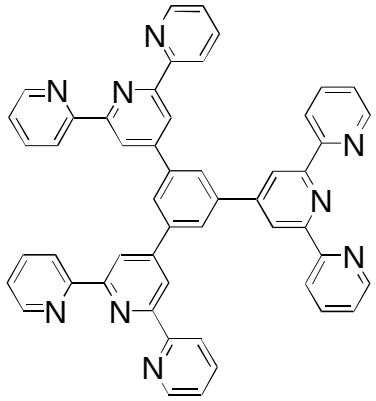

Figure 1.26 The trinucleating bridging ligand tris-tpy

Sauvage et al. have reported on many multimetallic porphyrin systems for use in photoinitiated electron and energy transfer.[47] One such system is a three component zinc porphyrin - ruthenium bis(terpyridine) - gold porphyrin system designed for photoinitiated electron transfer from the zinc porphyrin to the gold porphyrin through the ruthenium bis(terpyridine) component (see Figure 1.27).[47] The ruthenium bis(terpyridine) component holds the two porphyrin components in a rigid, linear fashion. Excitation of this complex at 586 nm, where the zinc component absorbs most of the light, results in electron transfer from the zinc porphyrin to the gold porphyrin with a rate of ca. 2×10^{10} s^{-1}. The zinc-gold distance is approximately 30 angstroms. The synthetic scheme for this complex is easily varied to provide for the synthesis of a wide range of porphyrins held in a rigid, linear fashion designed for various photoinitiated processes.

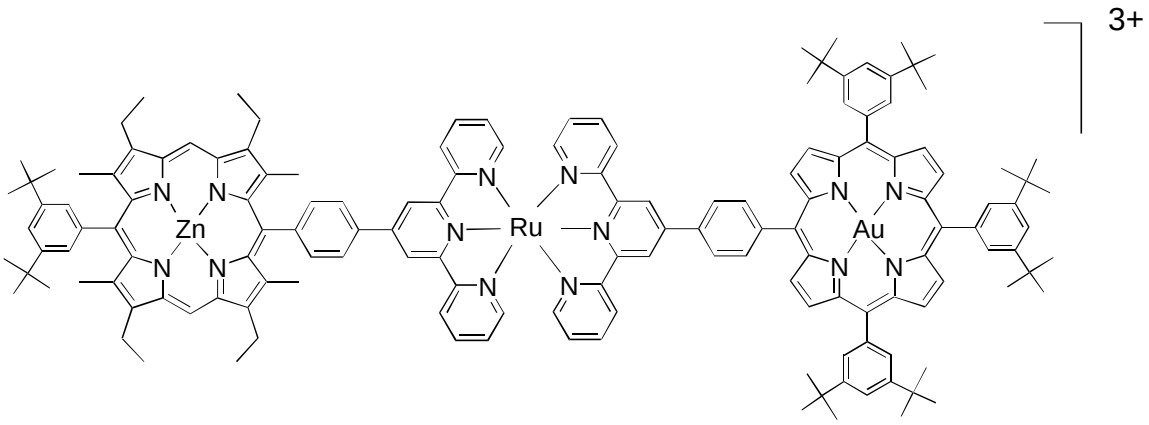

Figure 1.27 Zn^{II} Porphyrin-$Ru^{II}(tpy)_2$-Au^{III} Porphyrin

Statement of problem

The goal of this research was to develop stereochemically defined multimetallic systems for use as light absorbers and electron donor / light absorber dyads in molecular devices for photoinitiated electron transfer and electron collection. The basis of the stereochemical control is provided by the symmetric bridging ligands 2,3,5,6-tetra(pyridyl)pyrazine and 2,2′-bipyrimidine. The proposed ligand 4N-perylene could potentially be used as a symmetric bidentate to control the stereochemistry of polymetallic complexes.

A series of 2,3,5,6-tetra(pyridyl)pyrazine bridged ruthenium / osmium bimetallic complexes was investigated as potential light-absorber / electron-donor synthons for use in the construction of larger supramolecular complexes designed for photoinitiated electron collection. With two metal centers and up to three π accepting ligands, the electrochemistry and UV-vis spectroscopy can be extremely complex. UV-vis spectroelectrochemistry has been used to aid in the assignment of the electrochemistry as well as the UV-vis spectroscopy. The metal to metal charge transfer transition of the mixed valence species of these tpp bridged bimetallic complexes has been studied to gain an understanding of the degree of metal to metal communication through the tpp bridging ligand. A complete understanding of the

electrochemistry, UV-vis spectroscopy, and metal to metal communication of these light-absorber / electron donor complexes will greatly facilitate interpretation of photophysical studies of the larger, completed supramolecular devices.

The symmetric bidentate bridging ligand 2,2′-bipyrimidine was utilized in the synthesis of the LA-EC-LA complex $\{[(bpy)_2Ru(bpm)]_2IrCl_2\}^{5+}$. To aid in the understanding of the electrochemistry and UV-vis spectroscopy, UV-vis spectroelectrochemistry was used to study this trimetallic complex and the model compounds $[(bpy)_2Ru(bpm)]^{2+}$, $[(bpy)_2Ru(bpm)Ru(bpy)_2]^{4+}$, and $[IrCl_2(bpm)_2]^{+}$. A complete understanding of the UV-vis spectroscopy of the parent and reduced species of the complex $\{[(bpy)_2Ru(bpm)]_2IrCl_2\}^{5+}$ has aided in understanding the photophysical studies of this LA-EC-LA complex.

The symmetric ligand, 4N-perylene, was designed as a potential bidentate bridging ligand for use in polymetallic complexes. This ligand would have a large, planar π system that would likely result in a lower energy π* orbital compared to that of bpm. The principal reaction in the proposed synthetic route is the homo-coupling of a 1,8-di-substituted-2,7-naphthyridine. The potential synthon 1,8-dichloro-2,7-naphthyridine has been synthesized and characterized by NMR and EI-MS.

Chapter 2 Experimental

Materials. All chemicals were obtained from Aldrich Chemical Co. and used as received unless otherwise noted. Acetonitrile was obtained from Baxter Scientific. 2,3,5,6-Tetrakis(2-pyridyl)pyrazine was purchased from GFS Chemicals. The supporting electrolyte for the electrochemistry and spectroelectrochemistry was tetrabutylammonium hexafluorophosphate, prepared by the metathesis of tetrabutylammonium bromide with potassium hexafluorophosphate, recrystallized twice from ethanol, dried under vacuum, and stored in a vacuum desiccator. Lipophilic Sephadex LH-20 size exclusion chromatography resin was obtained from Sigma Chemical Company. Whatman 70 - 230 mesh silica for silica gel chromatography was obtained from VWR Scientific Products. Adsorption alumina (80 - 200 mesh) was obtained from Fisher Scientific. Dry ethanol was prepared by heating at reflux 10 mL ethanol (100 %), 0.5 g Mg, and 3 drops chloroform under nitrogen until all the Mg was converted to $Mg(OEt)_2$, addition of 90 mL EtOH to the mixture, heating at reflux for one hour followed by distillation. $Ru(bpy)_2Cl_2$[48], $Ru(tpy)Cl_3$[49], $Os(tpy)Cl_3$[50], $[(tpy)Ru(tpp)Ru(tpy)](PF_6)_4$[51], $[(tpy)Ru(tpp)RuCl_3](PF_6)$[27a], $[(tpy)Os(tpp)RuCl_3](PF_6)$[27a], $[(tpy)Ru(tpp)Ru(tpp)](PF_6)_4$[27a], and $[(tpy)Os(tpp)Ru(tpp)](PF_6)_4$[27a] were prepared as previously reported.

NMR Spectroscopy. ^1H NMR spectra were obtained on a Bruker 200 MHz instrument while the ^{13}C NMR spectra were obtained on a Bruker 360 MHz instrument. All spectra were obtained at room temperature using $CDCl_3$ as the solvent and trimethylsilane as an internal standard unless otherwise indicated.

FAB- and EI-Mass spectrometry. Mass spectral analysis was conducted on a Fisons VG Quattro triple-stage quadrupole mass spectrophotometer using *m*-nitrobenzyl alcohol as the matrix.

Electrochemistry. A Bioanalytical Systems, Inc. 100W electrochemical analyzer was used to record the cyclic voltammograms and to control the electrolysis in the spectroelectrochemical experiments. The supporting electrolyte was 0.1 M Bu_4NPF_6 and the measurements were made in Burdick and Jackson UV-grade acetonitrile. The three electrode system uses a 1.9 mm diameter platinum disk working electrode, a platinum wire auxiliary electrode, and a Ag/AgCl reference electrode (0.29 V vs. NHE). The Ag/AgCl reference electrode was calibrated against the $FeCp_2/FeCp_2^+$ couple which was assumed to be 0.665 V vs. NHE in 0.1 M TBAH in acetonitrile.[52] The $Ag/AgNO_3$ reference electrode (0.57 V vs. NHE) was also calibrated against the $FeCp_2/FeCp_2^+$ couple.

Electronic Absorption Spectroscopy. Spectra were recorded at room temperature using a Hewlett Packard 8452 diode array spectrophotometer with a 2 nm resolution and a range from 190 to 820 nm, interfaced to an IBM compatible computer. The solvent was Burdick and Jackson UV-grade acetonitrile. The cuvette was a 1 cm pathlength cell with quartz windows.

Near IR Spectroscopy. Spectra were recorded at room temperature using a Cary 5G spectrometer with 0.04 nm resolution and a range from 175 to 3300 nm interfaced to an IBM compatible computer. The solvent was Burdick and Jackson UV-grade acetonitrile. A 1 mm pathlength quartz cell was used to minimize the acetonitrile absorbances in the NIR region.

Spectroelectrochemistry. UV-vis electronic absorption spectra of electrogenerated oxidized or reduced species were recorded using an H-cell as shown in Figure 2.2, a modification of a previously reported cell.[34] The working compartment was a 1 cm quartz cuvette and contained the analyte in 0.1 M Bu_4NPF_6 in CH_3CN, a platinum mesh working electrode, and a Ag/AgCl reference electrode. The other compartment of the H-cell contained a platinum mesh auxiliary electrode and 0.1 M Bu_4NPF_6 in CH_3CN with no analyte. The two compartments are separated by a fine porosity glass frit. The auxiliary compartment was bubbled with CH_3CN saturated argon for ten minutes prior to the experiment and sealed for the duration of the experiment. The working compartment was bubbled with argon for 10

minutes prior to and during each experiment. The potential was controlled using a BAS 100W electrochemical analyzer. After establishing an initial maximum absorbance of 0.6-0.8, the solution was electrochemically oxidized or reduced and the redox process monitored by UV-vis spectroscopy. All processes gave clean isosbestic points. The oxidation or reduction was considered complete when there was no further change in the UV-vis spectra (± 2%). After the completion of the bulk electrolysis, the complex was returned electrochemically to its parent charge to determine the reversibility of the oxidation or reduction process.

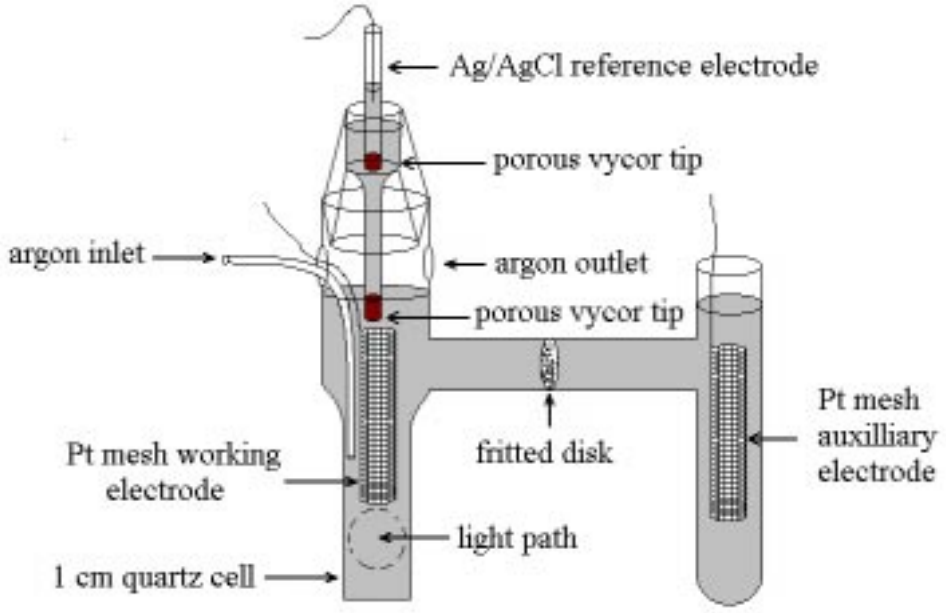

Figure 2.1 Spectroelectrochemistry cell.

Near IR Spectroelectrochemistry. NIR spectra were recorded using a 1 mm pathlength quartz cell attached to a H-cell used for bulk electrolysis (Figure 2.2). The working compartment of the H-cell contained the analyte in 0.1 M Bu_4NPF_6 in CH_3CN, a platinum mesh working electrode, and a $Ag/AgNO_3$ reference electrode (0.31 V vs. NHE, calibrated

against $FeCp_2/FeCp_2^+$). The other compartment of the H-cell contained a platinum mesh auxiliary electrode and 0.1 M Bu_4NPF_6 in CH_3CN with no analyte. The two compartments are separated by a fine porosity glass frit. The working compartment, the auxiliary compartment, and the cuvette compartment were all sealed with rubber septa and flushed with argon for ten minutes prior to the experiment to maintain an inert atmosphere. The working compartment was bubbled with argon during the bulk electrolysis to ensure mixing. After the complex was oxidized by one electron, the whole cell was tipped to allow the analyte solution to flow to the 1 mm pathlength cell. A tube connected the working compartment and the quartz cell to all the pressure to equalize during the transfer of the analyte. The whole apparatus was then placed in the NIR spectrophotometer. After the NIR spectrum was obtained, the cuvette portion of the cell was rotated up to allow the analyte

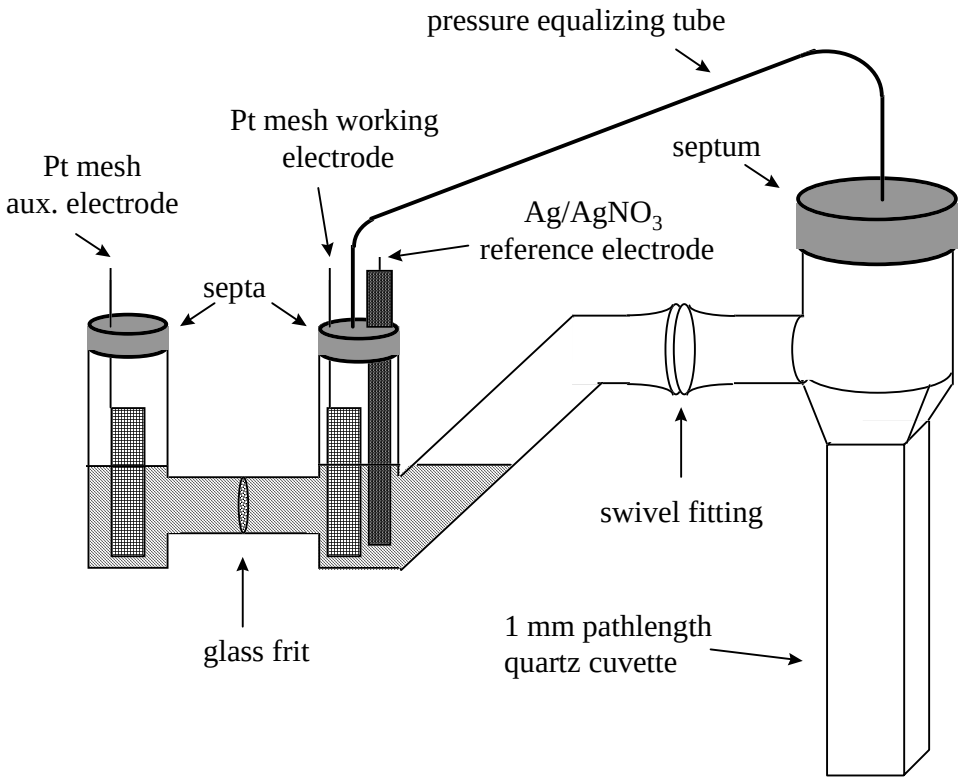

Figure 2.2 Near IR spectroelectrochemistry cell.

solution to flow back to the bulk electrolysis compartment. The complex was then electrochemically returned to the its parent charge and the spectrum obtained to determine the reversibility of the oxidation process.

Emission spectroscopy. Emission spectra were obtained at RT using a 1 cm quartz cell containing a deoxygenated acetonitrile solution of the analyte in a Photon Technologies Inc. Alphascan fluorimeter modified to detect red-shifted emissions using a thermoelectrically cooled Hamamatsu R666S photomultiplier tube.

Emission Lifetimes. Emission lifetimes were determined using a Photon Technologies Inc. PL 2300 nitrogen laser and a PL 201 continuously tunable dye laser (360-900nm) excitation source. The analyte was in deoxygenated acetonitrile solution in a 1 cm pathlength, four quartz window cell. The luminescence was detected at a right angle and passed through a monochromator. The emission was detected by a Hamamatsu R666S red-selective photomultiplier tube contained in a Products For Research thermoelectrically cooled housing. The signal was processed on a LeCroy oscilloscope by eliminating the initial data that contains the laser pulse and fit to a single exponential equation of the form $Y = A + B(\exp(-X/c))$ where $c = \tau = 1/k$ (in s).

2,3-bis(2-pyridyl)quinoxaline. 2,3-bis(2-pyridyl)quinoxaline (dpq) was synthesized by a modification of a previously published preparation by Goodwin and Lions.[21] 2, 2′-pyridyl (4.24 g, 20.0 mmol) and phenylenediamine (2.16 g, 20.0 mmol) were heated at reflux in 20 mL EtOH for 30 minutes. The reaction was cooled to room temperature and the crude product was separated by vacuum filtration. Purification was achieved by recrystallization from hot ethanol (~ 50 mL). The purity was checked by the lack of a C=O peak at ~1700 cm^{-1} in the IR spectrum. Yield: 3.86 g, 13.6 mmol, 68 %.

[(tpy)Ru(tpp)]$(PF_6)_2$. The synthesis of [(tpy)Ru(tpp)]$(PF_6)_2$ was a modification of a previously published procedure.[23] Ru(tpy)Cl_3 (300 mg, 0.681 mmol),

2,3,5,6-tetra(2-pyridyl)pyrazine (529 mg, 1.36 mmol), and triethylamine (2 mL) were heated at reflux under argon in 25 mL 2:1 EtOH/H_2O for 20 hours. The crude product was precipitated as the hexafluorophosphate salt by addition to 100 mL saturated aqueous KPF_6. The precipitate was separated by vacuum filtration and washed with 50 mL EtOH. Purification was achieved by alumina column chromatography using 1:1 toluene/acetonitrile as the eluent. The first, yellow band to elute was unreacted tpp. The second, orange-brown band was the product and was collected. The third, blue band was most likely the bimetallic $[(tpy)Ru(tpp)Ru(tpy)](PF_6)_4$. The solvent was removed from the product elution by rotary evaporation. The product was dissolved in a minimal amount of acetonitrile, flash precipitated in 150 mL diethylether, and collected by vacuum filtration. Yield: 220 mg, 0.217 mmol, 32 %. $E_{1/2}$ (V. vs. Ag/AgCl): +1.40, -0.97, -1.38, -1.60. λ_{max}^{abs} = 472 nm.

$[(tpy)Os(OH_2)_3](PF_6)_2$. $Os(tpy)Cl_3$ (300 mg, 0.566 mmol) and $AgCF_3SO_3$ (1.45 g, 5.66 mmol) were heated at reflux in 100 mL H_2O under Ar in the dark for 48 hours. The AgCl precipitate was removed by vacuum filtration. The reaction volume was reduced to ~25 mL by rotary evaporation. The product was precipitated by addition to 150 ml sat. aqueous KPF_6 and separated by vacuum filtration. Yield: 180 mg, 0.235 mmol, 41 %.

$[(tpy)Os(tpp)](PF_6)_2$. The synthesis of $[(tpy)Os(tpp)](PF_6)_2$ was a modification of a previously published procedure.[53] $[Os(tpy)(OH_2)_3](PF_6)_2$ (109 mg, 0.142 mmol) and tpp (70 mg, 0.18 mmol) were reacted in ethylene glycol (30 mL) at 160° C for 40 minutes under Ar. The reaction was monitored by electronic absorption spectroscopy. The lowest energy MLCT at 476 nm was seen growing in over the reaction time. The reaction mixture was cooled to RT in a water bath and the product was precipitated by the addition of 50 mL saturated aqueous KPF_6. The crude product was separated by vacuum filtration. Purification was achieved by alumina column chromatography using 1:1 toluene/acetonitrile as the mobile phase. The first, brown band was the desired product. The second band was the bimetallic $[(tpy)Os(tpp)Os(tpy)](PF_6)_4$. The product was collected and the solvent removed by rotary

evaporation. The product was then dissolved in minimal acetonitrile, flash precipitated in diethylether, and separated by vacuum filtration. Yield: 24 mg, 0.022 mmol, 15%. $E_{1/2}$ (V. vs. Ag/AgCl): +1.06, -0.97, -1.39. λ_{max}^{abs} = 468 nm.

$[(tpy)Ru(CH_3CN)_3](PF_6)_2$. $Ru(tpy)Cl_3$ (855 mg, 1.94 mmol) and $AgPF_6$ (1.6 g, 6.3 mmol) were heated at reflux in 70 mL 1:1 CH_3CN/H_2O under argon in the dark for 24 hours. The reaction mixture was filtered to remove solid AgCl and the solvent was removed by rotary evaporation. The crude product was dissolved in a minimal amount of acetonitrile and purified on a 3 inch alumina column, acetonitrile eluent. The first major yellow band was collected and the solvent was removed by rotary evaporation. The product was dissolved in minimal acetonitrile, flash precipitated in diethylether, and separated by vacuum filtration. Yield: 880 mg, 1.20 mmol, 60 %. $E_{1/2}$ (V. vs. Ag/AgCl): +1.54, -1.28. λ_{max}^{abs} = 446 nm.

Table 9. FAB Mass Spectral Data for $[(tpy)Ru(CH_3CN)_3](PF_6)_2$.[a]

m/z	rel. abund.	assignment
603	53	$[(tpy)Ru(CH_3CN)_3](PF_6)^+$
460	37	$[(tpy)Ru(CH_3CN)_3]^+$
375	80	$[(tpy)Ru(CH_3CN)]^+$
337	100	$[Ru(tpy)]^+$

[a] tpy = 2,2′:6′,2′′-terpyridine.

$[(tpy)Ru(tpp)Ru(CH_3CN)_3](PF_6)_4$. $[(tpy)Ru(tpp)RuCl_3](PF_6)_4$ (89.0 mg, 0.083 mmol) and $AgPF_6$ (200 mg, 0.79 mmol) were heated at reflux in 15 mL acetonitrile under argon in the dark for one hour. The reaction mixture was cooled to room temperature and filtered by vacuum to remove the AgCl precipitate. The filtrate was collected as the crude product. Purification was achieved by a four inch alumina column using acetonitrile as the mobile phase. The major, blue product band was collected and the acetonitrile was removed by rotary evaporation. The product was dissolved in minimal acetone, flash precipitated in 150 mL saturated, aqueous KPF_6, and separated by vacuum filtration. The pure product was then dissolved in minimal acetonitrile, flash precipitated in 100 mL diethylether, and separated by

vacuum filtration. Yield: 130 mg, 0.083mmol, 100%. $E_{1/2}$ (V. vs. Ag/AgCl): +1.80, +1.30, -0.30, -0.80, -1.67. λ_{max}^{abs} = 566 nm.

[(tpy)Ru(tpp)Ru(dpq)Cl](PF$_6$)$_3$. [(tpy)Ru(tpp)RuCl$_3$](PF$_6$) (100 g, 0.090 mmol) and dpq (130 mg, 0.44 mmol) were heated at reflux in 15 mL 95% EtOH under argon for 7 hours during which time the reaction mixture turned a blue color. The reaction mixture was cooled to room temperature, the crude product was precipitated by addition to 100 mL saturated aqueous KPF_6 and separated by vacuum filtration. Purification was achieved by size exclusion column chromatography using a 24 inch LH-20 column with 2:1 ethanol/ acetonitrile as the mobile phase. Fractions were monitored by UV-vis spectroscopy. The first part of the band to elute (λ_{max} > 590 nm with a low energy tail) was probably due to a tetrametallic complex. The second fraction (λ_{max} = 584 nm) was collected and the solvent removed by rotary evaporation. The product was dissolved in minimal acetonitrile, flash precipitated in diethylether, and collected by vacuum filtration. This complicated separation leads to a low yield of highly purified complex. A typical yield for this reaction was 34%. $E_{1/2}$ (V. vs. Ag/AgCl): +1.36, +0.87, -1.19, -1.42. λ_{max}^{abs} = 584 nm.

[Ir(bpm)$_2$Cl$_2$](PF$_6$). The synthesis of [Ir(bpm)$_2$Cl$_2$](PF$_6$) was a modification of a previously published procedure.[54] $IrCl_3 \cdot 3H_2O$ (250 mg, 0.710 mmol) and bpm (448 mg, 2.80 mmol) were heated at reflux in 20 mL ethylene glycol for 30 minutes. The reaction solution was cooled to room temperature and added to 100 mL saturated KPF_6 to induce precipitation. The precipitate was separated by vacuum filtration and washed with 30 mL water and 30 mL ethanol. Purification was achieved by alumina adsorption chromatography using 95:5 acetonitrile/methanol as the mobile phase. The first, yellow band to elute was unreacted bpm. The second, orange product band was collected and the solvent removed by rotary evaporation. The product was dissolved in minimal acetonitrile, flash precipitated in 150 mL diethylether, and collected by vacuum filtration. Yield: 110 mg, 0.152 mmol, 21 %. $E_{1/2}$ (V. vs. Ag/AgCl): -0.83, -1.00, -1.65.

$[Ru(bpy)_2(bpm)](PF_6)_2$. The synthesis of $[Ru(bpy)_2(bpm)](PF_6)_2$ was a modification of a previously published procedure.[10] $Ru(bpy)_2Cl_2$ (250 mg, 0.520 mmol) and 2,2'-bipyrimidine (326 mg, 2.06 mmol) were heated at reflux in 30 mL 2:1 EtOH/H_2O under argon for 12 hours during which time the reaction mixture turned a reddish color. The reaction was monitored by UV-vis spectroscopy. The crude product was precipitated as the hexafluorophosphate salt by adding the reaction solution to 100 mL saturated aqueous KPF_6. The precipitate was collected by vacuum filtration and air dried. Purification was achieved using alumina chromatography with 2:1 toluene/acetonitrile eluent. The first, red, product band was collected and the solvent removed by rotary evaporation. The product was dissolved in minimal acetonitrile, flash precipitated in diethylether, and collected by vacuum filtration. Yield: 310 mg, 0.360 mmol, 69 %. $E_{1/2}$ (V. vs. Ag/AgCl): 1.41, -1.01, -1.47.

$[(bpy)_2Ru(bpm)Ru(bpy)_2](PF_6)_4$. The synthesis of $[(bpy)_2Ru(bpm)Ru(bpy)_2](PF_6)_4$ was a modification of a previously published procedure.[10] $Ru(bpy)_2Cl_2$ (250 mg, 0.520 mmol) and 2,2'-bipyrimidine (41 mg, 0.26 mmol) were heated at reflux in 30 mL 2:1 EtOH/H_2O under argon for 7 hours. The crude product was precipitated as the hexafluorophosphate salt by adding the reaction solution to 100 mL saturated aqueous KPF_6. The precipitate was collected by vacuum filtration and air dried. Purification was achieved using LH 20 size exclusion chromatography with 2:1 EtOH/acetonitrile eluent. The first, green product band was collected and the solvent removed by rotary evaporation. The product was dissolved in minimal acetonitrile, flash precipitated in 150 mL diethylether, and collected by vacuum filtration. Yield: 160 mg, 0.102 mmol, 39 %. $E_{1/2}$ (V vs. Ag/AgCl): 1.80, 1.62, -0.37, -1.05.

$\{[(bpy)_2Ru(bpm)]_2IrCl_2\}(PF_6)_5$. $Ru(bpy)_2Cl_2$ (74 mg, 0.15 mmol) and $[Ir(bpm)_2Cl_2](PF_6)$ (37 mg, 0.051 mmol) were heated at reflux in 20 mL 2:1 EtOH/H_2O under argon for four days. The reaction mixture was cooled to room temperature and added to 80 mL sat. KPF_6 solution to induce precipitation. The precipitate was collected by vacuum filtration. The crude product was purified using LH 20 size exclusion chromatography with 2:1 EtOH/acetonitrile as the mobile phase. The first, brown band was followed by two closely

spaced green bands and an orange band. The first green band was collected and the solvent removed by rotary evaporation. The pure product was dissolved in minimal acetonitrile, flash precipitated in diethylether, and collected by vacuum filtration. This difficult separation led to a low yield of highly purified product. Yield: 28 mg, 0.013 mmol, 26%.

$E_{1/2}$ (V. vs. Ag/AgCl): 1.72, -0.11, -0.25, -0.95, -1.09.

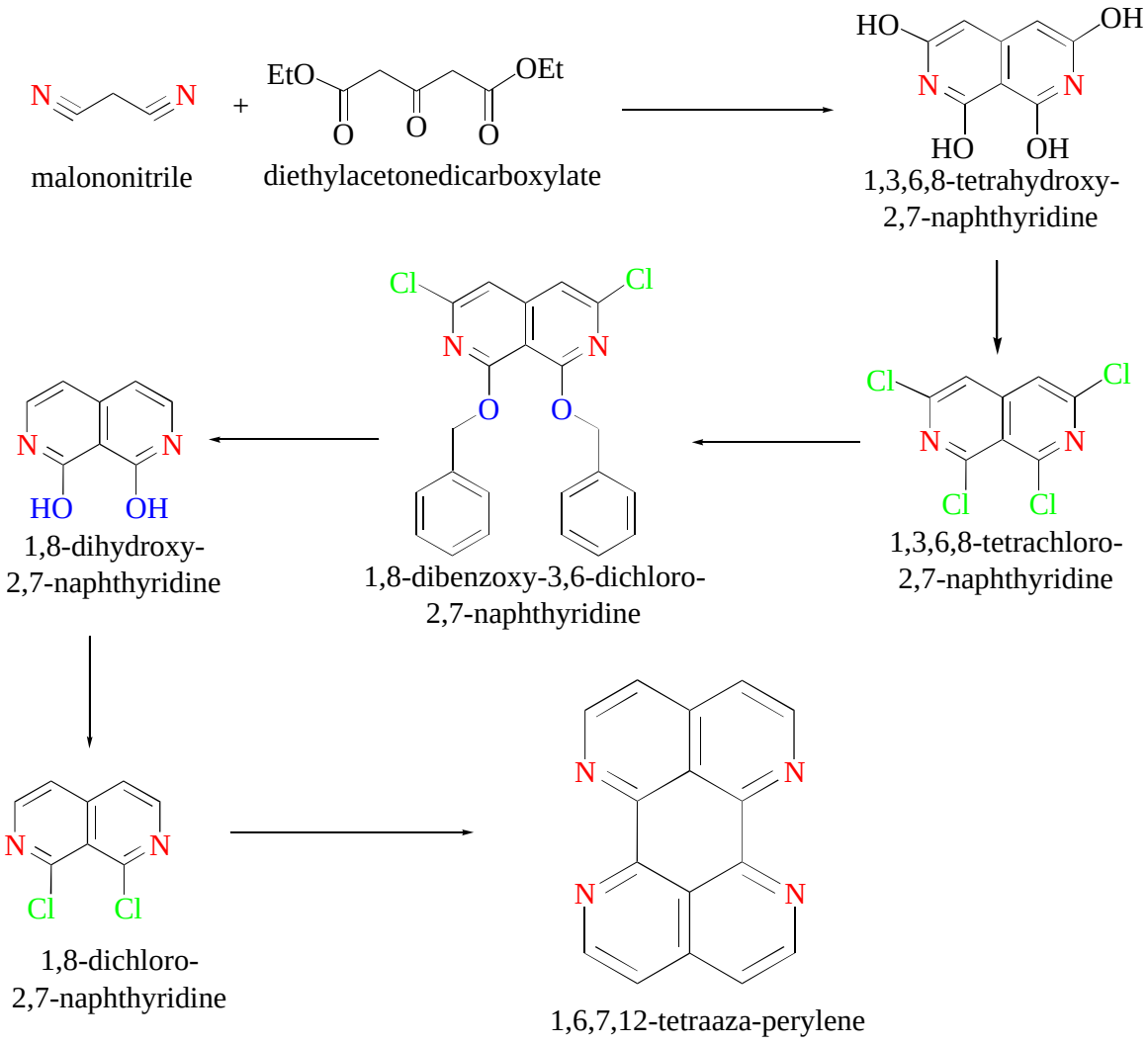

Figure 2.3 Overview of synthetic scheme for 1,6,7,12-tetraazaperylene.

1,6,7,12-Tetraazaperylene. An overview of the proposed synthetic route to 1,6,7,12-tetraazaperylene is shown in Figure 2.3. The principal reaction step is the coupling of the 1,8-dichloro-2,7-naphthyridine.

1,3,6,8-tetrahydroxy-2,7-naphthyridine. The synthesis of 1,3,6,8-tetrahydroxy-2,7-naphthyridine was a modification of a previously published procedure.[55] Malononitrile (1.1 g, 17 mmol), diethylacetonedicarboxylate (3.0 g, 15 mmol), and four drops diethylamine (dried over Na) were stirred in 25 mL dry ethanol for 48 hours under argon. The ethanol was removed under vacuum to yield a yellow oil. A 12 M H_2SO_4 solution (20 mL) was added and the reaction mixture brought to 110° C for 10 minutes. The reaction mixture was cooled to RT, added to 60 mL water, and filtered to yield a pale yellow solid. The product was washed with 75 mL water and 75 mL ethanol. Yield: 1.87 g, 9.63 mmol, 64%. Elemental analysis did not give satisfactory results probably due to water in the sample. (see Results and Discussion). Elemental analysis: C 49.49, H 3.11, N 14.43 (calc.), C 41.09, H 4.86, N 10.82 (found).

1,3,6,8-tetrachloro-2,7-naphthyridine. The synthesis of 1,3,6,8-tetrachloro-2,7-naphthyridine was a modification of previous methods.[55,56] 1,3,6,8-tetrahydroxy-2,7-naphthyridine (1.0 g, 5.2 mmol) and phosphoryl chloride (10 mL) were heated in a closed reaction tube at 180° C for 24 hours. The reaction mixture was cooled to RT, poured onto 150 g ice, and then made alkaline with K_2CO_3. The precipitate was collected by vacuum filtration. The crude product was obtained from the precipitate by extracting with diethylether using a Soxlet extractor for 24 hours. Removal of the diethylether by rotary evaporation gave a orange/yellow solid. Sublimation under vacuum at 130° C yielded a white powder. Yield : 0.68 g, 2.5 mmol, 48 %. m.p. 157-159° (157 - 161° lit. value). Elemental analysis: C 35.86, H 0.75, N 10.46, Cl 52.93 (calc.), C 35.88, H 0.73, N 10.28, Cl 53.29 (found). ^{1}H NMR: 7.55 (s). ^{13}C NMR: 118.108, 118.782, 147.166, 148.438, and 150.694 ppm.

Table 10. Electron Ionization Mass Spectral Data For 1,3,6,8-tetrachloro-2,7-naphthyridine.[a]

m/z	rel. abund. (found)	rel. abund. (calc.)
266	86	77
267	12	7
268	100	100
269	13	10
270	48	49
271	7	5
272	11	11

[a] Using *m*-nitrobenzyl alcohol as matrix.

1,8-dibenzoxy-3,6-dichloro-2,7-naphthyridine. 1,3,6,8-tetrachloro-2,7-naphthyridine (1.00 g, 3.73 mmol), benzyl alcohol (6.73 g, 62.2 mmol), K_2CO_3 (4.00 g, 28.9 mmol), and DMF (43 mL) were stirred under Ar at 60° C for 9 hours. The DMF was removed under vacuum at 60° C. Two 50 mL portions of benzene were added to the reaction mixture to dissolve the crude product and decanted off. The benzene portions were washed with water to remove any remaining DMF. The benzene was removed by rotary evaporation. Purification was achieved using silica gel column chromatography, 1:1 benzene/hexanes mobile phase. Elutions were checked by silica gel TLC, 1:1 benzene/hexanes mobile phase. Spots on the TLC plate were illuminated with a hand-held UV light. The first, product band was collected and the solvent removed by rotary evaporation. Yield: 1.10 g, 2.67 mmol, 72%. ^{1}H NMR: 5.54(s), 6.98(s), 7.28 - 7.48(mult). ^{13}C NMR (^{1}H coupled): 69.44(t), 102.44(s), 110.93(d), 127.79(d), 127.99(d), 128.35(d), 135.81(s), 147.95(s), 148.69(s), 161.00(s).

Table 11. Electron Ionization Mass Spectral Data For 1,8-dibenzoxy-3,6-dichloro-2,7-naphthyridine.[a]

m/z	rel. abund. (found)	rel. abund. (calc.)
410	100	100
411	30	25
412	56	68
413	16	17
415	4	3

[a] Using *m*-nitrobenzyl alcohol as matrix.

1,8-dihydroxy-2,7-naphthyridine. 1,8-dibenzoxy-3,6-dichloro-2,7-naphthyridine (400 mg, 0.980 mmol), potassium acetate (1.58 g, 16.1 mmol), methanol (60 mL), and 10% Pd/C (100 mg) were stirred under H_2 until the theoretical amount of hydrogen was taken up (3.92 mmol, 88.0 mL). The reaction mixture was filtered to remove the Pd/C catalyst and the methanol was removed under vacuum. Yield: 100 mg, 0.617 mmol, 63 %. The product was generally used directly in the synthesis of 1,8-dichloro-2,7-naphthyridine without characterization. ^{1}H NMR in MeOD showed doublets at 7.95 and 9.00 ppm and a large singlet at 6.41 ppm.

Table 12. Electron Ionization Mass Spectral Data For 1,8-dihydroxy-2,7-naphthyridine.[a]

m/z	rel. abund. (found)	rel. abund. (calc.)
162	100	100
163	10	10
164	3	1

[a] Using *m*-nitrobenzyl alcohol as matrix.

1,8-dichloro-2,7-naphthyridine. 1,8-dihydroxy-2,7-naphthyridine (100 mg, 0.617 mmol) and 20 mL $POCl_3$ were heated in a sealed reaction tube at 180° C for 36 hours. The reaction was cooled to room temperature, the reaction solution was poured onto 150 mL ice and the mixture was made alkaline with K_2CO_3. The precipitate was filtered by vacuum. The crude product was extracted from the precipitate with diethylether using a Soxlet extractor. Purification was achieved using silica gel column chromatography, 1:1 benzene/hexanes

mobile phase. Elutions were checked by spotting a silica gel TLC plate, developing in 1:1 benzene/hexanes, and illuminating with a hand-held UV light. Yield: 20 mg, 0.10 mmol, 17 %. ^{1}H NMR 8.47 (d), 7.59 (d). ^{13}C NMR 119.78, 120.93, 144.62, 145.54, 150.00.

Table 13. Electron Ionization Mass Spectral Data For 1,8-dichloro-2,7-naphthyridine.[a]

m/z	rel. abund. (found)	rel. abund. (calc.)
198	100	100
199	8	9
200	60	65
201	5	6
202	10	11
203	1	1

[a] Using *m*-nitrobenzyl alcohol as matrix.

Chapter 3 Results and Discussion

Ru and Os complexes containing the tridentate bridging ligand tpp

Synthesis. The synthesis of these light absorber - electron donor bimetallic systems bridged by tpp follows a building block approach where the complexes are assembled step by step by alternately adding a ligand and then a metal center. As an example, the synthetic scheme for $[(tpy)Ru(tpp)Ru(tpp)](PF_6)_4$ is shown in Figure 3.1. By following this step by step approach, the exact nature of each component can be chosen. Since the stereochemistry of these tpp bridged bimetallic complexes is defined, purification is simplified by not having to separate geometric isomers.

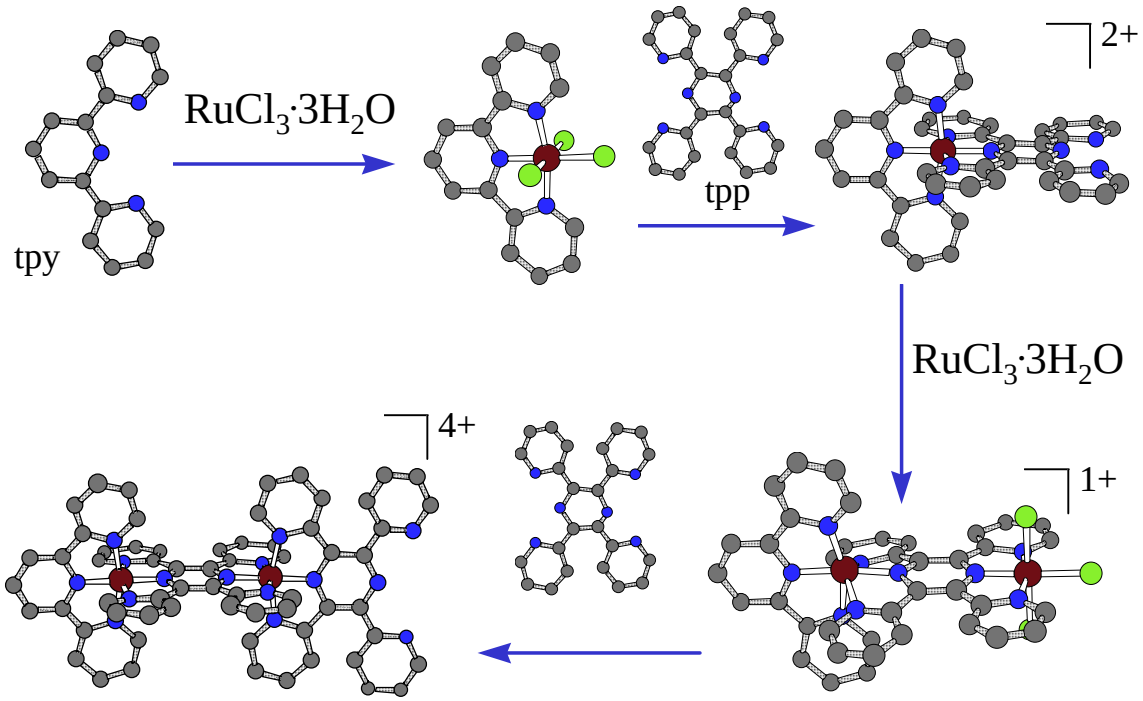

Figure 3.1 Synthetic scheme for $[(tpy)Ru(tpp)Ru(tpp)](PF_6)_4$.

In the following discussion of the series of bis-ruthenium complexes, a bold font will be used to indicate the ruthenium coordinated to tpy and tpp and a normal font will be used to indicate the other ruthenium, $[(tpy)\mathbf{Ru}(tpp)RuL_3]^{n+}$. In complexes that have two tpp ligands, a bold font will be used for the bridging tpp, $[(tpy)M(\mathbf{tpp})Ru(tpp)]^{4+}$.

Electrochemistry. The electrochemistry of $[(tpy)Ru(CH_3CN)_3](PF_6)_2$, $[Ru(tpy)(tpp)](PF_6)_2$, $[Os(tpy)(tpp)](PF_6)_2$, $[(tpy)Ru(tpp)Ru(tpy)](PF_6)_4$, $[(tpy)Ru(tpp)Ru(tpp)](PF_6)_4$, $[(tpy)Os(tpp)Ru(tpp)](PF_6)_4$, $[(tpy)Os(tpp)RuCl_3](PF_6)$, and $[(tpy)Ru(tpp)RuCl_3](PF_6)$ is summarized in Table 14.

The electrochemical behavior of these complexes is characterized by metal based oxidations and ligand based reductions. In $[(tpy)Ru(CH_3CN)_3]^{2+}$, the oxidation is ruthenium based

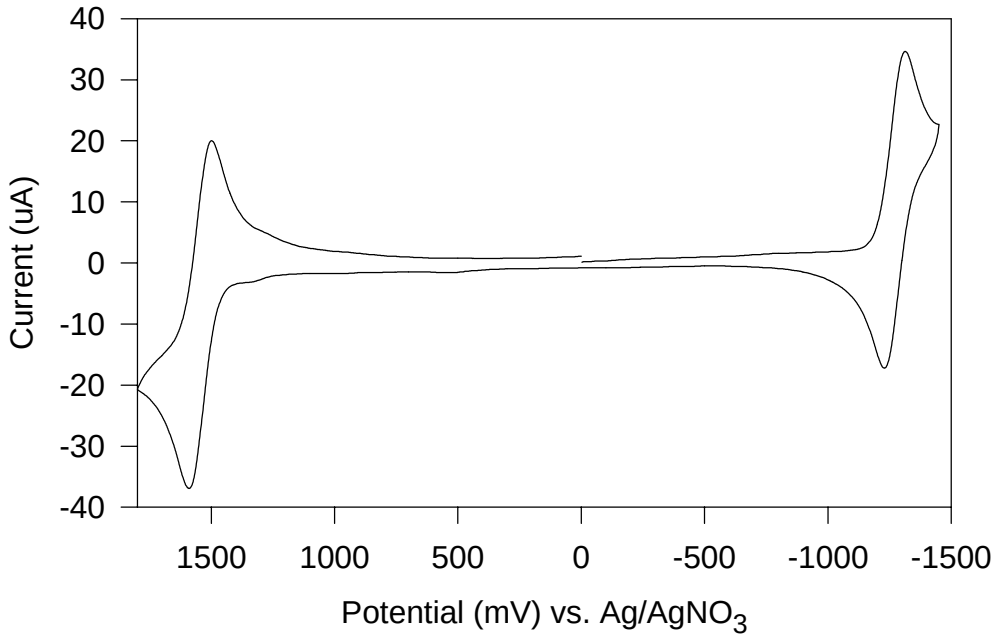

Figure 3.2 Cyclic voltammogram of $[(tpy)Ru(CH_3CN)_3](PF_6)_2$.

and the reduction is tpy based (see Figure 3.2). For $[M(tpy)(tpp)]^{2+}$ ($M = Ru^{II}$ or Os^{II}), the oxidation is assigned as $M^{II/III}$, the first reduction is assigned as $tpp^{0/-}$, and the second reduction is assigned as $tpy^{0/-}$. The $tpp^{0/-}$ couple occurs prior to the $tpy^{0/-}$ due to the larger π system of tpp as a result of the two extra pyridyl rings on tpp as well as the extra electron accepting character of the pyrazine ring. This results in tpp having a substantially lower energy π^* orbital than tpy. The osmium based oxidation occurs at a less positive potential than the ruthenium based process consistent with osmium having higher energy $d\pi$ orbitals.

Upon formation of a tpp bridged bimetallic complex, the bridging tpp becomes easier to reduce due to a stabilization of the π^* orbital induced by the coordination of the second electron deficient metal center. In $[(tpy)Ru(tpp)Ru(tpy)]^{4+}$, the first two reductions are assigned as $tpp^{0/-}$ and $tpp^{-/2-}$, occurring before the $tpy^{0/-}$ reduction of both terminal tpy ligands. The presence of a $tpp^{-/2-}$ couple prior to the reduction of the terminal tpy ligands is indicative of the bimetallic formulation of this complex. Oxidatively, it is notable that the two equivalent ruthenium centers oxidize at different potentials indicating electronic coupling of the two metal centers through the bridging tpp ligand. In these tpp bridged bimetallic complexes, the order of oxidation of the metal centers is determined by the metal used and its coordination environment. The spectroelectrochemical studies will serve to solidify the electrochemical assignments of the order of oxidation of the metal centers. In the complex $[(tpy)Ru(tpp)RuCl_3]^+$, the three chlorides donate significant electron density to the ruthenium bound to the three chlorides and tpp. The first oxidation in $[(tpy)Ru(tpp)RuCl_3]^+$ is therefore assigned to this ruthenium center. In the complex $[(tpy)Ru(tpp)Ru(tpp)]^{4+}$, the ruthenium bound to tpy and tpp is assigned as the first oxidation since tpp is a better π acceptor that tpy which makes the $(tpp)Ru^{II}(tpp)$ metal center less electron rich than the $(tpy)Ru^{II}(tpp)$ metal center. The complex $[(tpy)Ru(tpp)Ru(CH_3CN)_3]^{4+}$ displays two well separated reversible metal oxidations and two well behaved reversible reductions (see Figure 3.3). The ligand tpy

is more electron withdrawing than three acetonitrile ligands and the first oxidation is assigned to the ruthenium center coordinated to tpp and the three acetonitriles.

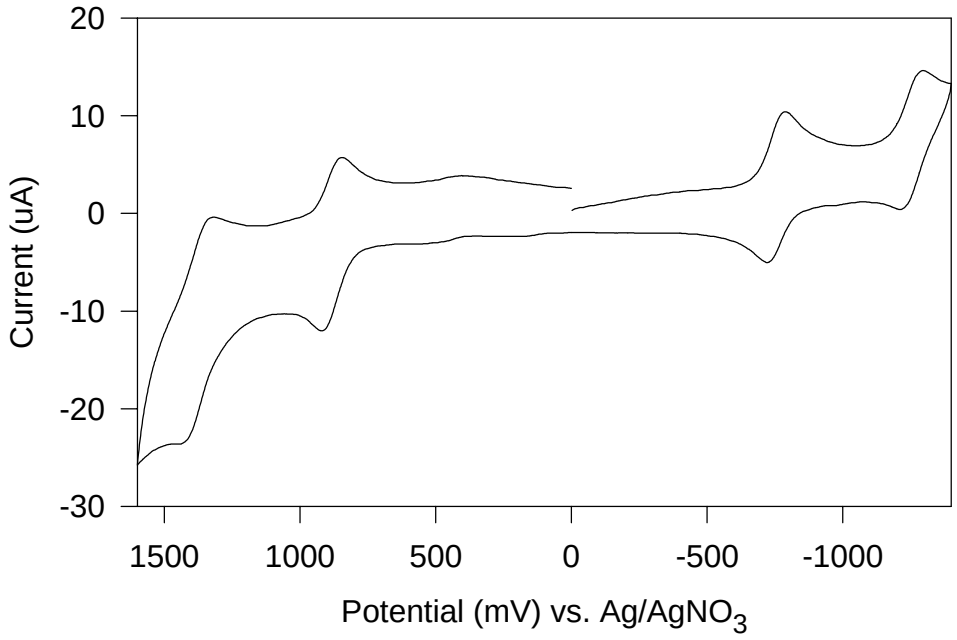

Figure 3.3 Cyclic voltammogram of $[(tpy)Ru(tpp)Ru(CH_3CN)_3](PF_6)_4$.

Substitution of two chlorides in $[(tpy)Ru(tpp)RuCl_3]^+$ by dpq gives $[(tpy)Ru(tpp)Ru(dpq)Cl]^{3+}$. This complex displays two well separated reversible metal oxidations and two well behaved reversible reductions (see Figure 3.4). Further reduction leads to adsorption onto the electrode surface and the observation of a desorption spike. The first oxidation, at 0.87 V, represents the oxidation of the Ru center bound to the chloride ligand due to the π accepting ability of the polyazine ligands on the $(tpy)Ru^{II}(tpp)$ moiety leading to a less electron rich metal relative to the $(tpp)Ru^{II}(dpq)Cl$ metal center. The (tpy)Ru(tpp) metal oxidation follows at 1.36 V, consistent with its coordination environment.

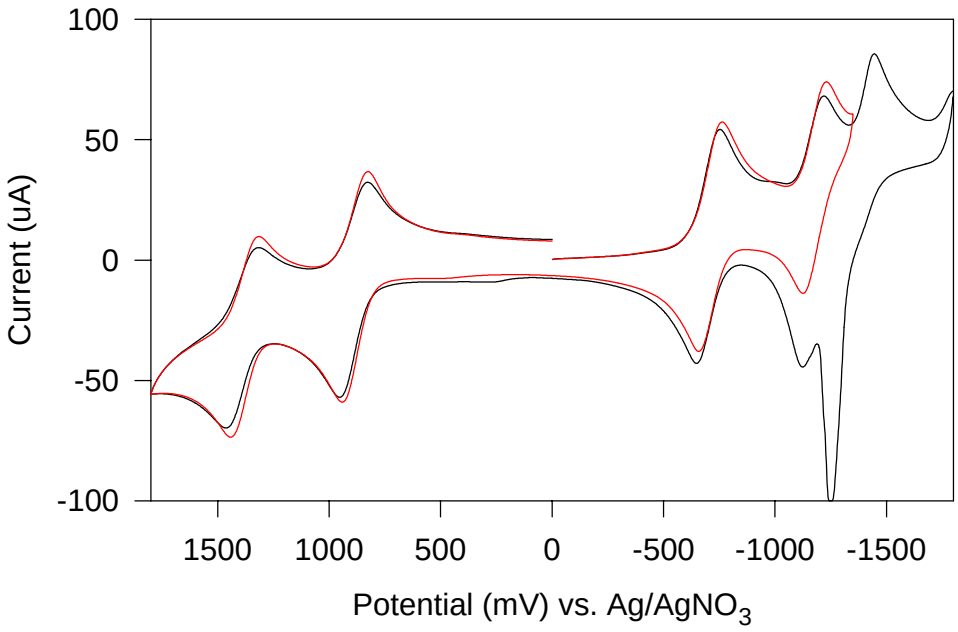

Figure 3.4 Cyclic voltammogram of [(tpy)Ru(tpp)Ru(dpq)Cl](PF$_6$)$_3$.

The first reduction at -0.72 V represents the reduction of the bridging tpp ligand, i.e. tpp$^{0/-}$. The tpp ligand is expected to display a second reversible reduction, tpp$^{-/2-}$, ca. 500 mV negative of the first reduction process and this occurs at -1.19 V. The third reduction should represent the dpq$^{0/-}$ couple since the dpq ligand has lower energy π^* orbitals than tpy. This redox couple appears at -1.42 V. The tpy$^{0/-}$ wave is expected to follow but is obscured by adsorption onto the electrode surface.

In these tpp bridged bimetallic complexes designed to be used in larger systems for photoinitiated electron collection, it is important to know nature of the redox processes since they give information about the nature and energy of the HOMO and LUMO in these systems. In these tpp bridged bimetallic complexes, it was found that the nature of the first oxidation

Table 14. Electrochemical Data for a Series of Osmium and Ruthenium Complexes Incorporating the Tridentate Bridging Ligand tpp.[a]

Complex	oxidations	reductions	reference
$[(tpy)Ru(CH_3CN)_3]^{2+}$	+1.54 $Ru^{II/III}$	-1.28 $tpy^{0/-}$	
$[(tpy)Ru(tpp)]^{2+}$	+1.40 $Ru^{II/III}$	-0.97 $tpp^{0/-}$ -1.38 $tpy^{0/-}$ -1.60 $tpp^{-/2-}$	22, 23, 27c
$[(tpy)Os(tpp)]^{2+}$	+1.06 $Os^{II/III}$	-0.97 $tpp^{0/-}$ -1.39 $tpy^{0/-}$	27a, 51, 53
$[(tpy)Ru(tpp)Ru(tpy)]^{4+}$	+1.44 $Ru^{II/III}$ +1.76 $Ru^{II/III}$	-0.35 $tpp^{0/-}$ -0.84 $tpp^{-/2-}$ -1.30 $2tpy^{0/-}$	22, 23, 51
$[(tpy)\mathbf{Ru}(\mathbf{tpp})Ru(tpp)]^{4+}$	+1.51 $\mathbf{Ru}^{II/III}$ +1.86 $Ru^{II/III}$	-0.30 $\mathbf{tpp}^{0/-}$ -0.82 $\mathbf{tpp}^{-/2-}$ -1.10 $tpp^{0/-}$	27a, 51
$[(tpy)Os(\mathbf{tpp})Ru(tpp)]^{4+}$	+1.17 $Os^{II/III}$ +1.81 $Ru^{II/III}$	-0.36 $\mathbf{tpp}^{0/-}$ -0.81 $\mathbf{tpp}^{-/2-}$ -1.07 $tpp^{0/-}$	27a
$[(tpy)\mathbf{Ru}(tpp)RuCl_3]^{+}$	+0.73 $Ru^{II/III}$ +1.61 $\mathbf{Ru}^{II/III}$	-0.60 $tpp^{0/-}$ -1.10 $tpp^{-/2-}$ -1.50 $tpy^{0/-}$	27a
$[(tpy)Os(tpp)RuCl_3]^{+}$	+0.66 $Ru^{II/III}$ +1.32 $Os^{II/III}$	-0.59 $tpp^{0/-}$ -1.07 $tpp^{-/2-}$ -1.47 $tpy^{0/-}$	27a
$[(tpy)\mathbf{Ru}(tpp)Ru(CH_3CN)_3]^{4+}$	+1.30 $Ru^{II/III}$ +1.80 $\mathbf{Ru}^{II/III}$	-0.30 $tpp^{0/-}$ -0.80 $tpp^{-/2-}$ -1.67 $tpy^{0/-}$	27b
$[(tpy)\mathbf{Ru}(tpp)Ru(dpq)Cl]^{3+}$	+0.87 $Ru^{II/III}$ +1.36 $\mathbf{Ru}^{II/III}$	-0.72 $tpp^{0/-}$ -1.19 $tpp^{-/2}$ -1.42 $dpq^{0/-}$	27c

[a] tpp = 2,3,5,6-tetrakis(2-pyridyl)pyrazine, tpy = 2,2',6',2"-terpyridine, and dpq = 2,3-bis(2-pyridyl)benzoquinoxaline

[b] Potentials reported in CH_3CN solution with 0.1 M TBAH and reported versus Ag/AgCl (0.29V vs. NHE).

was dependent upon the metal and the ligands used. In most cases, the first oxidation was centered on ruthenium coordinated to tpp and (LLL), $(tpp)Ru^{II}(LLL)$, where LLL = Cl_3, $(CH_3CN)_3$, or (dpq)Cl . However, in the case of the complexes with a terminal tpp, $[(tpy)\mathbf{Ru}(\mathbf{tpp})Ru(tpp)]^{4+}$ and $[(tpy)Os(\mathbf{tpp})Ru(tpp)]^{4+}$, the first oxidation in centered on the metal coordinated to tpy and tpp, $(tpy)M^{II}(tpp)$, where M = Ru or Os. In all the complexes the first reduction in centered on the bridging tpp due to coordination to two metal centers. When these bimetallic complexes are incorporated into larger multimetallic systems, the nature of the first oxidation and/or the first reduction could change when the terminal tpp or dpq takes on the role of a bridging ligand.

Electronic Absorption Spectroscopy. The spectroscopy of ruthenium and osmium based complexes with polypyridyl ligands is characterized by intense ligand $\pi \rightarrow \pi^*$ and $n \rightarrow \pi^*$ transitions in the ultraviolet and metal($d\pi$) $\rightarrow$ ligand(π^*) charge transfer transitions in the visible. Osmium based systems typically have spectroscopy similar to their ruthenium analogs with slight red shifts of the MLCT transitions due to the higher energy $d\pi$ orbitals of osmium. The osmium complexes also possess tails to the red of the lowest lying ^{1}MLCT and these represent the more intense ^{3}MLCT bands expected for the osmium based systems.

The electronic absorption spectrum of $[(tpy)Ru(CH_3CN)_3](PF_6)_2$ is shown in Figure 3.5. The lowest energy transition at 436 nm is expected to be a Ru($d\pi$) $\rightarrow$ tpy(π^*) CT transition. From comparison with other ruthenium polypyridyl complexes, the intense transitions in the UV region of the spectrum can be assigned as tpy $\pi \rightarrow \pi^*$ transitions.

The electronic absorption spectra of $[(tpy)Ru(tpp)](PF_6)_2$ and $[(tpy)Os(tpp)](PF_6)_2$ have been previously reported.[22,23,51] The lowest energy transitions at 474 nm and 468 nm, respectively, have been assigned as overlapping M($d\pi$) $\rightarrow$ tpp(π^*) and M($d\pi$) $\rightarrow$ tpy(π^*) CT transitions with the M($d\pi$) $\rightarrow$ tpp(π^*) CT transition occurring at slightly lower energy. The intense

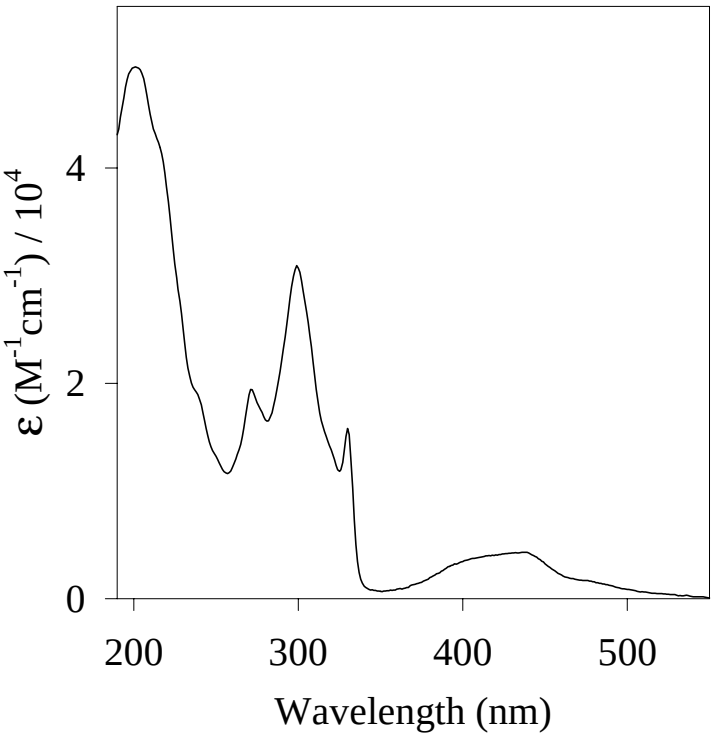

Figure 3.5 Electronic absorption spectrum of $[(tpy)Ru(CH_3CN)_3](PF_6)_2$ in acetonitrile.

transitions in the UV region have been assigned as tpy and tpp based $\pi \rightarrow \pi^*$ and $n \rightarrow \pi^*$ transitions.

The electronic absorption spectra of $[(tpy)M(tpp)RuCl_3](PF_6)$, where M = Os or Ru, have been reported previously but are presented here for discussion (see Figure 3.6).[27a] For $[(tpy)\mathbf{Ru}(tpp)RuCl_3](PF_6)$, the transition at 470 nm has been assigned as a **Ru**$(d\pi) \rightarrow tpy(\pi^*)$ CT transition. Formation of the bimetallic lowers the energy of the tpp π^* orbital which lowers the **Ru**$(d\pi) \rightarrow tpp(\pi^*)$ CT transition from ca. 470 nm to 525 nm. The three chlorides

donate significant electron density to the ruthenium center and the lowest energy transition at 612 nm is assigned as a Ru(dπ) → tpp(π*) CT transition. The intense transitions in the UV region have been assigned as tpp and tpy based π → π* and n → π* transitions. The electronic absorption spectrum of [(tpy)Os(tpp)$RuCl_3$](PF_6) is similar to the bis-ruthenium complex with a shift to lower energy for the lowest energy Ru(dπ) → tpp(π*) CT transition.

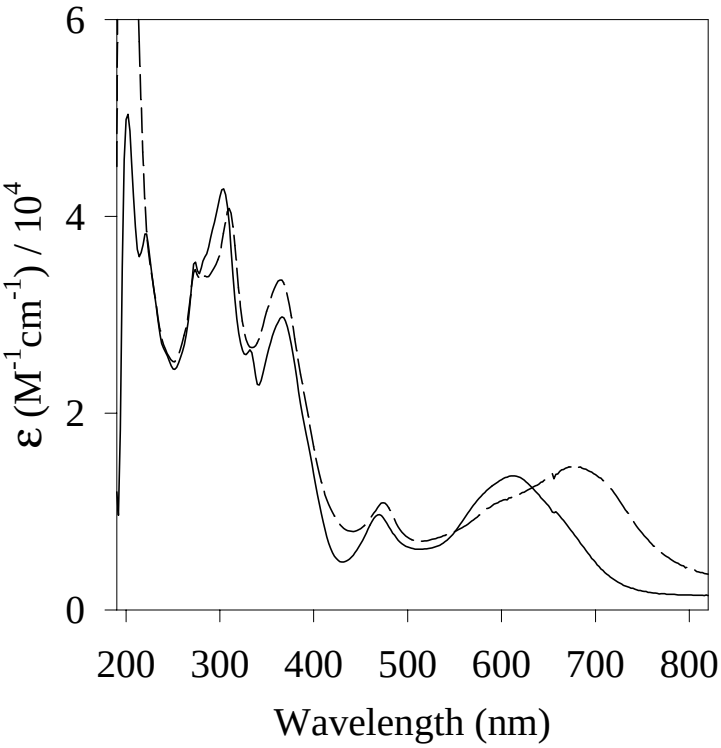

Figure 3.6 Electronic absorption spectrum of [(tpy)M(tpp)$RuCl_3$](PF_6) where M = Ru and Os. —— [(tpy)**Ru**(tpp)$RuCl_3$](PF_6), ----- [(tpy)Os(tpp)$RuCl_3$](PF_6).

The electronic absorption spectra of [(tpy)M(tpp)Ru(tpp)]$(PF_6)_4$, where M = Os or Ru, have been reported previously but are presented here for discussion (see Figure 3.7).[27a] In the complex [(tpy)**Ru**(**tpp**)Ru(tpp)]$(PF_6)_4$, the band centered at 548 nm has been assigned as overlapping Ru(dπ) $\rightarrow$ **tpp**(π*) and **Ru**(dπ) $\rightarrow$ **tpp**(π*) CT transitions. The peak at 360 nm has been assigned as overlapping Ru(dπ) $\rightarrow$ tpy(π*) and **Ru**(dπ) $\rightarrow$ tpp(π*) CT transitions. The intense transitions in the ultraviolet region were assigned as ligand based $\pi \rightarrow \pi^*$ and $n \rightarrow \pi^*$ transitions. The complex [(tpy)Os(**tpp**)Ru(tpp)]$(PF_6)_4$ shows nearly identical electronic absorption spectroscopy as the bis ruthenium complex with a low energy tail due to

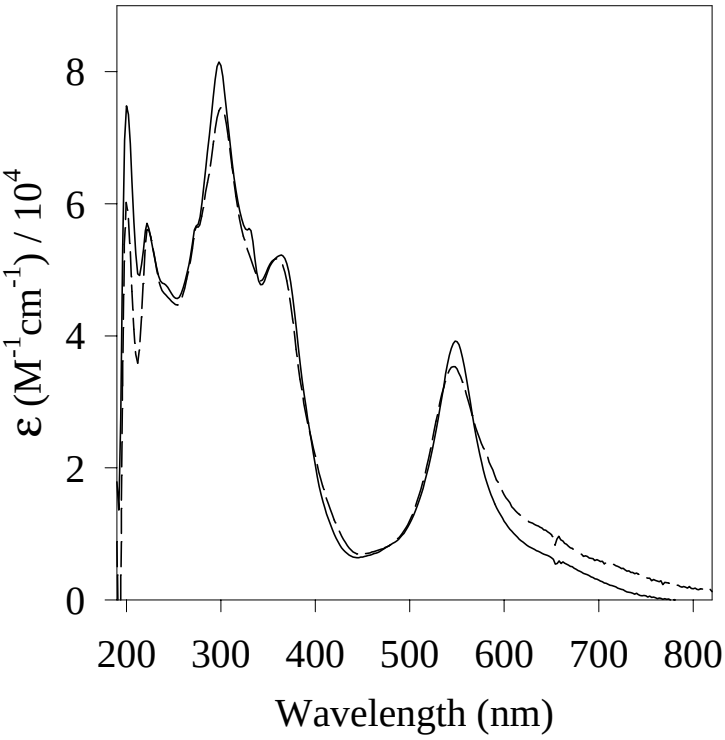

Figure 3.7 Electronic absorption spectrum of [(tpy)M(tpp)Ru(tpp)]$(PF_6)_4$ where M = Ru and Os. —— [(tpy)**Ru**(**tpp**)Ru(tpp)]$(PF_6)_4$, ----- [(tpy)Os(**tpp**)Ru(tpp)]$(PF_6)_4$.

stronger spin orbit coupling in the case of the osmium complex.

The electronic absorption spectrum of [(tpy)**Ru**(tpp)Ru(dpq)Cl]$(PF_6)_3$ is shown in Figure 3.8. The peak centered at 460 nm can be assigned as a **Ru**(dπ) $\rightarrow$ tpy(π*) CT transition. The peak centered at 584 can be assigned as overlapping **Ru**(dπ) $\rightarrow$ tpp(π*)and Ru(dπ) $\rightarrow$ tpp(π*) CT transitions. The Ru(dπ) $\rightarrow$ dpq(π*) CT transition would be expected to occur at slightly lower energy.

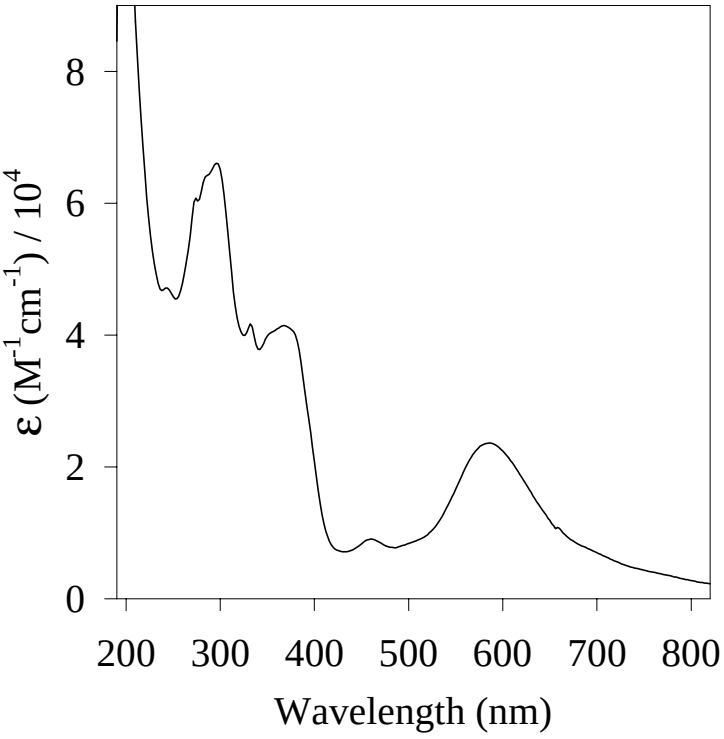

Figure 3.8 Electronic absorption spectrum of [(tpy)**Ru**(tpp)Ru(dpq)Cl]$(PF_6)_3$.

The electronic absorption spectrum of [(tpy)**Ru**(tpp)Ru$(CH_3CN)_3$]$(PF_6)_4$ is shown in Figure 3.9. The lowest energy transition can be assigned as overlapping Ru(dπ) $\rightarrow$ tpp(π*) and **Ru**(dπ) $\rightarrow$ tpp(π*) CT transitions. The peak centered at 464 nm can be assigned as a

Ru(dπ) → tpy(π*) charge transfer transition as this transition would be expected to stay at approximately the same energy as the Ru(dπ) → tpy(π*) transition in [(tpy)Ru(tpp)]$(PF_6)_2$. The intense transition at 376 nm can be assigned as a tpp π → π* transition, red shifted from the energy of the same transition in [(tpy)Ru(tpp)]$(PF_6)_2$.

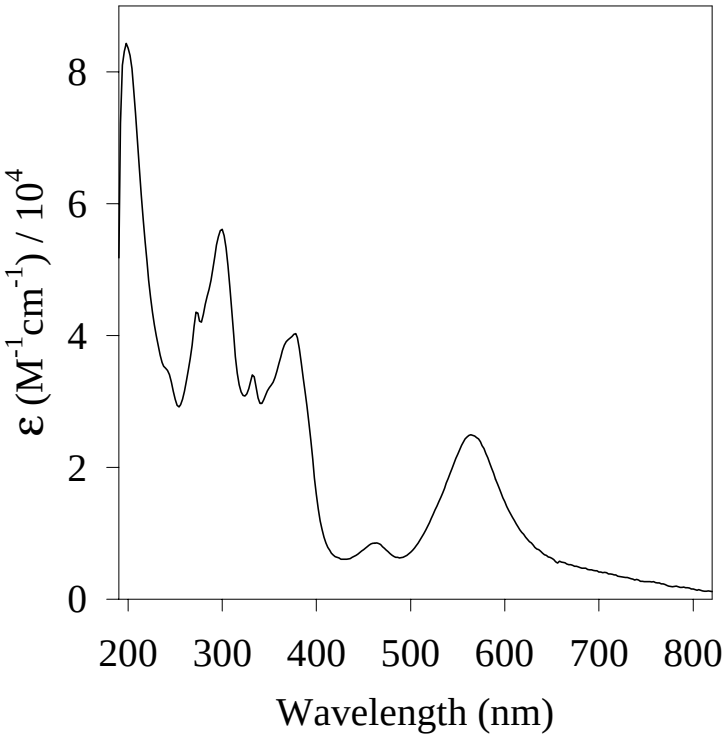

Figure 3.9 Electronic absorption spectrum of [(tpy)**Ru**(tpp)Ru$(CH_3CN)_3$]$(PF_6)_4$.

The electronic absorption spectroscopy for these tpp based complexes is summarized in Table 15.

Table 15. Electronic Absorption Spectroscopy of a Series of Osmium and Ruthenium Complexes Incorporating the Tridentate Bridging Ligand tpp.[a,b]

Complex	λ_{max} (nm)	$\varepsilon(M^{-1}cm^{-1})/10^4$	assignment	reference
$[Ru(tpy)(CH_3CN)_3]^{2+}$	436	0.43	$Ru(d\pi) \rightarrow tpy(\pi^*)$ CT	[c]
$[Ru(tpy)(tpp)]^{2+}$	472		$Ru(d\pi) \rightarrow tpp(\pi^*)$ CT $Ru(d\pi) \rightarrow tpp(\pi^*)$ CT	22, 23, 51
	354		tpp ($\pi \rightarrow \pi^*$)	24
	328		tpp ($\pi \rightarrow \pi^*$)	24
	310		tpy ($\pi \rightarrow \pi^*$)	24
$[Os(tpy)(tpp)]^{2+}$	468		$Os(d\pi) \rightarrow tpp(\pi^*)$ CT $Os(d\pi) \rightarrow tpy(\pi^*)$ CT	51
	350		tpp ($\pi \rightarrow \pi^*$)	53
	324		tpp ($\pi \rightarrow \pi^*$)	53
$[(tpy)Ru(tpp)Ru(tpy)]^{4+}$	548		$Ru(d\pi) \rightarrow tpp(\pi^*)$ CT	22, 23, 51
$[(tpy)Ru(tpp)Ru(tpp)]^{4+}$	548	3.92	$Ru(d\pi) \rightarrow tpp(\pi^*)$ CT $Ru(d\pi) \rightarrow tpp(\pi^*)$ CT	27a, 51
	360	5.20	$Ru(d\pi) \rightarrow tpy(\pi^*)$ CT $Ru(d\pi) \rightarrow tpp(\pi^*)$ CT	27a
$[(tpy)Os(tpp)Ru(tpp)]^{4+}$	546	3.53	$Ru(d\pi) \rightarrow tpp(\pi^*)$ CT $Os(d\pi) \rightarrow tpp(\pi^*)$ CT	27a, 51
	360	5.17	$Os(d\pi) \rightarrow tpy(\pi^*)$ CT $Ru(d\pi) \rightarrow tpp(\pi^*)$ CT	27a
$[(tpy)Ru(tpp)RuCl_3]^{+}$	612	1.36	$Ru(d\pi) \rightarrow tpp(\pi^*)$ CT	27a, 51
	525	0.63	$Ru(d\pi) \rightarrow tpp(\pi^*)$ CT	
	468	0.97	$Ru(d\pi) \rightarrow tpy(\pi^*)$ CT	
	366	2.98	tpp ($\pi \rightarrow \pi^*$)	
$[(tpy)Os(tpp)RuCl_3]^{+}$	678	1.46	$Ru(d\pi) \rightarrow tpp(\pi^*)$ CT	27a, 51
	606	1.12	$Os(d\pi) \rightarrow tpp(\pi^*)$ CT	27a
	474	1.09	$Os(d\pi) \rightarrow tpy(\pi^*)$ CT	27a
	364	3.35	tpp ($\pi \rightarrow \pi^*$)	

[a] Spectra recorded in CH_3CN at RT

[b] tpp = 2,3,5,6-tetrakis(2-pyridyl)pyrazine, tpy = 2,2',6',2"-terpyridine

[c] New assignments based on this work

Table 15 (continued).

Complex	λ_{max} (nm)	$\varepsilon(M^{-1}cm^{-1})/10^4$	assignment	ref.
$[(tpy)Ru(tpp)Ru(CH_3CN)_3]^{4+}$	566	2.48	$Ru(d\pi) \rightarrow tpp(\pi^*)$	[c]
	526	1.35	$Ru(d\pi) \rightarrow tpp(\pi^*)$ CT	
	464	0.85	$Ru(d\pi) \rightarrow tpy(\pi^*)$ CT	
	376	4.02	tpp ($\pi \rightarrow \pi^*$)	
$[(tpy)Ru(tpp)Ru(dpq)Cl]^{3+}$	584	2.36	$Ru(d\pi) \rightarrow tpp(\pi^*)$ CT	[c]
	584		$Ru(d\pi) \rightarrow tpp(\pi^*)$ CT	
	565	2.09	$Ru(d\pi) \rightarrow dpq(\pi^*)$ CT	
	460	0.90	$Ru(d\pi) \rightarrow tpy(\pi^*)$ CT	
	376	4.08	tpp ($\pi \rightarrow \pi^*$)	

[a] Spectra recorded in CH_3CN at RT

[b] tpp = 2,3,5,6-tetrakis(2-pyridyl)pyrazine, tpy = 2,2',6',2"-terpyridine, and dpq = 2,3-bis(2-pyridyl)benzoquinoxaline

[c] New assignments based on this work

Spectroelectrochemistry

Spectroelectrochemistry is a technique that is used to probe the electrochemistry and electronic absorption spectroscopy of complexes that are stable in a variety of oxidation states.[28-33] In this experiment the complex is oxidized or reduced and the change in the electronic absorption spectrum is monitored. This oxidation or reduction results in dramatic changes in any transitions involving the orbital that is involved in the electrochemical process. Transitions involving the redox orbital typically shift out of the observable spectroscopic region. New transitions can appear as a result of a newly occupied orbital via reduction or a newly partially unoccupied orbital via oxidation. Minor shifts in transitions not involving the redox orbital can also occur. In the complexes studied, the metals can be oxidized and the polyazine ligands can be reduced. Oxidation of a metal will cause a dramatic shift in the energy of any MLCT transitions involving that metal, typically shifting them out of the UV-vis region of the spectrum. Metal oxidation will also tend to stabilize the π^* orbitals of the polyazine ligands coordinated to that metal, giving rise to slight red shifts in transitions

involving that acceptor orbital. The reduction of the polyazine ligands in this study; tpp, tpy, and dpq, results in the electron formally residing in the π* orbital of that ligand. This results in a dramatic shift in the energy of any MLCT transitions and ligand centered $\pi \rightarrow \pi^*$ transitions involving that ligand, shifting them out of the observable UV-vis region. Reduction of the ligand can also cause the appearance of new ligand $\pi^* \rightarrow \pi^*$ transitions, typically in the visible region of the spectrum.

The oxidative spectroelectrochemistry of $[Ru(tpy)(CH_3CN)_3]^{2+}$ is shown in Figure 3.10. Upon oxidation of the ruthenium metal center, the Ru (dπ) → tpy (π*) CT transition at 436 nm is lost along with the higher energy Ru (dπ) → tpy (π*) CT transition at 300 nm.

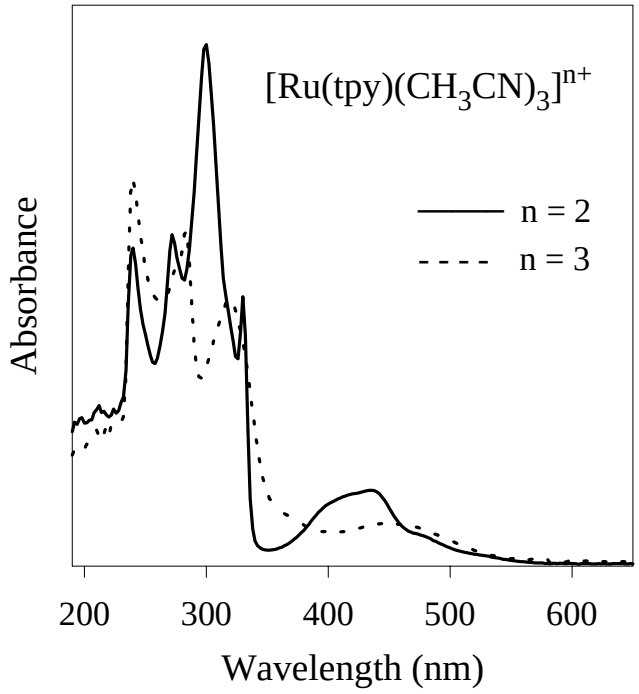

Figure 3.10 Oxidative spectroelectrochemistry of $[Ru(tpy)(CH_3CN)_3](PF_6)_2$.

The transition at 272 nm can be assigned as a tpy $\pi \rightarrow \pi^*$ transition and undergoes a slight red shift upon ruthenium oxidation due to stabilization of that tpy π^* orbital upon ruthenium oxidation. The new transition at 446 nm may represent a new tpy (π) $\rightarrow$ Ru ($d\pi$) ligand-to-metal charge transfer transition made possible by metal oxidation.

The spectroelectrochemistry of $[Ru(tpy)(tpp)]^{2+}$, shown in Figure 3.11, has been previously reported by our group but is presented here for more detailed analysis.[18] Upon oxidation of the ruthenium metal center, a number of spectroscopic changes are evident. The loss of the band centered at 472 nm upon oxidation of the Ru^{II} to Ru^{III} substantiates the previous assignment of this transition as overlapping Ru $\rightarrow$ tpy and Ru $\rightarrow$ tpp CT transitions.[18, 19] Oxidation of the ruthenium would also be expected to lower the energy of the tpp π^* orbitals

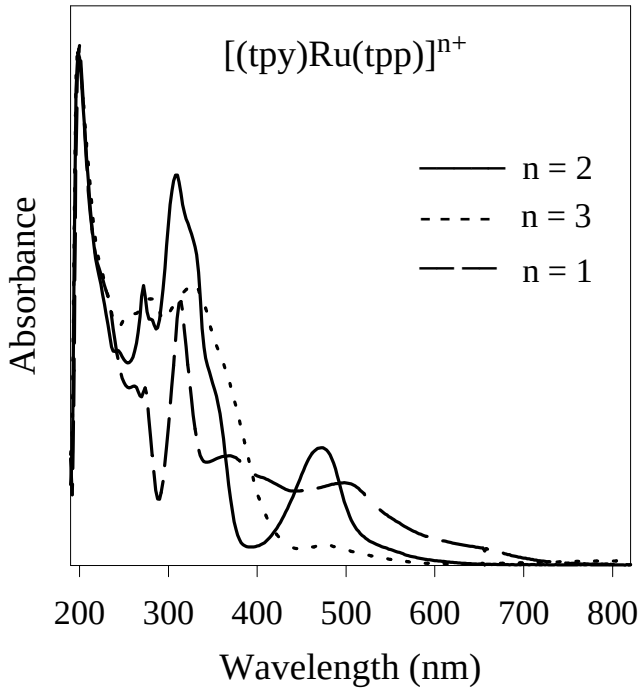

Figure 3.11 Spectroelectrochemistry of $[(tpy)Ru(tpp)](PF_6)_2$.

resulting in slight red shifts of the tpp $\pi \rightarrow \pi^*$ transitions. This effect is seen in the tpp $\pi \rightarrow \pi^*$ transitions at 328 nm and 354 nm. A peak at 310 nm is lost upon metal oxidation, consistent with a higher energy MLCT band in this region. This metal based oxidation is > 95% reversible under our conditions.

When $[Ru(tpy)(tpp)]^{2+}$ is reduced by one electron, one would expect that the added electron would reside formally on the lowest energy tpp π^* orbital. The loss of the transitions at 328 nm and 354 nm upon reduction of the complex supports the assignment of these transitions as tpp $\pi \rightarrow \pi^*$ based. Since the band at 472 nm represents overlapping Ru $\rightarrow$ tpy and Ru $\rightarrow$ tpp CT bands, this band should decrease in intensity upon tpp reduction due to the loss of the Ru $\rightarrow$ tpp CT component. Several new absorbances appear in the visible upon tpp reduction and can be attributed to new tpp $\pi^* \rightarrow \pi^*$ transitions. These new $\pi^* \rightarrow \pi^*$ based transitions obscure changes in this region. The transition at 310 nm can be assigned as a high energy Ru $\rightarrow$ tpy CT transition since oxidation of the ruthenium causes the loss of the transition while the transition remains when the tpp is reduced. A peak at 270 nm remains unchanged upon metal oxidation or tpp reduction and likely represents a higher energy tpy $\pi \rightarrow \pi^*$ band. The one electron reduced species was generated with > 75% reversibility.

The spectroelectrochemistry of $[Os(tpy)(tpp)]^{2+}$ is shown in Figure 3.12. It was possible to generate the one electron oxidized species $[Os(tpy)(tpp)]^{3+}$ with > 95 % reversibility. The one electron reduced species was electrogenerated with > 80 % reversibility. The spectroelectrochemistry of this osmium chromophore is virtually identical to that observed for the previously discussed ruthenium analog. Within the bis-tridentate framework, the spectroscopy of the ruthenium and osmium analogs is remarkably similar despite the fact that the osmium metal center is substantially easier to oxidize. The spectroelectrochemistry further illustrates this similarity showing that this phenomenon is true not only for the synthesized oxidation state but also for the one electron oxidized and reduced species. The

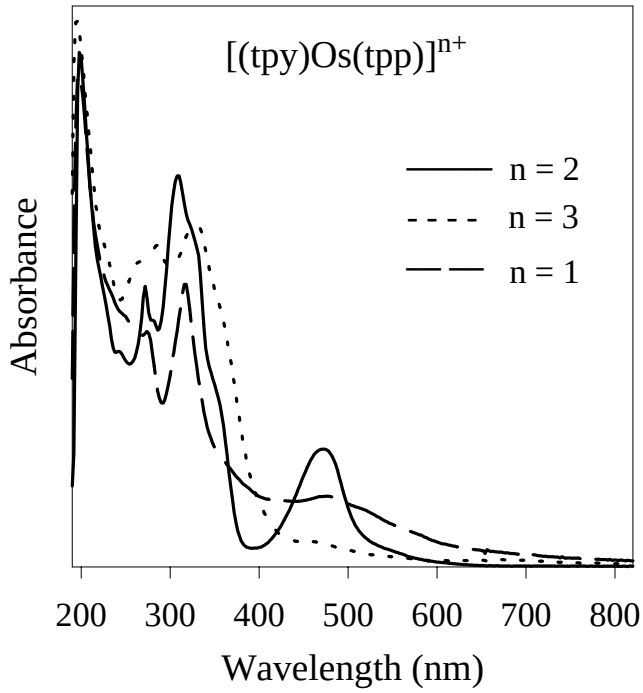

Figure 3.12 Spectroelectrochemistry of $[(tpy)Os(tpp)](PF_6)_2$.

550 - 750 nm region of $[Os(tpy)(tpp)]^{2+}$ exhibits an increased absorbance relative to the ruthenium analog. This region represents the ^{3}MLCT bands which have higher intensity in the osmium system due to a higher degree of spin orbit coupling. Peaks in this region are lost upon osmium oxidation consistent with this ^{3}MLCT assignment.

The oxidative spectroelectrochemistry of $[(tpy)Ru(tpp)Ru(tpy)]^{4+}$ is shown in Figure 3.13. The absorbance at 548 nm has been assigned as overlapping Ru $\rightarrow$ tpp CT transitions based on the two equivalent ruthenium centers. Oxidation of the first ruthenium metal decreases the intensity of the MLCT at 548 nm with the remaining intensity being due to the Ru $\rightarrow$ tpp CT transition involving the unoxidized ruthenium. One would expect $[(tpy)Ru(tpp)Ru(tpy)]^{4+}$ to have a Ru $\rightarrow$ tpy CT band at ca. 460 nm. A shoulder appears in this region which loses

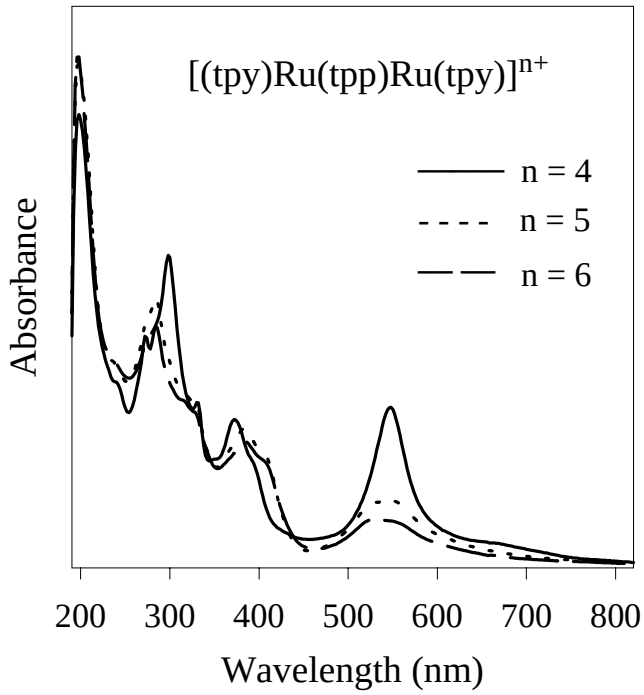

Figure 3.13 Oxidative spectroelectrochemistry of $[(tpy)Ru(tpp)Ru(tpy)](PF_6)_4$.

intensity upon metal oxidation consistent with an underlying Ru $\rightarrow$ tpy CT band in this region. Oxidation by one electron also results in a red shift of the tpp $\pi \rightarrow \pi^*$ transitions at 372 and 400 nm and a loss of intensity in the 298 nm region. Oxidation by a second electron results in further loss of the Ru$\rightarrow$tpp CT transition at 548 nm. The 298 nmregion exhibits a marked decrease in absorbance upon metal oxidation. This is consistent with a higher energy MLCT band occurring in this region and the peak at 298 nm is assigned as a higher energy Ru $\rightarrow$ tpy CT band. A band at 530 nm persists after both metals have been oxidized. It could be a result of incomplete oxidation but could also be attributed to a new tpp $\rightarrow Ru^{III}$ ligand-to-metal charge transfer (LMCT) transition made possible by metal oxidation. Electrogeneration

of these oxidized complexes is possible with > 95 % regeneration of their original oxidation state.

Reduction of $[(tpy)Ru(tpp)Ru(tpy)]^{4+}$ by one electron, shown in Figure 3.14, formally reduces the lowest energy tpp π^* orbital which results in a bleaching of the $Ru(d\pi) \rightarrow tpp(\pi^*)$ CT transitions at 548 nm, new tpp $\pi^* \rightarrow \pi^*$ transitions at 400 and 538 nm, and a bleaching of the tpp $\pi \rightarrow \pi^*$ transitions at 372 and 400 nm. The 298 nm region is unaffected by tpp reduction consistent with the Ru $\rightarrow$ tpy CT nature of this band. A band at ca. 290 nm is lost upon tpp reduction but remains upon metal oxidation. This is consistent with a tpp ($\pi \rightarrow \pi^*$) band in this region. The peak at 312 nm remains upon metal oxidation and tpp reduction and likely represents a tpy based $\pi \rightarrow \pi^*$ band.

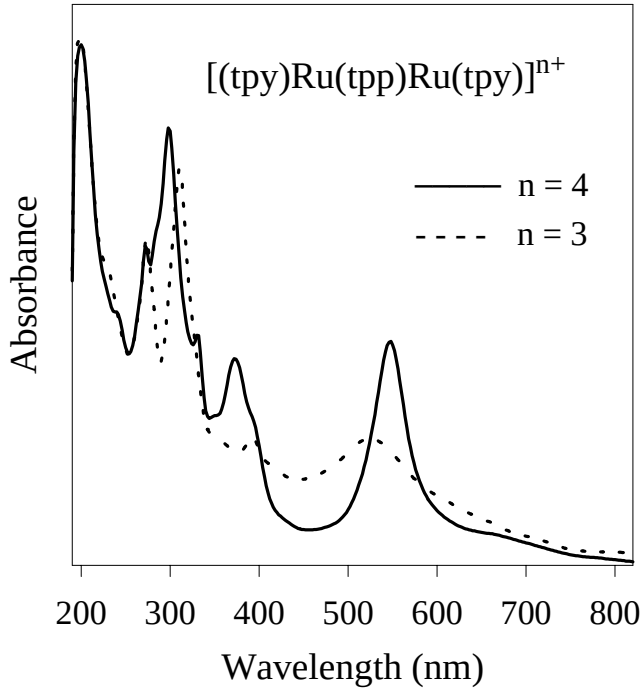

Figure 3.14 Reductive spectroelectrochemistry of $[(tpy)Ru(tpp)Ru(tpy)](PF_6)_4$.

Electrogeneration of the one electron reduced species is reversible with > 90 % regeneration of the original oxidation state. It was not possible to reversibly generate the two electron reduced form of this complex.

Figure 3.15 shows the oxidative spectroelectrochemical results for $[(tpy)\mathbf{Ru}(\mathbf{tpp})Ru(tpp)]^{4+}$. Electrogeneration of the one electron oxidized complex is possible with > 95 % regeneration of the original oxidation state. The band at 548 nm has been assigned as two overlapping Ru $\rightarrow$ **tpp** CT transitions involving the bridging ligand, with the lower energy component being attributed to the **Ru** $\rightarrow$ **tpp** CT transition localized on the $(tpy)\mathbf{Ru}^{II}(\mathbf{tpp})$ moiety. The

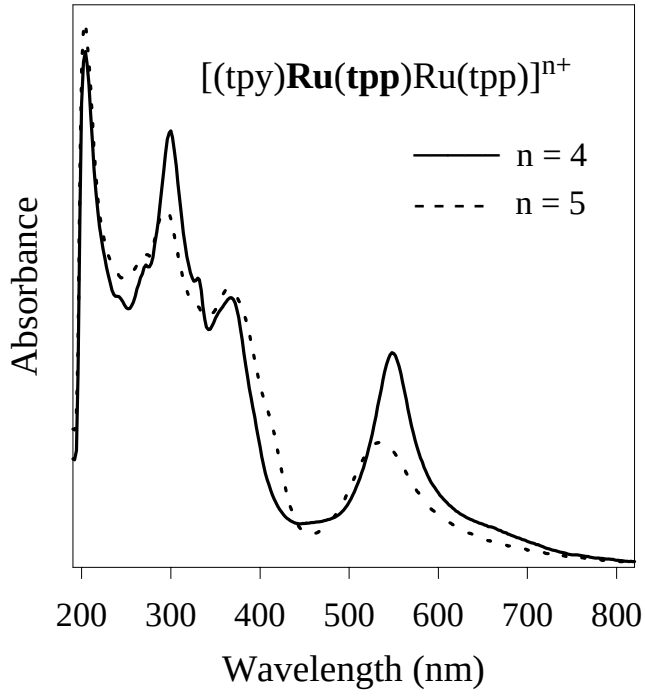

Figure 3.15 Oxidative spectroelectrochemistry of $[(tpy)\mathbf{Ru}(\mathbf{tpp})Ru(tpp)](PF_6)_4$.

first oxidation has been assigned as oxidation of the ruthenium metal that is coordinated to both tpy and tpp. Generation of the [(tpy)**Ru^{III}**(**tpp**)Ru^{II}(tpp)]$^{5+}$ species results in the loss of the lower energy component of the band at 548 nm with the remaining intensity due to the higher energy Ru $\rightarrow$ **tpp** MLCT transition involving the ruthenium coordinated to two tpp ligands. Oxidation of the ruthenium metal also lowers the energy of the lowest energy **tpp** π^* orbital of the bridging tpp, red shifting the $\pi \rightarrow \pi^*$ transitions at 400 and 360 nm associated with this bridging tpp. The terminal tpp should exhibit $\pi \rightarrow \pi^*$ bands in this region at ca. 335 nm that remain at the same energy upon oxidation of the (tpy)**Ru**(**tpp**) metal center. The tpy based $\pi \rightarrow \pi^*$ band at 320 nm experiences a slight red shift upon generation of the (tpy)Ru^{III}(tpp) moiety. A peak at 300 nm is lost upon oxidation to generate a (tpy)**Ru^{III}**(**tpp**) moiety. This is consistent with a higher energy **Ru** $\rightarrow$ tpy CT band in this region. Underlying **Ru** $\rightarrow$ tpy and Ru $\rightarrow$ tpp CT bands should be present in the 460 - 470 nm region. A loss of intensity in this region upon ruthenium oxidation indicates that these peaks are probably present. It was not possible to reversibly generate the two electron oxidized complex.

Figure 3.16 shows the reductive spectroelectrochemical results for [(tpy)**Ru**(**tpp**)Ru(tpp)]$^{4+}$. It was possible to generate the one electron reduced species with > 95 % reversibility. When reduced by one electron, the electron formally resides on the lowest energy π^* orbital of the bridging **tpp** and this bleaches both the Ru $\rightarrow$ **tpp** and the **Ru** $\rightarrow$ **tpp** CT transitions centered at 548 nm. Reduction of the bridging tpp results in the loss of the **tpp** $\pi \rightarrow \pi^*$ transitions at 368 and 400 nm. New tpp based $\pi^* \rightarrow \pi^*$ transitions appear at 550 and 400 nm upon reduction. The high energy **Ru** $\rightarrow$ tpy CT band originally at 300 nm is slightly red shifted by tpp reduction but a closely spaced band at ca. 290 nm is lost. This peak at 290 nm was seen to be retained upon one electron oxidation to generate the (tpy)Ru^{III}(tpp) moiety. These two observations point to a higher energy **tpp** based $\pi \rightarrow \pi^*$ transition in this 290 nm region. It was not possible to reversibly generate the two electron reduced species.

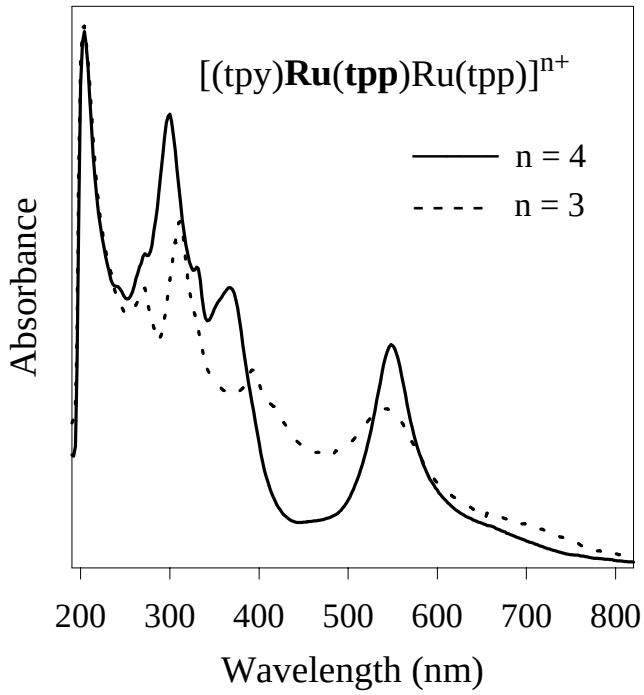

Figure 3.16 Reductive spectroelectrochemistry of [(tpy)**Ru**(**tpp**)Ru(tpp)]$(PF_6)_4$.

Figure 3.17 shows the oxidative spectroelectrochemical results for [(tpy)Os(**tpp**)Ru(tpp)]$^{4+}$. Electrogeneration of the one electron oxidized complex is possible with > 95 % regeneration of the original oxidation state. It is worth noting the very similar spectroscopy observed not only in the synthesized oxidation state of [(tpy)M(tpp)Ru(tpp)]$^{4+}$ (M = Ru^{II} or Os^{II}), but also in the electrogenerated states seen in the spectroelectrochemistry. Slight differences are observed in the 650 - 700 nm region with an increase in absorbance for the osmium analog. This results from the ^{3}MLCT bands occurring in this region having higher intensity for the osmium chromophore. The band at 546 nm has been assigned as overlapping Ru $\rightarrow$ **tpp** and Os $\rightarrow$ **tpp** CT transitions involving the bridging tpp ligand with the lower energy component being the osmium based transition. The first oxidative process has been assigned as the $Os^{II/III}$ oxidation. Electrogeneration of this state should result in a spectrum that closely matches

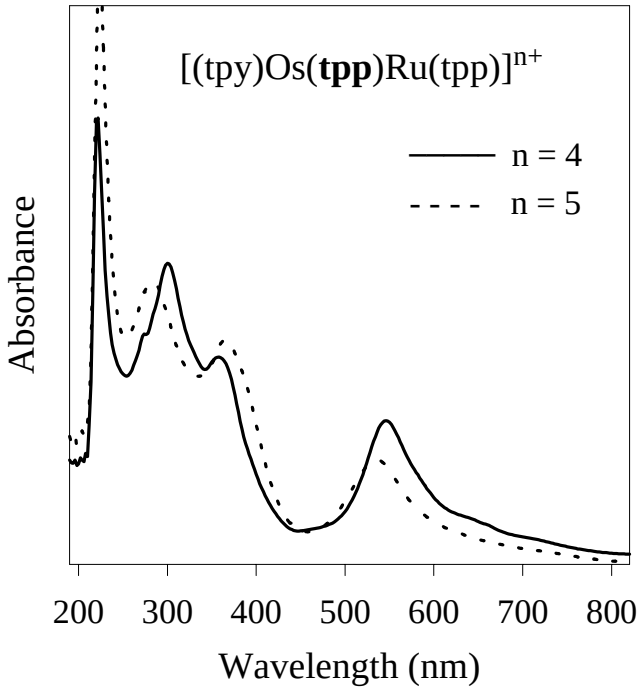

Figure 3.17 Oxidative spectroelectrochemistry of [(tpy)Os(**tpp**)Ru(tpp)]$(PF_6)_4$.

that of the one electron oxidized species [(tpy)**Ru**(**tpp**)Ru(tpp)]$^{5+}$ shown in Figure 3.15. As expected, the lower energy component of the band at 546 nm is lost upon osmium oxidation with the remaining intensity being assigned as the Ru $\rightarrow$ **tpp** CT involving the bridging tpp ligand. The lower energy 650 -700 nm region loses intensity due to the loss of the osmium based ^{3}MLCT transition in this region upon osmium oxidation. The peak at 470 nm is lost upon osmium oxidation, consistent with a Os $\rightarrow$ tpy CT band. The $\pi \rightarrow \pi^*$ transitions of the bridging **tpp** at 358 and 400 nm are red shifted upon osmium oxidation. The tpp $\pi \rightarrow \pi^*$ bands for the terminal tpp should remain unchanged by osmium oxidation. A shoulder at 330 nm also remains upon osmium oxidation and this complex is expected to have a tpy based $\pi \rightarrow \pi^*$ band in this region. There is a loss of intensity at 300 nm upon osmium oxidation that

can be attributed to the loss of the Os → tpy CT transition. The remaining intensity in the 290 nm region is due to the **tpp** π → π* transition. It was not possible to reversibly generate the two electron oxidized species of this complex.

The reductive spectroelectrochemistry of $[(tpy)Os(\mathbf{tpp})Ru(tpp)]^{4+}$ is also shown in Figure 3.18. It was possible to generate the one electron reduced species with > 80 % reversibility. When reduced by one electron, the electron is assigned as residing in the **tpp** π* orbital. This has the effect of bleaching the Os → **tpp** and Ru → **tpp** CT transitions at 546 nm and giving new **tpp** π* → π* transitions in the visible at 400 and 540 nm. The **tpp** π → π* transitions at 358 and 400 nm are lost upon **tpp** reduction. The higher energy terminal tpp π → π* component at ca. 335 nm is maintained upon **tpp** reduction. As in the all ruthenium analog,

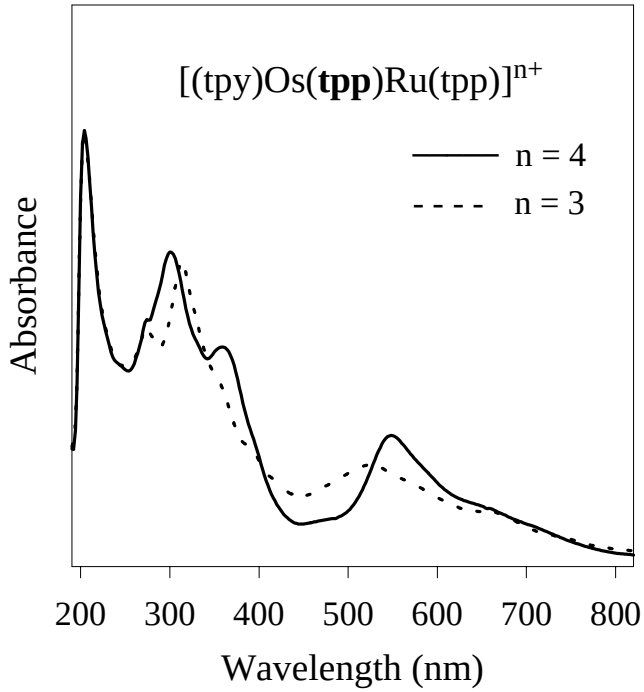

Figure 3.18 Reductive spectroelectrochemistry of $[(tpy)Os(\mathbf{tpp})Ru(tpp)](PF_6)_4$.

the loss of intensity at 290 nm upon one electron reduction of $[(tpy)Os(\mathbf{tpp})Ru(tpp)]^{4+}$ is consistent with the high energy **tpp** $\pi \rightarrow \pi^*$ assignment of this transition. It was not possible to reversibly generate the two electron reduced form of this complex.

The oxidative spectroelectrochemistry of $[(tpy)\mathbf{Ru}(tpp)RuCl_3]^+$ is shown in Figure 3.19. Electrogeneration of the one and two electron oxidized species is possible with > 95 % regeneration of the original oxidation state. Upon oxidation by one electron, the ruthenium bound to three chlorides is oxidized to the 3+ oxidation state and the absorbance at 612 nm is lost, consistent with the previous assignment of this transition as being a Ru $\rightarrow$ tpp CT transition.[12] The oxidation of Ru^{II} to Ru^{III} also stabilizes the tpp π^* orbital which should result in a red shift of the **Ru**($d\pi$) $\rightarrow$ tpp(π^*) CT transition. The intense band at 536 nm

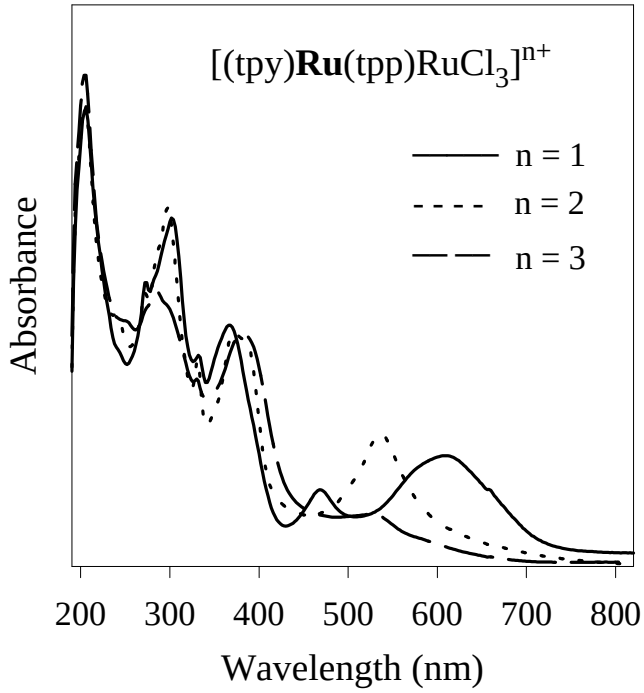

Figure 3.19 Oxidative spectroelectrochemistry of $[(tpy)\mathbf{Ru}(tpp)RuCl_3](PF_6)$.

represents this MLCT which seems to gain significant intensity and sharpen as the ruthenium bound to three chlorides is oxidized. The **Ru** $\rightarrow$ tpy CT transition at 468 nm is obscured by the intense **Ru** $\rightarrow$ tpp CT transition at 536 nm in the one electron oxidized complex. Stabilization of the tpp π^* orbital upon ruthenium oxidation will also red shift the tpp $\pi \rightarrow \pi^*$ transitions, establishing the 354 and 366 nm absorbances as a tpp $\pi \rightarrow \pi^*$ transitions. It is interesting to note that the visible portion of the spectrum for the one electron oxidized form, $[(tpy)\mathbf{Ru^{II}}(tpp)Ru^{III}Cl_3]^+$, is quite similar to the unoxidized $[(tpy)Ru(tpp)Ru(tpp)]^{4+}$. This indicates that the stabilizing effect on the tpp π^* orbitals of Ru^{II}tpy is about equal to that of $Ru^{III}Cl_3$. Oxidation of $[(tpy)\mathbf{Ru}(tpp)RuCl_3]^+$ by a second electron results in the loss of absorbance at 536 nm, verifying this as the **Ru** $\rightarrow$ tpp CT transition. The oxidation of this **Ru** would also be expected to bleach the higher energy **Ru** $\rightarrow$ tpy CT transition, as is seen for the transition at 302 nm. The peak at 332 nm is maintained upon Ru oxidation and slightly red shifted upon **Ru** oxidation consistent with a tpy $\pi \rightarrow \pi^*$ assignment.

The reductive spectroelectrochemistry of $[(tpy)\mathbf{Ru}(tpp)RuCl_3]^+$ is shown in Figure 3.20. The one electron reduced species is produced with > 75 % regeneration of the original oxidation state. The one electron reduction of $[(tpy)\mathbf{Ru}(tpp)RuCl_3]^+$ would result in the electron formally residing in the lowest energy tpp π^* orbital. The loss of the peaks at 354 and 366 nm is consistent with the assignment of these being tpp $\pi \rightarrow \pi^*$ transitions. Loss of the band at 612 nm upon reduction of tpp is consistent with this absorbance being due to the Ru(dπ) $\rightarrow$ tpp(π^*) CT transition. New tpp $\pi^* \rightarrow \pi^*$ transitions are expected in the visible and obscure changes to this region. A peak at 290 nm is lost upon tpp reduction consistent with a tpp based $\pi \rightarrow \pi^*$ band occurring in this region. It was not possible to reversibly reduce this complex by two electrons.

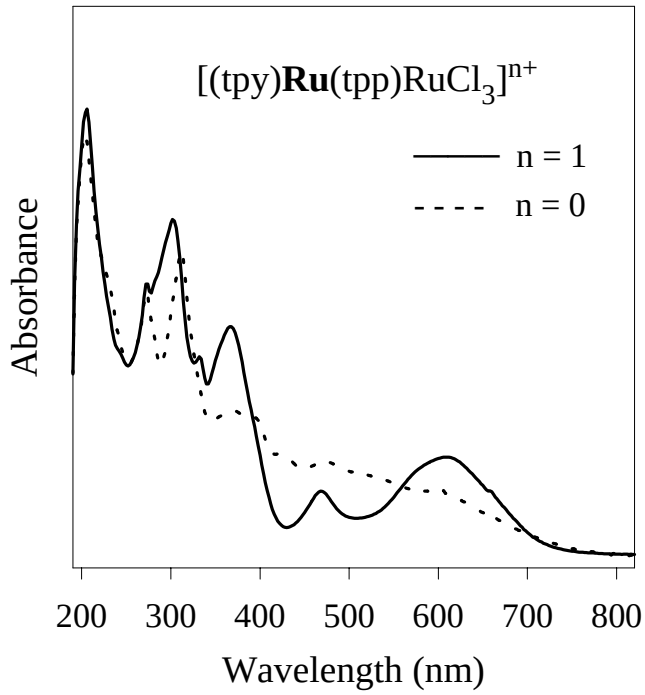

Figure 3.20 Reductive spectroelectrochemistry of [(tpy)**Ru**(tpp)$RuCl_3$](PF_6).

Figure 3.21 shows the oxidative spectroelectrochemical results for [(tpy)Os(tpp)$RuCl_3$]$^+$. It was possible to generate the one electron oxidized species with > 75 % reversibility. The first oxidation for this complex has been assigned as the $Ru^{II/III}$ couple and the second as the $Os^{II/III}$ couple. Oxidation of the ruthenium should lead to the loss of the ruthenium based MLCT transitions. The one electron oxidation results in a loss of the band at 678 nm, verifying the assignment of this band as a Ru $\rightarrow$ tpp CT transition. The peak at 606 nm in the parent complex has been assigned as a Os $\rightarrow$ tpp CT band and is relatively unaffected upon ruthenium oxidation. The Os $\rightarrow$ tpy CT band at 474 nm is still present in the one electron oxidized species although it is somewhat obscured by the peak at 522 nm that grows in intensity in this [(tpy)Os^{II}(tpp)$Ru^{III}Cl_3$]$^{2+}$ form. The tpp based $\pi \rightarrow \pi^*$ bands at 354 and

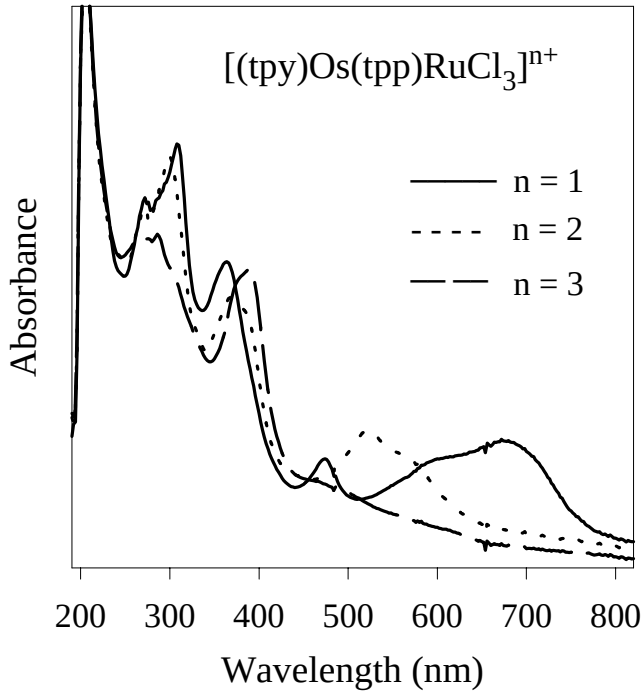

Figure 3.21 Oxidative spectroelectrochemistry of $[(tpy)Os(tpp)RuCl_3](PF_6)$.

364 nm shift to lower energy upon ruthenium oxidation as expected. The peak at 606 nm is lost upon oxidation by two electrons to generate an oxidized osmium center. This is consistent with the assignment of this peak being an Os $\rightarrow$ tpp CT transition. The Os $\rightarrow$ tpy CT band at 474 nm is also lost as expected upon osmium oxidation. The band at 522 nm that gains intensity upon ruthenium oxidation is lost upon osmium oxidation. This is consistent with an Os $\rightarrow$ tpp CT assignment. A peak at ca. 300 nm is also lost upon osmium oxidation and represents a high energy Os $\rightarrow$ tpy CT transition. A shoulder at 320 nm is relatively unchanged by metal oxidation and tpy is expected to exhibit a $\pi \rightarrow \pi^*$ band in this region.

In the spectrum of the one electron reduced form of $[(tpy)Os(tpp)RuCl_3]^+$, shown in

Figure 3.22, the electron resides formally on the tpp π* orbital. The one electron reduced complex was generated with > 75 % reversibility. As in the Ru/Ru analog, this bleaches the tpp π → π* transitions at 354 and 366 nm and the Ru(dπ) → tpp(π*) and Os → tpp CT transitions at 678 and 606 nm, helping to solidify these assignments. Other changes in the visible region of the spectrum are obscured by new tpp π* → π* transitions. A peak at 290 nm is lost upon tpp reduction and represents a higher energy tpp based π → π* transition. It was not possible to reversibly generate the two electron reduced species.

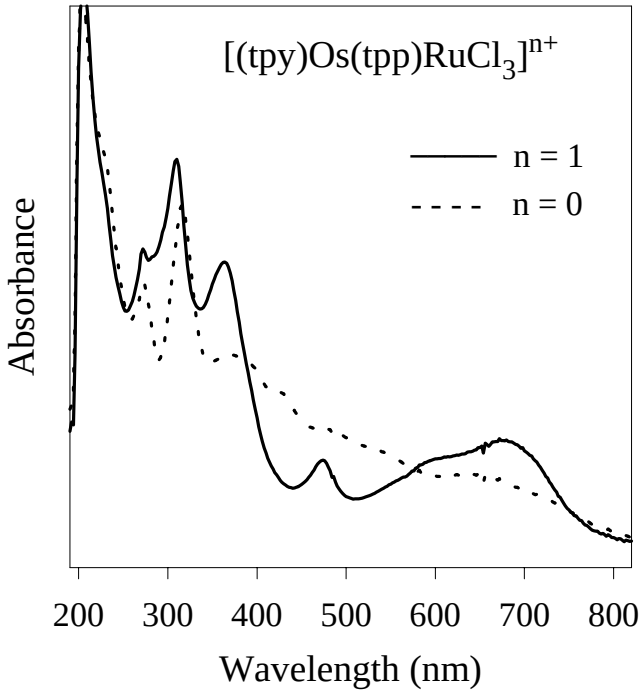

Figure 3.22 Reductive spectroelectrochemistry of [(tpy)Os(tpp)$RuCl_3$](PF_6).

Figure 3.23 shows the oxidative spectroelectrochemistry of [(tpy)**Ru**(tpp)Ru($CH_3CN)_3$]$^{4+}$. Electrogeneration of the one and two electron oxidized species is possible with > 95% regeneration of the original oxidation state. Upon one electron oxidation, Ru is oxidized to

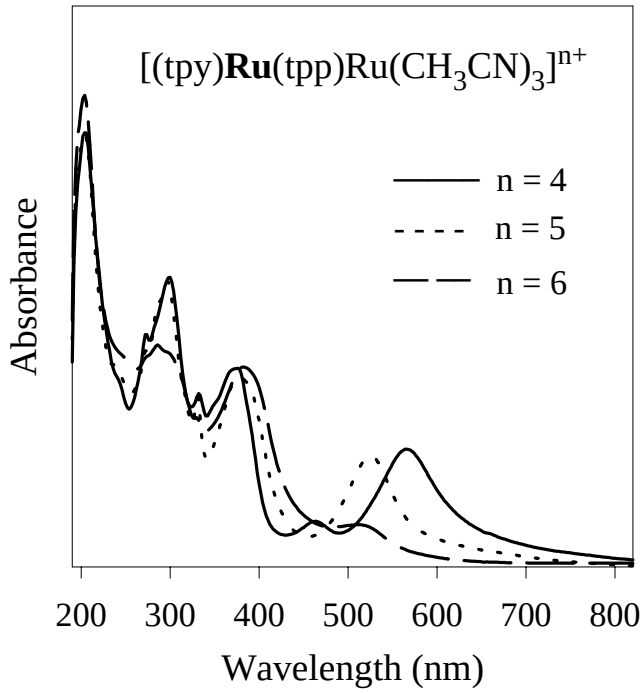

Figure 3.23 Oxidative spectroelectrochemistry of [(tpy)**Ru**(tpp)Ru$(CH_3CN)_3$]$(PF_6)_4$.

the 3+ oxidation state. This bleaches the Ru $\rightarrow$ tpp CT transition at 566 nm. The absorbance at 526 nm that remains is due to the higher energy **Ru** $\rightarrow$ tpp CT component of this band. The tpp $\pi \rightarrow \pi^*$ transitions at 366 and 376 nm are red shifted from the parent compound upon Ru oxidation. No changes in the ultraviolet are observed upon generation of this (tpy)$Ru^{III}(CH_3CN)_3$ moiety. This clearly establishes the first oxidation of this complex as based on the ruthenium bound to the three acetonitriles since generation of a (tpy)Ru^{III}(tpp) moiety has been shown to result in changes in the 300 nm region. When oxidized by two electrons, the second ruthenium is now oxidized to the 3+ oxidationstate. The **Ru** $\rightarrow$ tpp CT transition at 526 nm is lost. The tpp based $\pi \rightarrow \pi^*$ transitions originally at 366 and 376 nm experience a slight additional red shift as the second ruthenium metal center is oxidized to the

3+ oxidation state. A peak at ca. 300 nm is lost upon generation of the (tpy)Ru^{III}(tpp) moiety consistent with a higher energy Ru $\rightarrow$ tpy CT assignment. The peak at 332 nm is relatively unaffected by metal oxidation and represents a tpy $\pi \rightarrow \pi^*$ band.

The reductive spectroelectrochemistry of $[(tpy)\mathbf{Ru}(tpp)Ru(CH_3CN)_3]^{4+}$ is shown in Figure 3.24. Electrogeneration of the one electron reduced species is possible with > 75% regeneration of the original oxidation state. When reduced by one electron, the electron formally resides in the lowest energy tpp π^* orbital causing the loss of the tpp $\pi \rightarrow \pi^*$ transitions at 366 and 376 nm. The **Ru** $\rightarrow$ tpy CT transition at 300 nm is still evident after reduction of tpp indicating that tpy serves as the acceptor ligand for this transition. A peak at

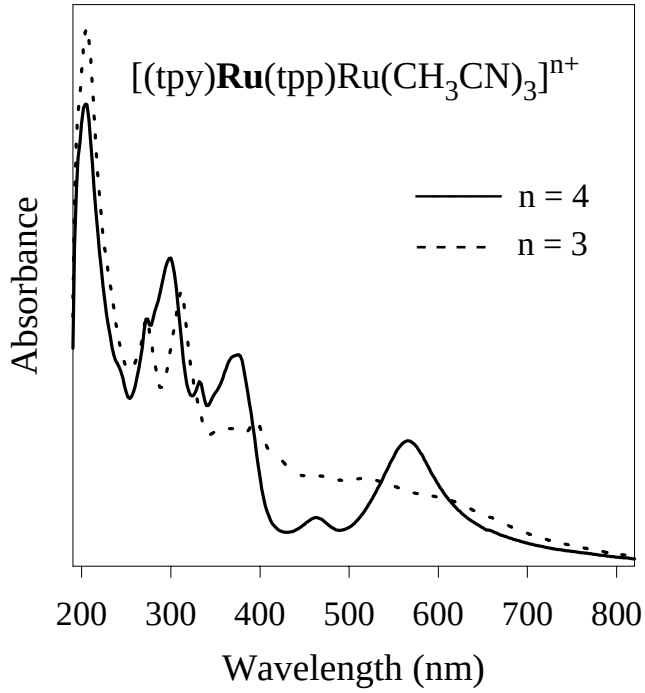

Figure 3.24 Reductive spectroelectrochemistry of $[(tpy)\mathbf{Ru}(tpp)Ru(CH_3CN)_3](PF_6)_4$.

290 nm is lost upon tpp reduction and most likely represents a higher energy tpp based $\pi \rightarrow \pi^*$ transition. The reduction of tpp also causes the appearance of new tpp $\pi^* \rightarrow \pi^*$ transitions at ca. 400 and 540 nm, partially obscuring other changes in the visible region of the spectrum. It is still evident that the peak at 566 nm is lost upon tpp reduction consistent with the assignment of two Ru $\rightarrow$ tpp CT bands in this region. It was not possible to reversibly generate the two electron reduced species.

The oxidative spectroelectrochemistry of $[(tpy)\mathbf{Ru}(tpp)Ru(dpq)Cl]^{3+}$ is shown in Figure 3.25. Electrogeneration of the one electron oxidized species is possible with > 95% regeneration of the original oxidation state. Oxidation by one electron oxidizes the ruthenium bound to dpq and Cl. This bleaches the low energy Ru $\rightarrow$ tpp CT band at 584 nm and the higher energy

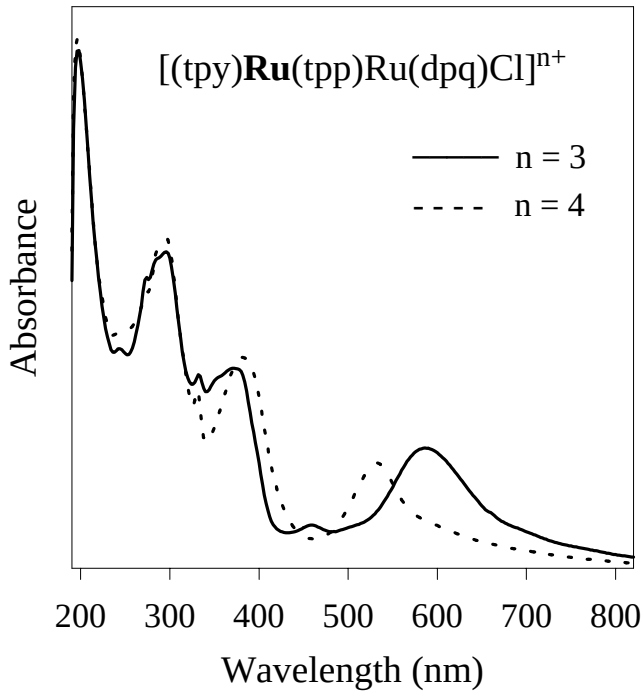

Figure 3.25 Oxidative spectroelectrochemistry of $[(tpy)\mathbf{Ru}(tpp)Ru(dpq)Cl](PF_6)_3$.

Ru → dpq CT band that is expected to occur in the visible region. The **Ru** → tpp CT transition at 525 nm increases in intensity as the other metal center is oxidized and the **Ru** → tpy CT band becomes buried in this more intense **Ru** → tpp CT peak. As with the other compounds, oxidation of one metal center lowers the energy of the tpp π* orbital which can be seen in a red shift of the tpp π → π* transitions at 366 and 376 nm. The ultraviolet region of the spectrum is not affected by the generation of the $(tpp)Ru^{III}(dpq)Cl$ moiety establishing the first oxidation as oxidation of this ruthenium center since generation of a $(tpy)Ru^{III}(tpp)$ moiety has been shown above to dramatically alter the 300 nm region of the spectrum. It was not possible to reversibly generate the two electron oxidized species.

The reductive spectroelectrochemistry of $[(tpy)\mathbf{Ru}(tpp)Ru(dpq)Cl]^{3+}$ is shown in Figure 3.26.

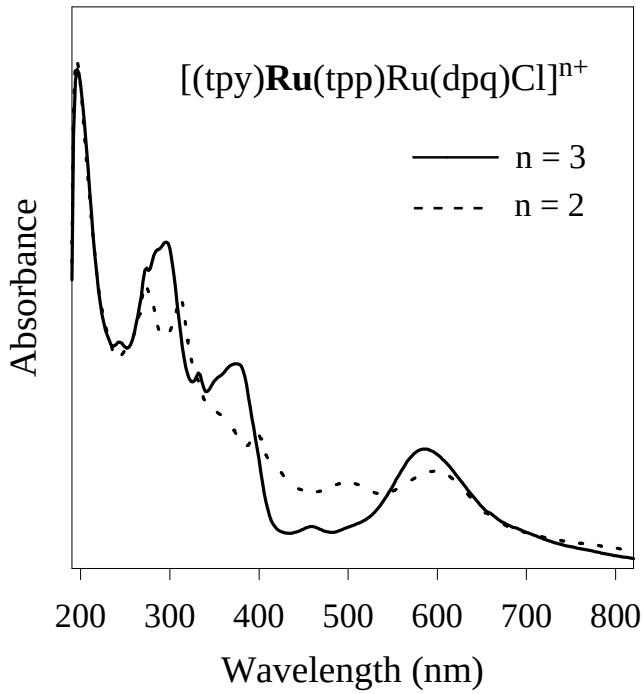

Figure 3.26 Reductive spectroelectrochemistry of $[(tpy)\mathbf{Ru}(tpp)Ru(dpq)Cl](PF_6)_3$.

Electrogeneration of the one electron reduced species is possible with > 80% regeneration of the original oxidation state. When the complex is reduced by one electron, tpp is reduced resulting in the loss of the Ru $\rightarrow$ tpp CT transition at 584 nm and the tpp based $\pi \rightarrow \pi^*$ transitions at 366 and 376 nm. The absorbance at 598 nm is due to a Ru $\rightarrow$ dpq CT transition. Other changes in the visible portion of the spectrum are obscured by new tpp $\pi^* \rightarrow \pi^*$ transitions which have typically appeared at ca. 400 and 540 nm upon reduction of a bridging tpp. As expected, the Ru $\rightarrow$ tpy CT transition at 460 nm is slightly red shifted upon tpp reduction. A peak at 290 nm is lost upon tpp reduction consistent with a higher energy tpp based $\pi \rightarrow \pi^*$ transition occurring in this region. Loss of this peak uncovers a transition at 296 nm which in similar complexes appears to be a higher energy Ru $\rightarrow$ tpy CT band. The peak at 332 nm is relatively unaffected by metal oxidation and tpp reduction and represents a tpy $\pi \rightarrow \pi^*$ band. It was not possible to reversibly generate the two electron reduced species.

The electronic absorption spectroscopy of the tpp bridged complexes with the additional assignments determined from spectroelectrochemistry is presented in Table 16.

Spectroelectrochemistry has been used here to elucidate much of the electronic absorption spectroscopy as well as the electrochemistry of these tpp bridged complexes. The light absorbing properties of these complexes can be quite difficult to understand due to the complicated UV-vis spectroscopy. In these complexes there are metal to ligand charge transfer transitions as well as ligand based $\pi \rightarrow \pi^*$ and $n \rightarrow \pi^*$ transitions. With two metals and up to three different ligands in these $[(tpy)M(tpp)Ru(LLL)]^{n+}$ complexes, the number of possible transitions is quite large and leads to very complicated UV-vis spectra. UV-vis spectroelectrochemistry has been used to determine the nature of many characteristic transitions in the complicated spectra of these complexes. The lowest energy band is overlapping M $\rightarrow \mu$-tpp and Ru $\rightarrow \mu$-tpp CT transitions in the area of 540 to 650 nm. There is a M $\rightarrow$ tpy CT transition located at approximately 470 nm and a higher energy M $\rightarrow$ tpy CT transition at ca. 300 nm which is lost from this region of the spectrum upon oxidation of M.

Table 16. Electronic Absorption Spectroscopy of a Series of Osmium and Ruthenium Complexes Incorporating the Tridentate Bridging Ligand tpp.[a,b]

Complex	λ_{max} (nm)	assignment	reference
$[Ru(tpy)(CH_3CN)_3]^{2+}$	436	Ru(dπ) → tpy(π*) CT	[c]
	330	tpy (π → π*)	[c]
	300	Ru(dπ) → tpy(π*) CT	[c]
	272	tpy (π → π*)	[c]
$[Ru(tpy)(tpp)]^{2+}$	472	Ru(dπ) → tpp(π*) CT	22, 23, 51
		Ru(dπ) → tpp(π*) CT	22, 23, 51
	354	tpp (π → π*)	24
	328	tpp (π → π*)	24
	310	Ru(dπ) → tpy(π*) CT	[c]
	290	tpp (π → π*)	[c]
	272	tpy (π → π*)	[c]
$[Os(tpy)(tpp)]^{2+}$	468	Os(dπ) → tpp(π*) CT	51
		Os(dπ) → tpy(π*) CT	51
	350	tpp (π → π*)	53
	324	tpp (π → π*)	53
	314	Os(dπ) → tpy(π*) CT	[c]
	290	tpp (π → π*)	[c]
	272	tpy (π → π*)	[c]
$[(tpy)Ru(tpp)Ru(tpy)]^{4+}$	548	Ru(dπ) → tpp(π*) CT	22, 23, 51
	460	Ru(dπ) → tpy(π*) CT	22, 23, 51
	400	tpp (π → π*)	[c]
	372	tpp (π → π*)	[c]
	332	tpy (π → π*)	[c]
	298	Ru(dπ) → tpy(π*) CT	[c]
	290	tpp (π → π*)	[c]
	272	tpy (π → π*)	[c]

[a] Spectra recorded in CH_3CN at RT.
[b] tpp = 2,3,5,6-tetrakis(2-pyridyl)pyrazine, tpy = 2,2',6',2"-terpyridine.
[c] New assignment

Table 16 (continued).

Complex	λ_{max} (nm)	assignment	reference
[(tpy)**Ru**(**tpp**)Ru(tpp)]$^{4+}$	548	**Ru**(dπ) → **tpp**(π*) CT	27a, 51
		Ru(dπ) → **tpp**(π*) CT	27a
	460	**Ru**(dπ) → tpy(π*) CT	[c]
	400	**tpp** (π → π*)	[c]
	368	**tpp** (π → π*)	27a
	340	tpp (π → π*)	[c]
	332	tpy (π → π*)	[c]
	300	Ru(dπ) → tpy(π*) CT	[c]
	290	**tpp** (π → π*)	[c]
	272	tpy (π → π*)	[c]
[(tpy)Os(**tpp**)Ru(tpp)]$^{4+}$	546	Ru(dπ) → **tpp**(π*) CT	27a, 51
		Os(dπ) → **tpp**(π*) CT	27a
	470	Os(dπ) → tpy(π*) CT	[c]
	400	tpp (π → π*)	[c]
	358	tpp (π → π*)	27a
	330	tpy (π → π*)	[c]
	300	Os(dπ) → tpy(π*) CT	[c]
	290	tpp (π → π*)	[c]
	272	tpy (π → π*)	[c]
[(tpy)**Ru**(tpp)$RuCl_3$]$^{+}$	612	Ru(dπ) → tpp(π*) CT	27a
	525	**Ru**(dπ) → tpp(π*) CT	27a
	468	**Ru**(dπ) → tpy(π*) CT	27a
	366	tpp (π → π*)	[c]
	354	tpp (π → π*)	[c]
	332	tpy (π → π*)	[c]
	302	**Ru**(dπ) → tpy(π*) CT	[c]
	290	tpp (π → π*)	[c]
	272	tpy (π → π*)	[c]

[a] Spectra recorded in CH_3CN at RT.
[b] tpp = 2,3,5,6-tetrakis(2-pyridyl)pyrazine, tpy = 2,2',6',2"-terpyridine.
[c] New assignments based on this work.

Table 16 (continued).

Complex	λ_{max} (nm)	assignment	reference
$[(tpy)Os(tpp)RuCl_3]^+$	678	Ru(dπ) → tpp(π*) CT	27a
	606	Os(dπ) → tpp(π*) CT	27a
	474	Os(dπ) → tpy(π*) CT	27a
	364	tpp (π → π*)	[c]
	354	tpp (π → π*)	[c]
	330	tpy (π → π*)	[c]
	308	Os(dπ) → tpy(π*) CT	[c]
	290	tpp (π → π*)	[c]
	272	tpy (π → π*)	[c]
$[(tpy)\mathbf{Ru}(tpp)Ru(CH_3CN)_3]^{4+}$	566	Ru(dπ) → tpp(π*)	27b
	526	**Ru**(dπ) → tpp(π*) CT	[c]
	464	**Ru**(dπ) → tpy(π*) CT	[c]
	376	tpp (π → π*)	[c]
	366	tpp (π → π*)	[c]
	332	tpy (π → π*)	[c]
	300	**Ru**(dπ) → tpy(π*) CT	[c]
	290	tpp (π → π*)	[c]
	272	tpy (π → π*)	[c]
$[(tpy)\mathbf{Ru}(tpp)Ru(dpq)Cl]^{3+}$	584	Ru(dπ) → tpp(π*) CT	[c]
		Ru(dπ) → tpp(π*) CT	[c]
	565	Ru(dπ) → dpq(π*) CT	[c]
	460	**Ru**(dπ) → tpy(π*) CT	[c]
	376	tpp (π → π*)	[c]
	366	tpp (π → π*)	[c]
	332	tpy (π → π*)	[c]
	296	**Ru**(dπ) → tpy(π*) CT	[c]
	290	tpp (π → π*)	[c]
	272	tpy (π → π*)	[c]

[a] Spectra recorded in CH_3CN at RT.

[b] tpp = 2,3,5,6-tetrakis(2-pyridyl)pyrazine, tpy = 2,2',6',2"-terpyridine, and dpq = 2,3-bis(2-pyridyl)benzoquinoxaline.

[c] New assignments based on this work.

This drastic change in the 300 nm region upon oxidation of M is very useful in determining which metal is oxidized first in these systems. There are typically three bands at ca. 290, 350, and 380 nm associated with μ-tpp $\pi \rightarrow \pi^*$ transitions that are lost from this area of the spectrum upon tpp reduction and red shifted upon metal oxidation. The are two bands at 272 and ca. 325 nm that are associated with the tpy $\pi \rightarrow \pi^*$ transitions. The characteristic transitions identified by spectroelectrochemistry has helped to understand the complicated light absorbing characteristics of these compounds and will also aid in understanding the excited state properties of these promising light absorber - electron donor complexes.

Metal to Metal Charge Transfer Spectroscopy. In the complexes of the type $[(tpy)M(tpp)Ru(LLL)]^{n+}$, when the mixed valence species is produced, either $[(tpy)M^{II}(tpp)Ru^{III}(LLL)]^{n+}$ or $[(tpy)M^{III}(tpp)Ru^{II}(LLL)]^{n+}$, there is a metal to metal charge transfer transition that is present usually in the near infrared region of the spectrum. The mixed valence species can be generated by electrochemically oxidizing the parent $[(tpy)M^{II}(tpp)Ru^{II}(LLL)]^{n+}$ complex. The metal to metal charge transfer transition parameters for the tpp bridged complexes are given in Table 17.

Table 17. Metal to Metal Charge Transfer Transition Data for Ruthenium Complexes Bridged by 2,3,5,6-tetra(2-pyridyl)pyrazine.[a,b]

complex	λ_{max} (nm)	ε (M^{-1} cm^{-1})	$\Delta\nu_{1/2}$ (cm^{-1})	H_{ab} (eV)
$[(tpy)Ru(tpp)Ru(tpy)]^{5+}$	1521	5,132	1159	0.405[d]
$[(tpy)Ru(tpp)Ru(tpp)]^{5+}$	1450	2,200	2,300	0.430[d]
$[(tpy)Ru(tpp)RuCl_3]^{2+}$	[c]			
$[(tpy)Ru(tpp)Ru(CH_3CN)_3]^{5+}$	1333	720	3,200	0.052[e]
$[(tpy)Ru(tpp)Ru(dpq)Cl]^{4+}$	1282	400	3,900	0.044[e]

[a] Measured at room temperature in 0.1 M TBAH acetonitrile.
[b] tpp = 2,3,5,6-tetra(2-pyridyl)pyrazine, tpy = 2,2',6',2''-terpyridine, and dpq = 2,3-bis(2-pyridyl)quinoxaline
[c] Not detected
[d] Calculated as a Class III complex
[e] Calculated as a Class II complex

In the calculation for the metal to metal coupling parameter, H_{ab}, it is assumed that the free energy change for electron transfer from one metal to the other is zero. This is only the case for the symmetric bimetallic $[(tpy)Ru(tpp)Ru(tpy)]^{5+}$. In all the other complexes studied, the free energy change of electron transfer is not zero and the equation would be

$$\Delta\overline{\nu}_{1/2}(\text{calc}) = 48.06(E_{op} - \Delta G°)^{½}(\text{cm}^{-1})$$

where $E_{op} = \lambda + \Delta G°$

and $\Delta G°$ can be calculated as

$$\Delta G° = \overline{\nu}_{max} - [(\Delta\overline{\nu}_{1/2})^2/2310]$$

Therefore, in asymmetric systems, if

$$\Delta\overline{\nu}_{1/2} \geq 48.06(E_{op} - \Delta G°)^{½}$$

the compound is classified as Class II. If

$$\Delta\overline{\nu}_{1/2} < 48.06(E_{op} - \Delta G°)^{½}$$

the compound is classified as Class III.

For these tpp bridged systems, the MMCT data indicates that there is significant electronic coupling between the two metal centers, even when there is a large difference in the coordination environment between the two metal centers as in $[(tpy)Ru(tpp)Ru(dpq)Cl]^{4+}$. While $[(tpy)Ru(tpp)RuCl_3]^{2+}$ does not display a detectable MMCT transition, there may still be significant electronic communication between the metal centers. It has been pointed out that weakly coupled systems can undergo electron transfer processes without having optical transitions with large extinction coefficients.[57]

Ru and Ir complexes containing the bridging ligand bpm

Synthesis. The trimetallic complex $\{[(bpy)_2Ru(bpm)]_2IrCl_2\}(PF_6)_5$ was synthesized by the reaction of three equivalents of $Ru(bpy)_2Cl_2$ and one equivalent of $[Ir(bpm)_2Cl_2](PF_6)$. The excess $Ru(bpy)_2Cl_2$ was used in an attempt to reduce the yield of the bimetallic $[(bpy)_2Ru(bpm)IrCl_2(bpm)]^{3+}$.

Electrochemistry. The electrochemistry of ruthenium and iridium complexes incorporating the ligand 2,2′-bipyrimidine is summarized in Table 18.

Table 18. Electrochemical Data for Complexes Incorporating the Ligand 2,2′-bipyrimidine.[a,b,c]

complex	$E_{1/2}$ oxidation (V)	$E_{1/2}$ reduction (V)
$[Ir(bpm)_2Cl_2]^+$		-0.83 (bpm,bpm/bpm,bpm$^-$) -1.00 (bpm,bpm$^-$/bpm$^-$,bpm$^-$) -1.65 (Ir^{III}/Ir^{I})
$[(bpy)_2Ru(bpm)]^{2+}$	+1.44 (Ru^{II}/Ru^{III})	-1.01 (bpm/bpm$^-$) -1.47 (bpy/bpy$^-$) -1.75 (bpy/bpy$^-$)
$[(bpy)_2Ru(bpm)Ru(bpy)_2]^{4+}$	+1.80 (Ru^{II}/Ru^{III}) +1.62 (Ru^{II}/Ru^{III})	-0.37 (bpm/bpm$^-$) -1.05 (bpm$^-$/bpm^{2-}) -1.50 (2bpy/2bpy$^-$)
$\{[(bpy)_2Ru(bpm)]_2IrCl_2\}^{5+}$	+1.72 (Ru^{II}/Ru^{III})	-0.08 (bpm,bpm/bpm,bpm$^-$) -0.21 (bpm,bpm$^-$/bpm$^-$,bpm$^-$) -0.90 (bpm$^-$,bpm$^-$/bpm^{2-},bpm$^-$) -1.07 (bpm^{2-},bpm$^-$/ bpm^{2-},bpm^{2-}) -1.60 (2bpy/2bpy$^-$) -1.70 (Ir^{III}/Ir^{I})

[a] Recorded in acetonitrile with 0.1 M TBAH at room temperature. Reported vs. Ag/AgCl.
[b] bpm = 2,2′-bipyrimidine and bpy = 2,2′-bipyridine
[c] All complexes use the counterion PF_6^-.

The complex $[Ir(bpm)_2Cl_2](PF_6)$ shows two reversible bpm based reductions followed by an irreversible two electron iridium based reduction.[6d] When the Ir^I metal center is generated, there is an irreversible loss of two chloride ligands and the square planar complex $[(bpm^-)Ir(bpm^-)]^-$ is formed.

In all of the ruthenium complexes, bpm reduces prior to the bpy ligands due to the lower energy of the bpm π^* orbital. In the monometallic $[(bpy)_2Ru(bpm)]^{2+}$, the first bpm based reduction is followed by two sequential bpy based reductions. The oxidation at +1.44 V has been previously assigned as a Ru^{II}/Ru^{III} couple.[13] In the bimetallic $[(bpy)_2Ru(bpm)Ru(bpy)_2]^{4+}$, the first two reductions have been previously assigned as two sequential bpm based reductions.[11] These two bpm based reductions occur prior to any bpy based reduction which is characteristic of bimetallic formation. The two oxidations have been assigned as two Ru^{II}/Ru^{III} couples and are split by ca. 180 mV indicating significant metal to metal coupling through the bridging bpm.[11]

The electrochemistry of the trimetallic $\{[(bpy)_2Ru(bpm)]_2IrCl_2\}^{5+}$ shows two closely spaced oxidations and four reversible reductions, see Figure 3.27. The first oxidation wave is assigned as two closely spaced one electron Ru^{II}/Ru^{III} couples since ΔE_p is large. The overlapping nature of these two oxidations indicates that there is not significant coupling between the two ruthenium centers. The first two reductions are assigned as two closely spaced reductions of the two bridging bpm ligands. The splitting of the two bpm reductions is attributed to a small degree of communication through the iridium center. The next two reductions are also assigned as reduction of the two bpm ligands. This generates a $(bpm^{2-})Ir^{III}Cl_2(bpm^{2-})$ central core. The next reductions are assigned as bpy/bpy^- waves but are difficult to characterize due to the irreversible Ir^{III}/Ir^I redox couple in that region. The reversibility of the first two bpm based reductions indicates that this trimetallic complex is stable with two electrons collected on the $(bpm)Ir^{III}Cl_2(bpm)$ central core. The simultaneous

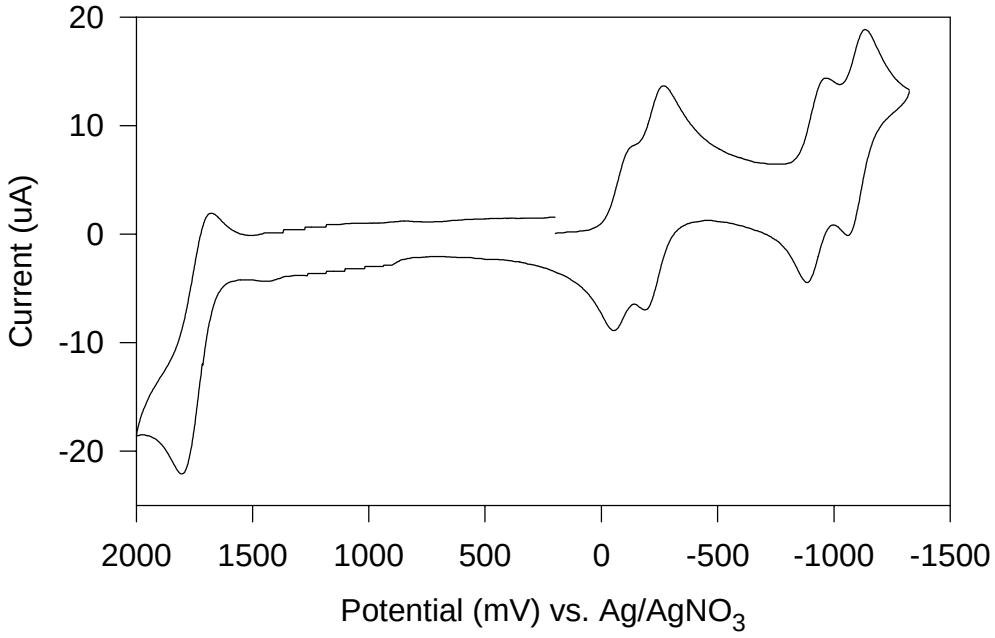

Figure 3.27 Cyclic voltammogram of $\{[(bpy)_2Ru(bpm)]_2IrCl_2]\}(PF_6)_5$

oxidation of the two ruthenium centers indicates that they are largely electronically uncoupled and can function as two independent light absorbers in this molecule.

Electronic Absorption Spectroscopy. Table 19 summarizes the previously made electronic absorption spectroscopy assignments for complexes utilizing the bridging ligand 2,2′-bipyrimidine as well as the electronic absorption data for iridium complexes using the ligand 2,2′-bipyrimidine.

The lowest energy transition for $[(bpy)_2Ru(bpm)]^{2+}$ is a $Ru(d\pi) \rightarrow bpm(\pi^*)$ CT transition.[10-13] Upon formation of the multimetallic complexes $[(bpy)_2Ru(bpm)Ru(bpy)_2]^{4+}$ and $\{[(bpy)_2Ru(bpm)]_2IrCl_2\}^{5+}$, the bpm π^* orbital is lowered in energy resulting in the lowest

Table 19. Electronic Absorption Spectroscopy Data for Ruthenium Complexes Using the Ligand 2,2′-bipyrimidine.[a,b,c]

Complex	λ_{max}^{abs} (nm)	assignment	reference
$[(bpy)_2Ru(bpm)]^{2+}$	478 (sh)	Ru(dπ) → bpm(π*) CT	11[d]
	422	Ru(dπ) → bpy(π*) CT	11[d]
	360	Ru(dπ) → (π*)	11[d]
	284	bpy,bpm π → π*	11[d]
$[(bpy)_2Ru(bpm)Ru(bpy)_2]^{4+}$	594	Ru(dπ) → bpm(π*) CT	11[d], 12
	545 (sh)	Ru(dπ) → bpm(π*) CT	11[d], 12
	412	Ru(dπ) → bpy(π*) CT	11[d], 12
	280	bpy,bpm π → π*	11[d], 12
$[Ir(bpm)_2Cl_2]^{+}$	460 (sh)	Ir(dπ) → bpm(π*)	6d
	426 (sh)	Ir(dπ) → bpm(π*)	6d
	386		6d
	332	bpm π → π*	6d
	254	bpm π → π*	6d
$\{[(bpy)_2Ru(bpm)]_2IrCl_2\}^{5+}$	598	Ru(dπ) → bpm(π*) CT	14
	412	Ru(dπ) → bpy(π*) CT	14
	280	bpy π → π*, n → π*	14

[a] Recorded in acetonitrile at room temperature.
[b] bpy = 2,2′-bipyridine, bpm = 2,2′-bipyrimidine.
[c] All complexes are the PF_6^- salt unless noted.
[d] Reported as for the ClO_4^- salt.

energy transition being a Ru(dπ) → bpm(π*) CT transition at lower energy. In $[(bpy)_2Ru(bpm)]^{2+}$ and $[(bpy)_2Ru(bpm)Ru(bpy)_2]^{4+}$, the intense transitions in the UV region of the spectrum have been assigned as bpy and bpm based π → π* and n → π* transitions. In $[(bpy)_2Ru(bpm)Ru(bpy)_2]^{4+}$, the absorption at approximately 412 nm has been previously assigned as the sum of Ru(dπ) → bpy(π*) CT transitions and higher energy Ru(dπ) → bpm(π*) CT transitions.[12]

More detailed assignments of the electronic absorption spectroscopy of these bpm bridged compounds can be obtained through the use of UV-vis spectroelectrochemistry.

Spectroelectrochemistry. In order to better understand the spectroelectrochemistry of 2,2′-bipyrimidine containing compounds, the reductive spectroelectrochemistry of free bpm is shown in Figure 3.24. Free bpm shows absorption bands at 240 and 285 nm that can be attributed to $\pi \rightarrow \pi^*$ and $n \rightarrow \pi^*$ transitions. Upon reduction by one electron, new transitions appear at 368, 422, 508, and 535 nm. These new transitions can be attributed to new $\pi^* \rightarrow \pi^*$ transitions. The transition at 240 nm decreases in intensity slightly upon one electron reduction and likely is a result of the loss of the $\pi \rightarrow \pi^*$ portion of this band.

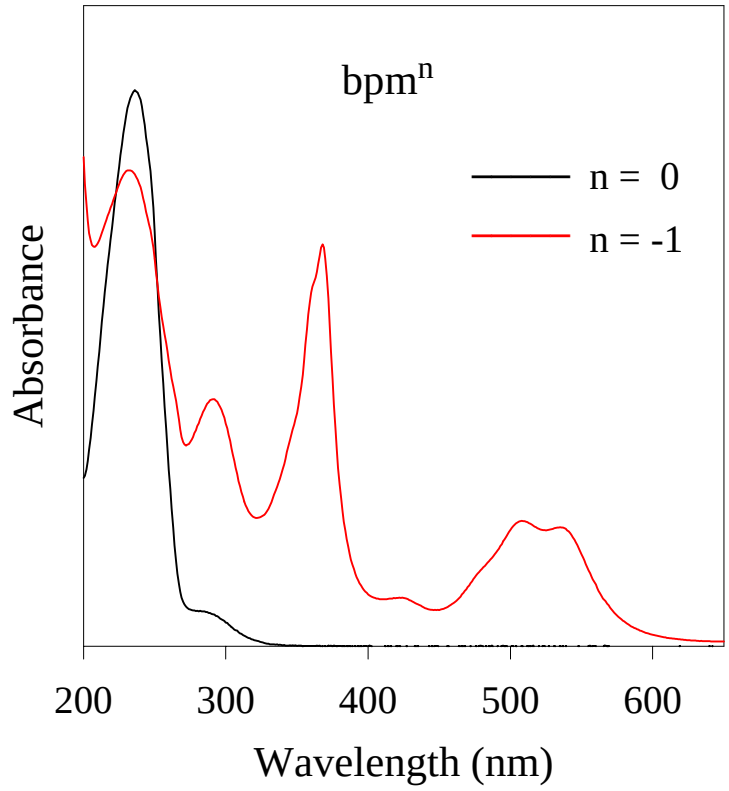

Figure 3.28 Reductive spectroelectrochemistry of 2,2′-bipyrimidine.

For the discussion of the electronic absorption spectroscopy of bpm complexes containing $Ru^{II}(bpy)_2$ fragments, it is informative to look at the electronic absorption spectrum of $[Ru(bpy)_3](PF_6)_2$ (see Figure 3.29). The spectrum has been previously assigned.[58] The two peaks at 240 and 450 nm have been assigned as Ru(dπ) → bpy(π*) transitions, each showing two vibronic components. The intense peaks at 185 and 285 nm have been assigned as ligand centered (LC) bpy π → π* transitions. The intensity at 322 and 344 nm has been attributed to metal centered (MC) Ru d → d transitions. Many of these transitions can be seen in the spectra of bpm complexes that have $Ru^{II}(bpy)^2$ fragments.

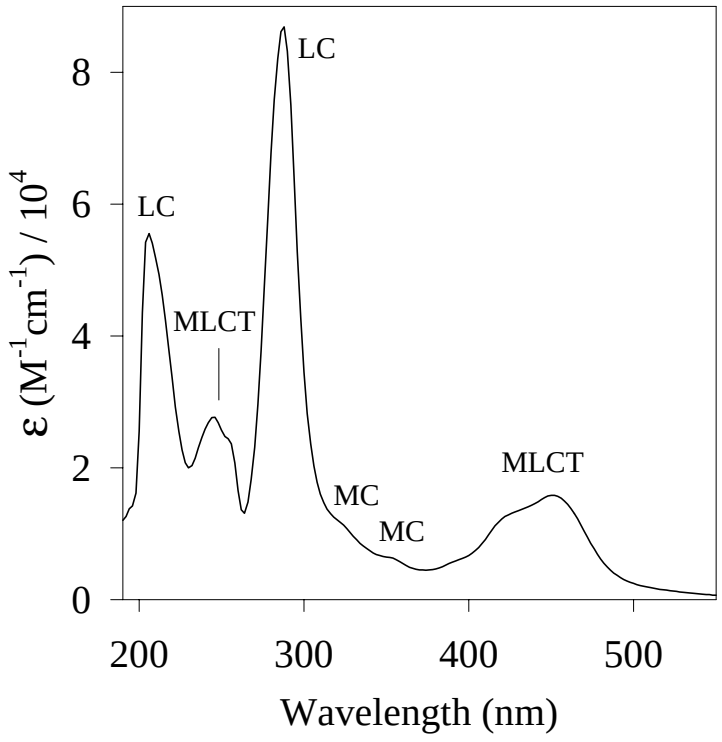

Figure 3.29 Electronic absorption spectrum of $[Ru(bpy)_3](PF_6)_2$.

The oxidative spectroelectrochemistry of $[(bpy)_2Ru(bpm)](PF_6)_2$ is shown in Figure 3.30. Upon oxidation by one electron, the absorbances centered at 422 and 478 nm are lost, as expected for Ru(dπ) → bpy(π*) and Ru(dπ) → bpm(π*) CT transitions. The absorbance centered at 360 nm decreases in intensity upon ruthenium oxidation and can be attributed to a ruthenium based d → d transition, red shifted from the 344 nm ruthenium based d → d transition in $[Ru(bpy)_3](PF_6)_2$. The remaining intensity in the visible region appears to be incomplete oxidation of the compound. The transition at 285 nm has been previously assigned as overlapping bpm and bpy π → π* transitions[11a] but likely contains only bpy π → π* and n → π* transitions which shift to lower energy and split upon oxidation by one electron. The shoulder at 268 nm can be attributed to either a Ru(dπ) → bpm(π*) CT

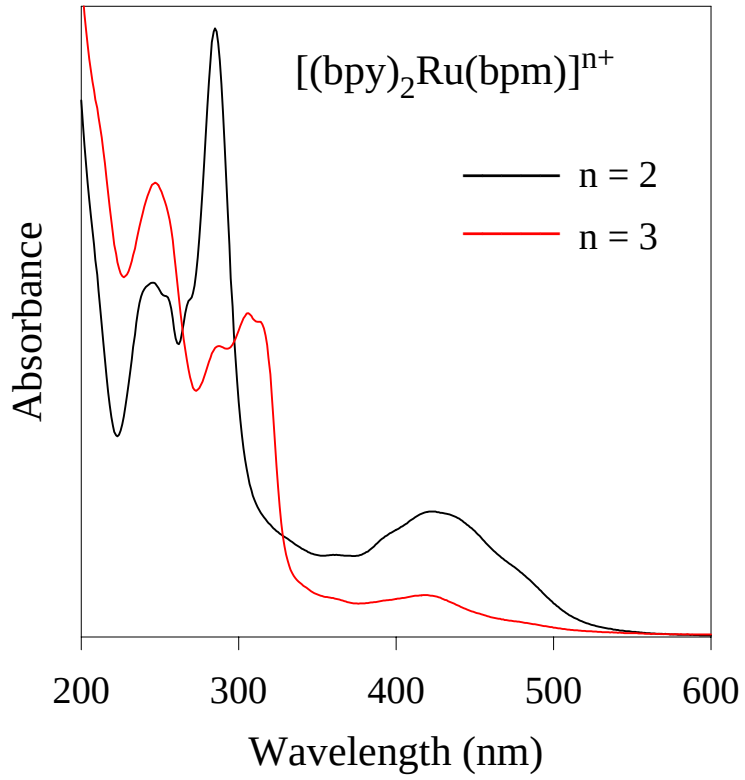

Figure 3.30 Oxidative spectroelectrochemistry of $[(bpy)_2Ru(bpm)](PF_6)_2$.

transition or a bpm $\pi \rightarrow \pi^*$ transition. For a Ru(dπ) $\rightarrow$ bpm(π^*) CT transition, oxidation would be expected to cause a shift of the transition out of the UV-vis region. For a bpm $\pi \rightarrow \pi^*$ transition, it is expected that oxidation would cause a small red shift of the transition. With the large absorbance in the 280 to 300 nm region, it is difficult to tell whether the shoulder at 268 nm is red shifted only slightly or whether it is shifted completely out of the UV-vis region of the spectrum. The transitions centered at 254 and 245 nm can be attributed to bpm $\pi \rightarrow \pi^*$ transitions by comparison with the electronic absorption spectrum of free bpm. From the comparison with the electron absorption spectrum of $[Ru(bpy)_3](PF_6)_2$, it is also expected that there will be a Ru(dπ) $\rightarrow$ bpy(π^*) CT transition with two vibronic components in this region. The one electron oxidized species was generated with > 90 % reversibility.

The reductive spectroelectrochemistry of $[(bpy)_2Ru(bpm)](PF_6)_2$ is shown in Figure 3.31. The one electron reduced species was generated with > 80 % reversibility. Upon reduction by one electron, it is expected that there will be a drastic change in the energy of the Ru $\rightarrow$ bpm CT transitions at 422 and 478 nm. These changes are obscured by new bpm $\pi^* \rightarrow \pi^*$ transitions in the visible. The absorbance band at 285 nm likely does not contain bpm $\pi \rightarrow \pi^*$ and $n \rightarrow \pi^*$ transitions as previously reported[11a] since the intensity and energy of this band does not change significantly upon bpm reduction. The peak at 285 nm most likely represents only bpy $\pi \rightarrow \pi^*$ and $n \rightarrow \pi^*$ transitions. Upon reduction by one electron, there is a loss of intensity in the shoulder at 268 nm which is consistent with either a bpm based $\pi \rightarrow \pi^*$ or $n \rightarrow \pi^*$ transition or a Ru(dπ) $\rightarrow$ bpm(π^*) CT transition. Upon reduction, the peak centered at ca. 250 nm decreases in intensity which can be attributed to the loss of the bpm $\pi \rightarrow \pi^*$ portion of this band. The remaining intensity can be attributed to a higher energy Ru(dπ) $\rightarrow$ bpy(π^*) CT transition.

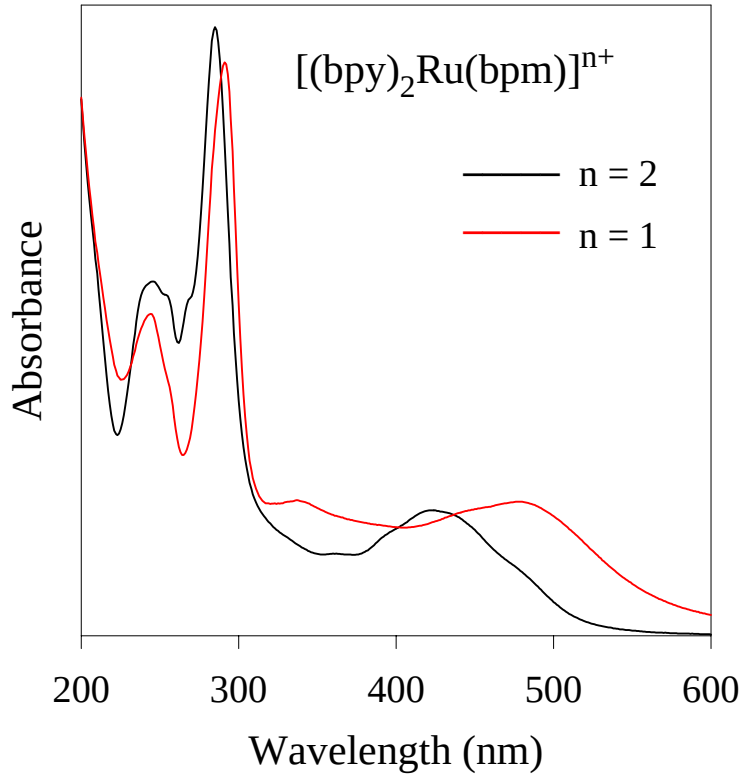

Figure 3.31 Reductive spectroelectrochemistry of $[(bpy)_2Ru(bpm)](PF_6)_2$.

The oxidative spectroelectrochemistry of $[(bpy)_2Ru(bpm)Ru(bpy)_2](PF_6)_4$ is shown in Figure 3.32. Upon oxidation by one electron, the transitions centered at 412, 545, and 595 nm all decrease in intensity by approximately one half, consistent with Ru(dπ) → bpm(π*) and Ru(dπ) → bpy(π*) CT transitions. As previously assigned,[11] the transitions at 545 and 594 nm can be attributed to Ru(dπ) → bpm(π*) CT transitions since the bridging bpm would be expected to have a lower energy π* orbital than bpy. The transition centered at 412 nm can be attributed to a Ru(dπ) → bpy(π*) CT transition,[11] blue shifted compared to the 450 nm Ru(dπ) → bpy(π*) CT transition in $[Ru(bpy)_3](PF_6)_2$ as a result of the electron withdrawing character of the bridging bpm. As in $[(bpy)_2Ru(bpm)](PF_6)_2$, oxidation by one electron lowers

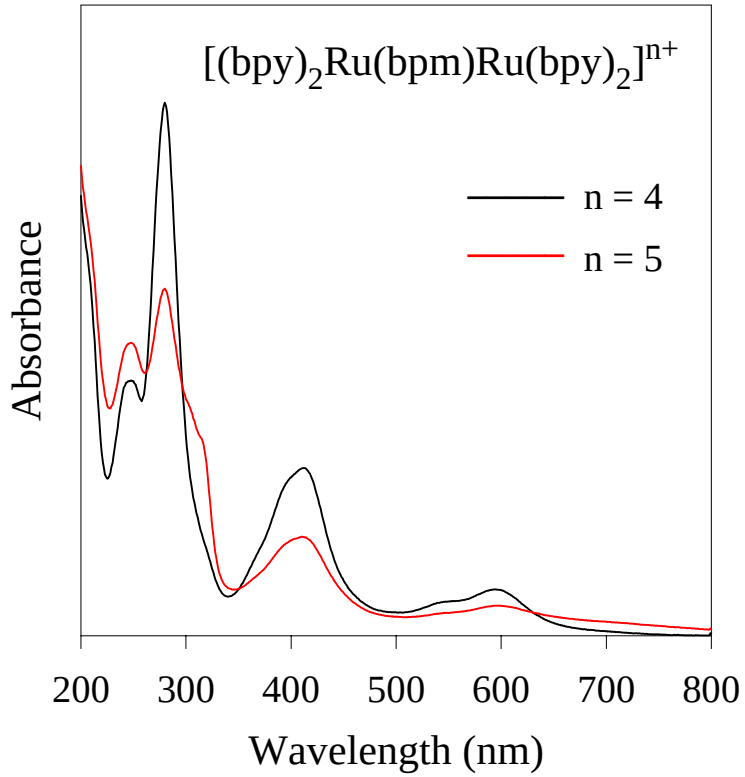

Figure 3.32 Oxidative spectroelectrochemistry of $[(bpy)_2Ru(bpm)Ru(bpy)_2](PF_6)_4$.

the intensity of the transition at 280 nm and shifts the bpy $\pi \rightarrow \pi^*$ and $n \rightarrow \pi^*$ transitions. In $[(bpy)_2Ru(bpm)Ru(bpy)_2](PF_6)_4$ this results in the shoulder at 316 nm. The one electron oxidized species was generated with > 90 % reversibility.

The reductive spectroelectrochemistry of $[(bpy)_2Ru(bpm)Ru(bpy)_2](PF_6)_4$ for the one and two electron reduced species is shown in Figure 3.33 and agrees with the spectra previously reported[12]. The one and two electron reduced species were generated with > 90 % reversibility. Reduction by one electron places an electron in a bpm π^* based orbital and it is expected that any Ru $\rightarrow$ bpm CT transitions will shift out of the UV-vis region of the

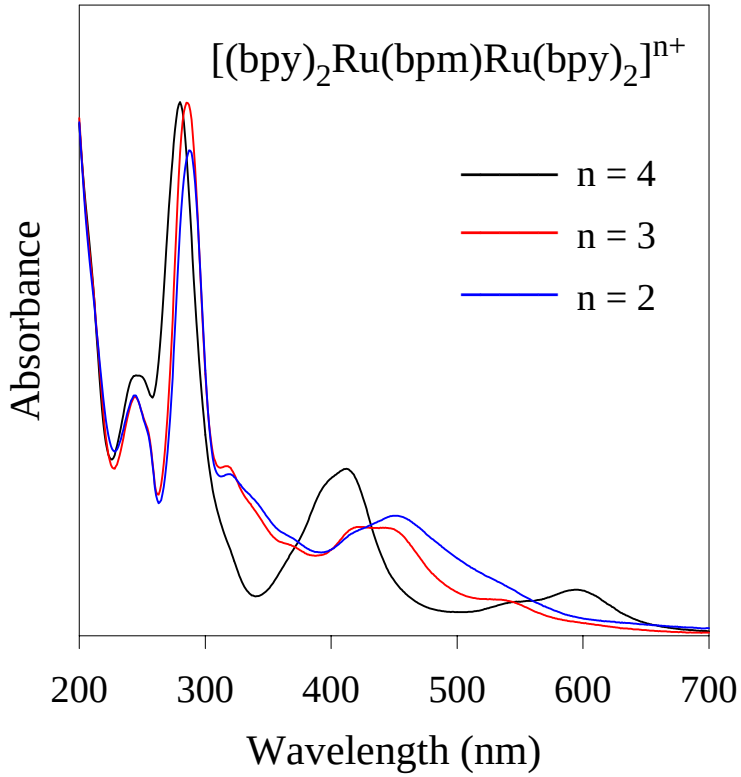

Figure 3.33 Reductive spectroelectrochemistry of $[(bpy)_2Ru(bpm)Ru(bpy)_2](PF_6)_4$.

spectrum. This can be seen in the loss of intensity at 594 nm. The Ru(dπ) → bpy(π*) CT transition centered at 412 nm shifts to lower energy upon reduction. These changes are partially obscured by new bpm π → π* transitions in the visible region of the spectrum, as previously assigned.[12] It is interesting to note that the absorbance centered at 545 nm remains upon one electron reduction. It has been previously proposed that this corresponds to a new Ru(dπ) → bpm^-(π*) CT transition[12] but is more likely due to a new bpm π* → π* transition. In the spectrum of free, reduced bpm there is a transition at 535 nm. In $[(bpy)_2Ru(bpm)Ru(bpy)_2](PF_6)_4$, reduction by one and two electrons does not significantly

change the energy or intensity of the absorbance band at 280 nm helping to confirm the absence of bpm $\pi \rightarrow \pi^*$ and n $\rightarrow \pi^*$ transitions in this area.

The reductive spectroelectrochemistry of $[Ir(bpm)_2Cl_2](PF_6)$, shown in Figure 3.34, was investigated to determine the nature of the doubly reduced central core of the trimetallic $\{[(bpy)_2Ru(bpm)]_2IrCl_2\}^{5+}$. Reduction by two electrons results in the complex $[Ir^{III}(bpm^{-})_2Cl_2]^{-}$. The new absorbance at 484 nm can be attributed to two bpm $\pi^* \rightarrow \pi^*$ transitions or possibly a bpm(π^*) $\rightarrow$ Ir(dπ) LMCT transitions. It is most likely due to two bpm $\pi^* \rightarrow \pi^*$ transitions since reduction by a second electron increases the intensity of this band by a factor of approximately two. For bpm(π^*) $\rightarrow$ Ir(dπ) LMCT transitions it would be

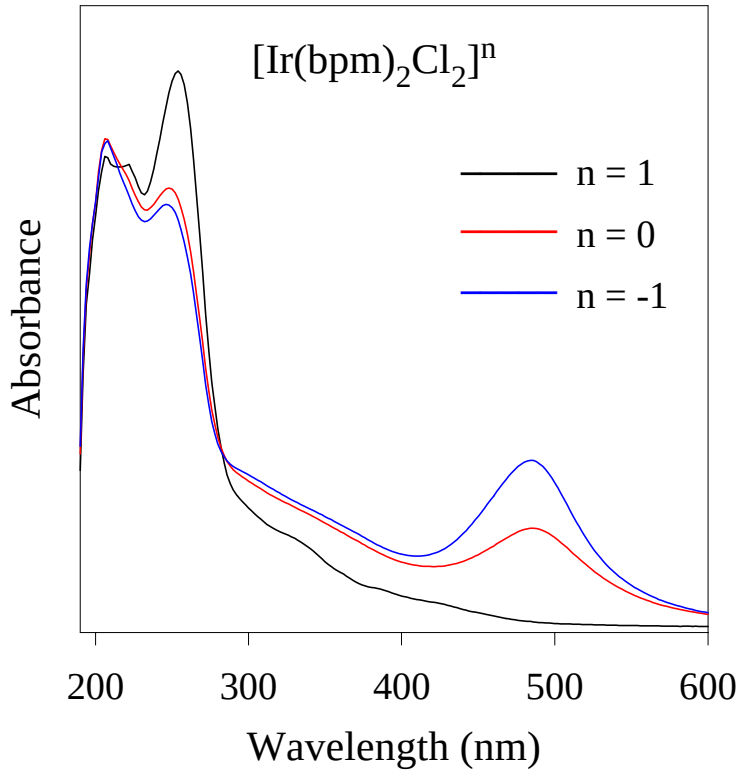

Figure 3.34 Spectroelectrochemistry of $[Ir(bpm)_2Cl_2](PF_6)$.

expected that reduction by a second electron would not increase the intensity of this band but would shift the energy of the transition. The two electron reduced species was generated with 70 % reversibility. The low reversibility of this electrochemical process may be due in part to the generation of the neutral $Ir(bpm)(bpm^{-})Cl_2$ complex en route to the doubly reduced species. The neutral complex is insoluble in acetonitrile and adsorbs onto the electrode.

The oxidative spectroelectrochemistry of $\{[(bpy)_2Ru(bpm)]_2IrCl_2\}^{5+}$ is shown in Figure 3.35. Oxidation by two electrons was achieved with > 70 % reversibility. Oxidation by two

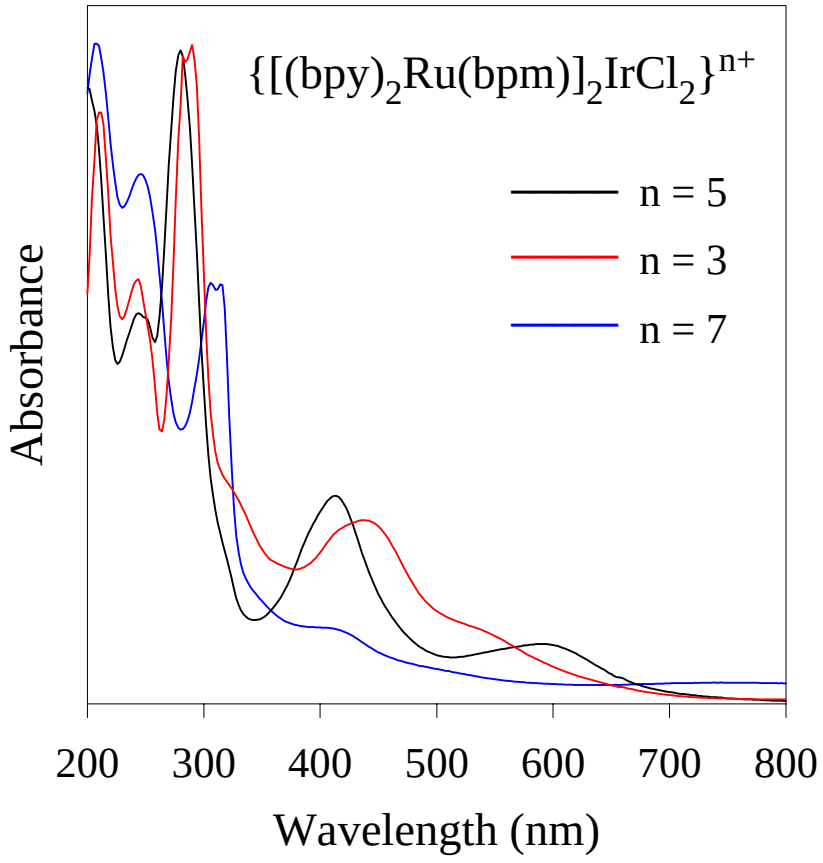

Figure 3.35 Spectroelectrochemistry of $\{[(bpy)_2Ru(bpm)]_2IrCl_2\}(PF_6)_5$.

electrons formally oxidizes both ruthenium centers and results in the loss of the Ru → bpm and Ru → bpy CT transitions at 598 and 412 nm. The reductive spectroelectrochemistry of $\{[(bpy)_2Ru(bpm)]_2IrCl_2\}^{5+}$ is also shown in Figure 3.35. The two electron reduced species was generated with > 80 % reversibility. The doubly reduced species has both bpm ligands reduced by one electron. This results in the loss of the two overlapping Ru(dπ) → bpm(π*) CT transitions at 598 nm. Reduction by two electrons also results in a shift to lower energy for the Ru(dπ) → bpy(π*) CT transitions at 412 nm. These changes are obscured by new bpm π* → π* transitions in the visible. Upon reduction by two electrons, the Ru(dπ) → bpy(π*) CT transitions at 280 nm retain their intensity but shift to slightly lower energy.

Spectroelectrochemistry has proved to be a very powerful tool in the elucidation of the UV-vis spectra of bpm containing complexes. These complexes all have bpm π → π* in the UV region at approximately 250 nm, Ru → bpy CT transitions in the UV at approximately 250 nm, and Ru → bpy and Ru → bpm CT transitions in the visible. The complete assignment of the UV-vis spectrum of these complexes is crucial to the understanding of the light absorbing properties of large systems incorporating these bpm containing metal complexes.

The electronic absorption spectroscopy assignments of ruthenium and iridium complexes using the ligand 2,2′-bipyrimidine made with the aid of spectroelectrochemistry are presented in Table 20.

Table 20. Electronic Absorption Spectroscopy Data for Ruthenium Complexes Using the Ligand 2,2′-bipyrimidine.[a,b,c]

Complex	λ_{max}^{abs} (nm)	assignment	reference
$[(bpy)_2Ru(bpm)]^{2+}$	478	Ru(dπ) → bpm(π*) CT	11[d]
	422	Ru(dπ) → bpy(π*) CT	11[d]
	360	Ru dπ → dπ*	[e]
	284	bpy π → π*	11[d]
		bpy n → π*	[e]
	268 (sh)	bpm π → π*	[e]
		Ru(dπ) → bpm(π*) CT	[e]
	254	bpm π → π*	[e]
		Ru(dπ) → bpy(π*) CT	[e]
	245	bpm π → π*	[e]
		Ru(dπ) → bpy(π*) CT	[e]
$[(bpy)_2Ru(bpm)Ru(bpy)_2]^{4+}$	594	Ru(dπ) → bpm(π*) CT	11[d], 12
	545 (sh)	Ru(dπ) → bpm(π*) CT	11[d], 12
	412	Ru(dπ) → bpy(π*) CT	11[d], 12
	280	bpy π → π*	11[d], 12
		bpy n → π*	[e]
	248	bpm π → π*	[e]
		Ru(dπ) → bpy(π*) CT	[e]
$[Ir(bpm)_2Cl_2]^{+}$	460 (sh)	Ir(dπ) → bpm(π*)	6d
	426 (sh)	Ir(dπ) → bpm(π*)	6d
	386		6d
	332	bpm π → π*	6d
	254	bpm π → π*	6d
$\{[(bpy)_2Ru(bpm)]_2IrCl_2\}^{5+}$	598	Ru(dπ) → bpm(π*) CT	14
	412	Ru(dπ) → bpy(π*) CT	14
	280	bpy π → π*	14
		bpy n → π*	
	250	bpm π → π*	[e]
		Ru(dπ) → bpy(π*) CT	[e]

[a] Recorded in acetonitrile at room temperature.

[b] bpy = 2,2′-bipyridine, bpm = 2,2′-bipyrimidine.

[c] All complexes are the PF_6^- salt unless noted.

[d] Reported as for the ClO_4^- salt.

[e] New assignments based on this work.

Photolysis studies. The photostability of $\{[(bpy)_2Ru(bpm)]_2IrCl_2\}(PF_6)_5$ was tested by photolyzing the complex with a Xe arc lamp at the energy of the MLCT (600 nm, 20 nm bandpass filter) and monitoring the UV-vis spectrum. The sample had a maximum absorbance of 1.5 at 280 nm. There was no change in the spectrum after ten minutes, indicating that the complex is stable under intense light.

Initial photolysis studies of $\{[(bpy)_2Ru(bpm)]_2IrCl_2\}^{5+}$ using triethanolamine as the sacrificial electron donor indicated that the triethanolamine reduced the compound by two electrons either very quickly or even in the absence of light. A solution of triethanolamine (0.03M) was added by syringe to a solution of the trimetallic in a septum-capped UV-vis cell wrapped tightly in tinfoil to rigorously exclude light. A spectrum was then taken in the dark and was nearly identical to that of the two electron reduced complex. It was not expected that the triethanolamine would react with the ground state of$\{[(bpy)_2Ru(bpm)]_2IrCl_2\}^{5+}$ since the oxidation potential of triethanolamine is ca. 0.70 V while the reduction potential of the trimetallic is -0.44 V.

Conclusions. The bpm bridged trimetallic $\{[(bpy)_2Ru(bpm)]_2IrCl_2\}^{5+}$ is a light absorber - electron collector - light absorber system capable of having two electrons at the central $(bpm)Ir^{III}Cl_2(bpm)$ core without decomposition of the complex. This complex is weakly emissive at room temperature in acetonitrile solution with a λ_{max}^{em} = ca. 800 nm and an emission lifetime of ca. 10 ns.[14] This is longer than the lifetime of $\{[(bpy)_2Ru(dpb)]_2IrCl_2\}^{5+}$ (< 4.5 ns) and should contribute to a greater quantum yield for photoinitiated electron collection. The use of the symmetric bridging ligand bpm leads to well defined stereochemistry and well defined metal-to-metal distances.

1,6,7,12-tetraazaperylene

Desiring to have a symmetric A-A type bidentate bridging ligand with an extended π system, the ligand 1,6,7,12-tetraazaperylene (4N-perylene), Figure 3.36, was designed. 4N-perylene would hold bridged metal centers at a greater distance than in analogous bipyrimidine

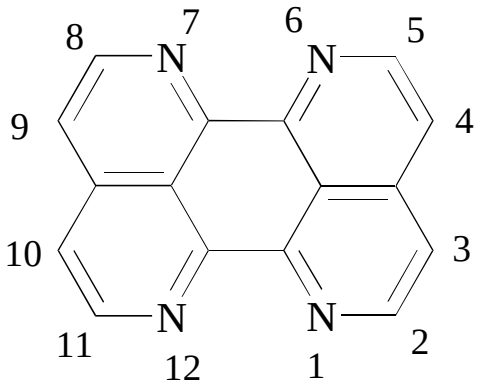

Figure 3.36 1,6,7,12-tetraazaperylene (4N-perylene).

systems. This may allow easier synthesis of multimetallic systems. From initial molecular modeling studies using Cambridge Soft Chem3D Pro Molecular Modeling and Analysis software, $[(bpy)_2Ru(4N\text{-perylene})Ru(bpy)_2]^{4+}$ would have a Ru-Ru distance of 7.75 Å while $[(bpy)_2Ru(bpm)Ru(bpy)_2]^{4+}$ has a Ru-Ru distance of 5.35 Å. The large π system in 4N-perylene would be a low energy π orbital which could be used as an acceptor in complexes designed for photoinitiated electron transfer. Also, tuning the electronic structure of the ligand could be done by adding electron withdrawing or electron donating groups at the 3, 4, 9, and 10 positions. Groups at these positions would most likely not sterically hinder the ability of 4N-perylene to coordinate to two metal centers.

Synthesis. The principal step in the proposed synthetic scheme of 4N-perylene is the coupling of 1,8-dichloro-2,7-naphthyridine. The overall proposed synthesis is shown in Figure 3.37.

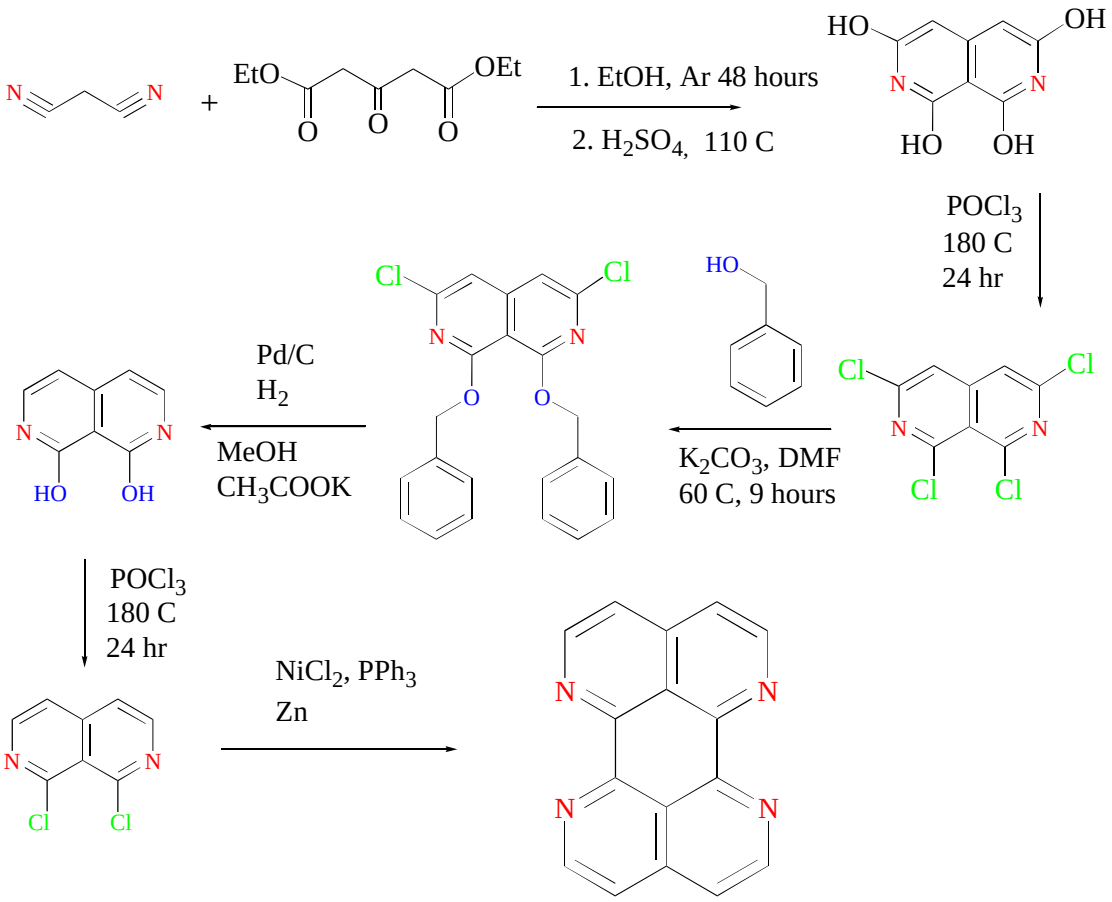

Figure 3.37 Synthetic scheme for 4N-perylene.

The numbering system for the substituted 2,7-naphthyrides is shown in Figure 3.38.

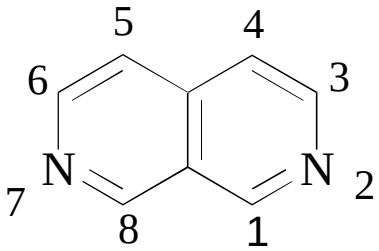

Figure 3.38 Numbering system for 2,7-naphthyridines.

In the first step of the synthesis, a modification of a previously published procedure[55], malononitrile and diethylacetonedicarboxylate were reacted to yield 1,3,6,8-tetrahydroxy-2,7-naphthyridine in 64 % yield. The product proved difficult to characterize due to the lack of solubility in common solvents and the tautomerization between the tetrahydroxy and tetraketone forms. ^{1}H NMR spectroscopy in DMSO gave a broad peak centered at 4 ppm which may indicate tautomerization. Elemental analysis did not give results consistent with the product probably due to the presence of water in the sample. 1,3,6,8-tetrahydroxy-2,7-naphthyridine was typically used directly in the synthesis of 1,3,6,8-tetrachloro-2,7-naphthyridine without characterization.

In the second step of the synthesis, a modification of a previously published procedure[55], 1,3,6,8-tetrahydroxy-2,7-naphthyridine was reacted with $POCl_3$ to give 1,3,6,8-tetrachloro-2,7-naphthyridine in 48 % yield. Given the low cost of the initial starting materials, the low yields of the first two synthetic steps are acceptable. The ^{1}H NMR spectrum showed one singlet at 7.55 ppm consistent with two equivalent protons. Using proton decoupled and proton coupled ^{13}C NMR spectroscopy, it was possible to assign all the carbon peaks of 1,3,6,8-tetrachloro-2,7-naphthyridine as in Table 21.

Table 21. ^{13}C NMR Assignments for 1,3,6,8-tetrachloro-2,7-naphthyridine.[a]

Peak value (ppm)	Multiplicity	Assignment (position)
118.1	dd	4,5
118.8	t	bridgehead between 4,5 positions
147.2	t	bridgehead between 1,8 positions
148.4	s	1,8
150.7	s	3,6

[a] Spectrum obtained using $CDCl_3$ as solvent.

The third step in the synthesis, using a previously published procedure for the synthesis of 1,8-dimethoxy-3,6-dichloro-2,7-naphthyridine as a guide[55], involves the reaction of 1,3,6,8-tetrahydroxy-2,7-naphthyridine with benzyl alcohol to give 1,8-dibenzoxy-3,6-

dichloro-2,7-naphthyridine in 72 % yield. The ^{1}H NMR spectrum showed a singlet at 6.98 ppm that can be assigned to the two equivalent naphthyridine protons, a singlet at 5.54 ppm that can be assigned to the two equivalent methylene protons, and a complex multiplet between 7.28 and 7.48 ppm that can be assigned to the benzyl protons. Using proton decoupled and proton coupled ^{13}C NMR spectroscopy, it was possible to assign all the carbon peaks of 1,8-dibenzyl-3,6-dichloro-2,7-naphthyridine as in Table 22.

Table 22. ^{13}C NMR Assignments for 1,8-dibenzyl-3,6-dichloro-2,7-naphthyridine.[a]

Peak value (ppm)	Multiplicity	Assignment (position)
69.4	t	methylene
102.4	s	1,8 of naphthyridine
110.9	d	4,5 of naphthyridine
127.8	d	benzyl
128.0	d	benzyl
128.3	d	benzyl
135.8	s	tert. carbon of benzyl
147.9	s	naphthyridine
148.7	s	naphthyridine
161.0	s	naphthyridine

[a] Spectrum obtained using $CDCl_3$ as solvent.

The fourth step in the synthesis involved the Pd catalyzed hydrogenation of 1,8-dibenzyl-3,6-dichloro-2,7-naphthyridine to give 1,8-dihydroxy-2,7-naphthyridine in 63 % yield. As with 1,3,6,8-tetrahydroxy-2,7-naphthyridine, 1,8-dihydroxy-2,7-naphthyridine proved difficult to characterize and was generally used directly in the synthesis of 1,8-dichloro-2,7-naphthyridine.

The fifth step in the synthesis involves the reaction of 1,8-dihydroxy-2,7-naphthyridine with $POCl_3$ to give 1,8-dichloro-2,7-naphthyridine in 17 % yield. The reason for the low yield in this reaction is not known. The ^{1}H NMR spectrum showed two doublets at 7.59 and 8.47 ppm, consistent with two sets of two equivalent protons. Based on the ^{13}C NMR of the tetrachloro and dibenzoxy-dichloro compounds, it was possible to assign the ^{13}C spectrum of 1,8-dichloro-2,7-naphthyridine as in Table 23.

Table 23. ^{13}C NMR Assignments for 1,8-dichloro-2,7-naphthyridine.[a]

Peak value (ppm)	Assignment (position)
119.8	4,5
120.9	bridgehead between 4,5 positions
144.6	bridgehead between 1,8 positions
145.5	3,6
150.0	1,8

[a] Spectrum obtained using $CDCl_3$ as solvent.

Attempts to couple 1,8-dichloro-2,7-naphthyridine using $Ni(PPh_3)_4$ / Zn as a catalyst system were not successful as indicated by FAB-MS.

Conclusions. The synthesis and characterization of the synthetic precursor 1,8-dichloro-2,7-naphthyridine has been achieved. A homo-coupling reaction of 1,8-dichloro-2,7-naphthyridine or 1,8-dibromo-2,7-naphthyridine is needed to synthesize the target complex 1,6,7,12-tetraazaperylene (4N-perylene). The ligand 4N-perylene is a symmetric bidentate ligand with an extended π system that would allow the synthesis of stereochemically defined multimetallic systems.

Chapter 4 Conclusions and Future Work

Bimetallic light absorber - electron donor complexes containing the bridging ligand 2,3,5,6-tetra(2-pyridyl)pyrazine have been developed and the electronic structure of these complexes has been elucidated using UV-vis spectroelectrochemistry. The symmetric bidentate bridging ligand 2,2'-bipyrimidine was used in the synthesis of the trimetallic $\{[(bpy)_2Ru(bpm)]_2IrCl_2\}(PF_6)_5$ and the electronic absorption spectroscopy was investigated using UV-vis spectroelectrochemistry. The majority of the synthesis of the symmetric bidentate bridging ligand 1,6,7,12-tetraazaperylene has been developed.

Complexes containing 2,3,5,6-tetra(2-pyridyl)pyrazine

The complexes $[(tpy)M(tpp)Ru(LLL)]^{n+}$ have been synthesized and characterized, where M = Ru^{II} or Os^{II} and LLL = tpy, tpp, Cl_3, $(CH_3CN)_3$, or (dpq)Cl. Electronic absorption spectroelectrochemistry has facilitated the assignment of most of the electronic transitions in the UV-vis region as well as the electrochemical assignments. These systems display a characteristic change in the $M(d\pi) \rightarrow tpy(\pi^*)$ CT transition at ca. 300 nm upon oxidation that aids in the assignment of the electrochemistry as well as the electronic absorption spectroscopy. The electrochemistry shows that the energy levels of the metal centers are suitable for these bimetallic complexes to act at electron donor / light absorber dyads in larger supramolecular systems designed for photoinitiated electron collection.

In most of these systems, the mixed valence species, $M^{II}(tpp)M^{III}$ exhibits a metal to metal charge transfer transition in the near IR region. Characterization of the metal to metal charge transfer transition in the mixed valence species has provided information on the degree of metal to metal coupling in these tpp bridged bimetallics. The tpp bridging ligand appears to

give rise to Class III or strongly coupled Class II systems with a large degree of metal to metal coupling which is crucial for the proposed use of these bimetallic complexes as electron donor / light absorber complexes for use in supramolecular systems for photoinitiated electron collection and electron transfer. There must be a sufficient amount of metal to metal coupling between the metals for the electron donor metal center to donate an electron to the light absorber metal center.

These bimetallic complexes are useful electron donor / light absorber systems that can be incorporated into larger multimetallic complexes designed for electron transfer and electron collection. The complexes containing terminal bridging ligands with open coordination sites, namely $[(tpy)Ru(tpp)Ru(tpp)](PF_6)_4$, $[(tpy)Os(tpp)Ru(tpp)](PF_6)_4$, and $[(tpy)Ru(tpp)Ru(dpq)Cl](PF_6)_3$, are capable of being attached to an electron collector. Attachment of two [(tpy)M(tpp)Ru(dpq)Cl] light absorber - electron donor units to a central iridium catalytic metal center would give the complex $\{[(tpy)M(tpp)RuCl(dpq)]IrCl_2[(dpq)RuCl(tpp)M(tpy)]\}^{9+}$ (see Figure 4.1). Depending on the nature of the M and the ligands on the ruthenium, it is possible that the HOMO for this complex would be localized on M and the LUMO would be localized on dpq. This would

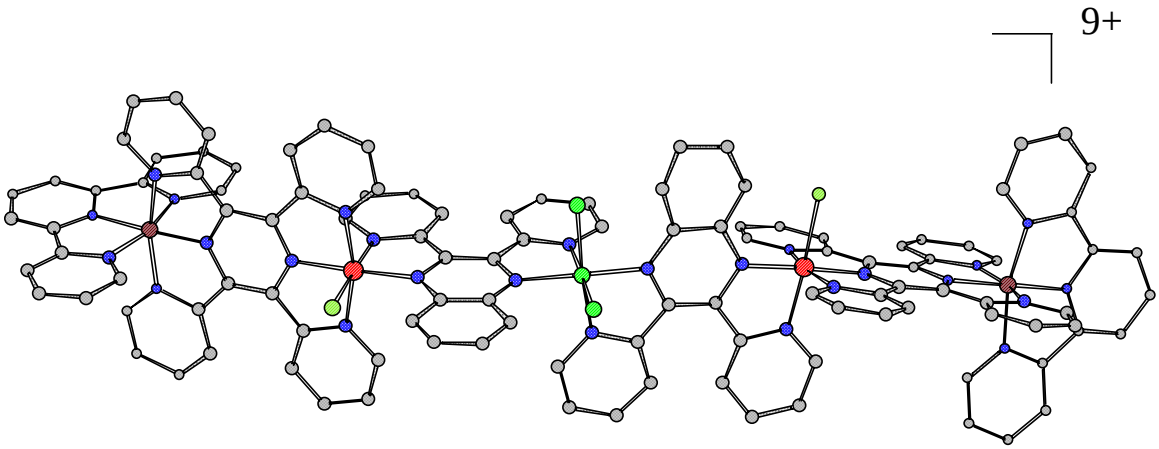

Figure 4.1 $\{[(tpy)M(tpp)RuCl(dpq)]IrCl_2[(dpq)RuCl(tpp)M(tpy)]\}^{9+}$.

result in a spatially separated electron and electron hole in the lowest energy excited state and would lead to a longer excited state lifetime than in complexes such as $\{[(bpy)_2Ru(dpq)]IrCl_2[(dpq)Ru(bpy)_2]\}^{5+}$ where the electron and electron hole are not as spatially separated. From molecular modeling studies, the M to pyrazine nitrogen of dpq distance in $\{[(tpy)M(tpp)Ru(dpq)]_2IrCl_2\}^{9+}$ would be approximately 8.4 Å while in $\{[(bpy)_2Ru(dpq)]_2IrCl_2\}^{5+}$ the Ru to pyrazine nitrogen of dpq distance is approximately 1.9 Å. The nature of the HOMO and LUMO in this complex could be determined using spectroelectrochemistry. Upon reduction, the electron in the LUMO would cause drastic shifts in any transitions involving that orbital. There could also be new $\pi^* \rightarrow \pi^*$ transitions in the visible region. From comparison with the spectroelectrochemistry of $[(tpy)Ru(tpp)Ru(dpq)Cl](PF_6)_3$, it would be possible to determine if the LUMO was dpq based or tpp based. It is expected that the HOMO in $\{[(tpy)M(tpp)Ru(dpq)]_2IrCl_2\}^{9+}$ would be M based since tpp and dpq are more electron withdrawing than tpp and tpy. Upon one electron oxidation there would be drastic shifts in any transitions involving the HOMO. The characteristic changes in the higher energy $M(d\pi) \rightarrow tpy(\pi^*)$ CT transition discovered in the extensive spectroelectrochemistry of the series of tpp bridged complexes could be used to solidify the assignment of the HOMO. Quenching of the emission from the $M \rightarrow tpp$ CT excited state could be used to probe intramolecular electron transfer to generate the $M^{III}(tpp)Ru(dpq^-)$ state. The excited state lifetime of this complex could then be determined using transient absorption spectroscopy. Changes in either the $Ru(d\pi) \rightarrow dpq(\pi^*)$ CT transition or the $M(d\pi) \rightarrow tpy(\pi^*)$ CT transition could be measured. A longer excited state lifetime for this pentametallic system should result in a higher quantum yield for photoinitiated electron collection in the presence of an electron donor. To determine the quantum yield for photoinitiated electron collection, it would be necessary to photolyze the complex in the presence of an electron donor to produce the two electron reduced species. The presence of the two electron reduced species would be confirmed by comparison to the electrochemically two electron reduced species.

Complexes containing the bridging ligand 2,2′-bipyrimidine (bpm)

The complex $\{[(bpy)_2Ru(bpm)]_2IrCl_2\}^{5+}$ has been synthesized and characterized. The complexes $[(bpy)_2Ru(bpm)]^{2+}$ and $[(bpy)_2Ru(bpm)Ru(bpy)_2]^{4+}$ have been previously reported but were prepared for a more detailed study. The use of the symmetric bridging ligand bpm eliminates some of the isomers associated with the coordination of the dpq or dpb bridging ligands around the central Ir metal center in the trimetallic complex $\{[(bpy)_2Ru(bpm)]_2IrCl_2\}^{5+}$ (see Figure 4.2). This leads to sharper waves in the cyclic voltammetry compared to those for the trimetallic systems using the asymmetric dpq or dpb bridging ligands.

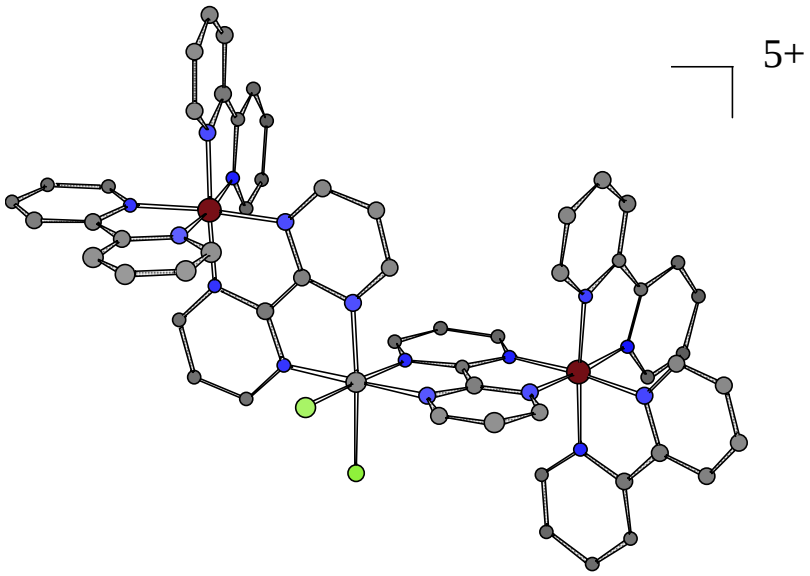

Figure 4.2 $\{[(bpy)_2Ru(bpm)]_2IrCl_2\}^{5+}$.

The electrochemistry of all the bpm containing complexes shows a bpm based LUMO and a Ru based HOMO. The cyclic voltammetry of $\{[(bpy)_2Ru(bpm)]_2IrCl_2\}^{5+}$ shows a lack of a large coupling of the two ruthenium centers. This means that the two ruthenium centers can act as separate light absorbers. Spectroelectrochemistry has helped in the assignment of the electronic absorption spectrum of this complex. The two electron reduced species,

$\{[(bpy)_2Ru(bpm)]_2IrCl_2\}^{3+}$, with two electrons formally located on the bpm bridging ligands, can be generated with > 80 % reversibility, demonstrating the stability of the molecule when two electrons are collected at the central iridium core.

Future work will include photolysis studies with sacrificial electron donors to determine the quantum yield for photoinitiated electron collection. The incorporation of covalently attached electron donors to the $\{[(bpy)_2Ru(bpm)]_2IrCl_2\}^{5+}$ complex to increase the excited state lifetime and the quantum yield for photoinitiated electron collection could then be studied.

The bridging ligand 1,6,7,12-tetraazaperylene (4N-perylene)

The synthesis of the ligand 4N-perylene should be possible by the homo-coupling reaction of 1,8-dihalo-2,7-naphthyridine. While attempts to couple 1,8-dichloro-2,7-naphthyridine using a $Ni(PPh_3)_4$/Zn catalyst did not succeed, it should be possible to successfully couple the dichloro or dibromo 2,7-naphthyridine using a different catalyst.

The symmetric bridging ligand 4N-perylene could be used as a bridging ligand in polymetallic systems for use in photoinitiated electron collection and electron transfer. 4N-perylene would have a large extended π system that should facilitate electronic communication between bridged metal centers. The monometallic $[(bpy)_2Ru(4N\text{-perylene})]^{2+}$ could be synthesized by the reaction of a 1:2 stoichiometric ratio of $Ru(bpy)_2Cl_2$: 4N-perylene (see Figure 4.3). It is expected that the LUMO for this complex would be 4N-perylene based and that reduction would occur at a more positive potential than the bpm based reduction of $[(bpy)_2Ru(bpm)]^{2+}$ due to the extended π system of 4N-perylene. The lowest energy electronic absorption transition would be expected to be $Ru(d\pi) \rightarrow$ 4N-perylene(π^*) CT in nature. The bimetallic $[(bpy)_2Ru(4N\text{-perylene})Ru(bpy)_2]^{4+}$ could be synthesized by the reaction of a 1:2 stoichiometric ratio of 4N-perylene : $Ru(bpy)_2Cl_2$ (see Figure 4.4). The first reduction in this complex would be expected to be 4N-perylene based and occur at a more positive potential

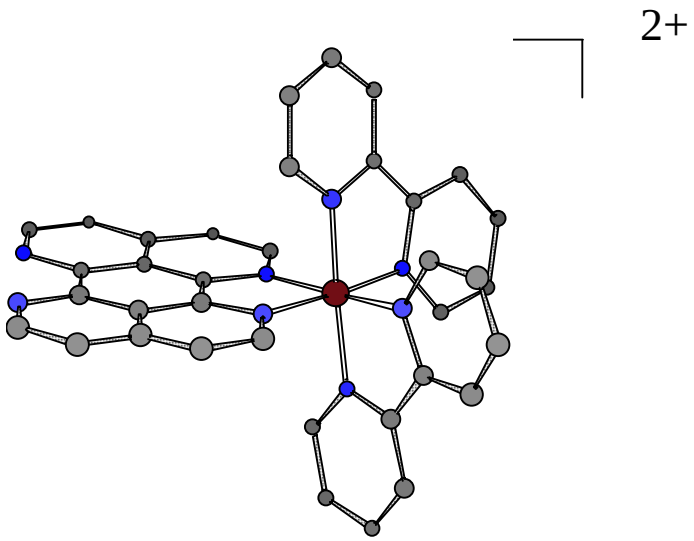

Figure 4.3 $[(bpy)_2Ru(4N\text{-perylene})]^{2+}$.

than in the monometallic $[(bpy)_2Ru(4N\text{-perylene})]^{2+}$. The ruthenium based oxidations are expected to be split as in the bpm bridged bimetallic system, $[(bpy)_2Ru(bpm)Ru(bpy)_2]^{4+}$. It will be informative to compare the $\Delta E_{1/2}$ of the ruthenium oxidations potentials of the 4N-perylene bridged bimetallic and the bpm bridged bimetallic. It is expected that the bpm

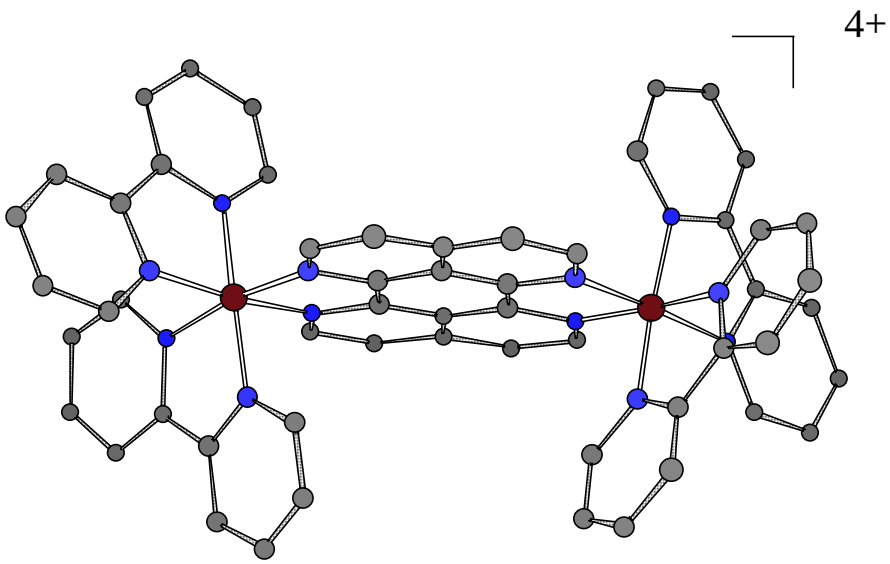

Figure 4.4 $[(bpy)_2Ru(4N\text{-perylene})Ru(bpy)_2]^{4+}$.

bridged bimetallic will have a larger split in the oxidation potentials of the two ruthenium centers. This is partly due to the larger Ru-Ru distance in $[(bpy)_2Ru(4N\text{-perylene})Ru(bpy)_2]^{4+}$ compared to that in $[(bpy)_2Ru(bpm)Ru(bpy)_2]^{4+}$. From initial molecular modeling studies using CambridgeSoft Chem3D Pro Molecular Modeling and Analysis software, $[(bpy)_2Ru(4N\text{-perylene})Ru(bpy)_2]^{4+}$ would have a Ru-Ru distance of 7.75 Å while $[(bpy)_2Ru(bpm)Ru(bpy)_2]^{4+}$ has a Ru-Ru distance of 5.35 Å. The lowest energy electronic transition of $[(bpy)_2Ru(4N\text{-perylene})Ru(bpy)_2]^{4+}$ would be expected to be $Ru(d\pi) \rightarrow$ 4N-perylene(π^*) CT in nature. It should be possible to observe a metal to metal charge transfer transition in the mixed valence compound, $[(bpy)_2Ru^{II}(4N\text{-perylene})Ru^{III}(bpy)_2]^{5+}$. The characteristics of this MMCT transition would give information concerning the degree of metal to metal communication in this 4N-perylene bridged system. The symmetric nature of this complex would facilitate the analysis of this MMCT transition.

The ligand 4N-perylene could be used as a bridging ligand in place of bpm in the trimetallic complex $\{[(bpy)_2Ru(bpm)]_2IrCl_2\}^{5+}$. This would give the complex $\{[(bpy)_2Ru(4N\text{-perylene})]_2IrCl_2\}^{5+}$, shown in Figure 4.5. As in the bpm bridged system, 4N-perylene would eliminate isomers associated with coordination of a unsymmetric bridging ligand such as dpq or dpb around the central Ir metal center when the chlorides are cis to each other.

The ligand 4N-perylene could be used as a ligand in a variety of applications of transition metal complexes such as catalysis, photoinitiated electron collection, and nonlinear optics.

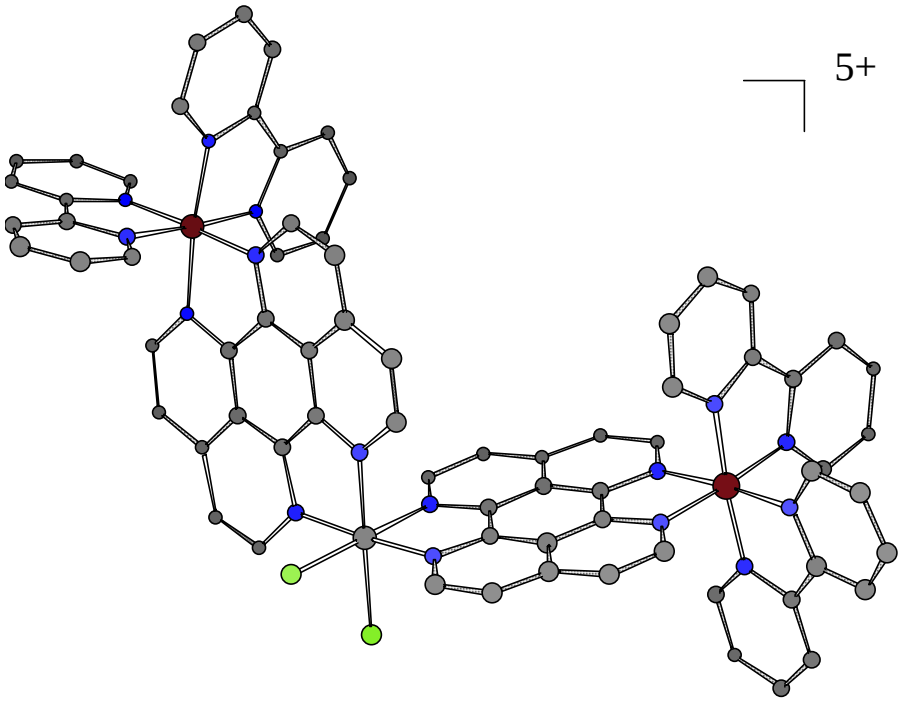

Figure 4.5 $[(bpy)_2Ru(4N\text{-perylene})IrCl_2(4N\text{-perylene})Ru(bpy)_2]^{5+}$.

1. Balzani, V.; Juris, A.; Venturi, M.; Campagna, S.; Seroni, S. *Coord. Chem. Rev.* **1996**, *96*, 759
2. Juris, A.; Balzani, V.; Barigelletti, F.; Campagna, S.; Belser, P.; Von Zelewsky, A. *Coord. Chem. Rev.* **1988**, *84*, 85
3. Kalyanasundaram, K. *Coord. Chem. Rev.* **1982**, *46*, 159 and references therein.
4. Bard, A. J.; Faulkner, L. R. *Electrochemical Methods, Fundamentals and Applications* **1980,** John Wiley and Sons, New York, 213
5. Balzani, V.(ed.); Moggi, L.; Scandola, F. *Supramolecular Photochemistry* **1987**, D. Reidel Publishing Co., 1
6. a) Molnar, S. M.; Nallas, G.; Bridgewater, J. S.; Brewer, K. J. *J. Am. Chem. Soc.* **1994**, *116*, 5206 b) Molnar, S. M.; Jensen, G. E.; Vogler, L. M.; Jones, S. W.; Laverman, L.; Bridgewater, J. S.; Richter, M. M.; Brewer, K. J. *J. Photochem. Photobiol. A: Chem.* **1994**, *80*, 315 c) Bridgewater, J. S.; Vogler, L. M.; Molnar, S. M.; Brewer, K. J. *Inorg. Chim. Acta* **1993**, *208*, 179 d) Rasmussen, S. C.; Richter, M. M.; Yi, E.; Place, H.; Brewer, K. J. *Inorg. Chem*. **1990**, *29*, 3926
7. Petersen, J. D.; Murphy, Jr., W. R.; Sahai, R.; Brewer, K. J.; Ruminski, R. R. *Coord. Chem. Rev.* **1985**, *64*, 261
8. Braunstein, C. H.; Baker, A. D.; Strekas, T. C.; Gafney, H. D. *Inorg. Chem.* **1984**, *23*, 857
9. von Zelewsky, A. *Stereochemistry of Coordination Compounds* **1996**, John Wiley and Sons, Ltd., England, 183
10. Hunziker, M.; Ludi, A. *J. Amer. Chem. Soc.* **1977**, *99*, 7370
11. a) Rillema, D, P.; Mack, K. B. *Inorg. Chem.* **1982**, *21*, 3849 b) Rillema, D, P.; Allen, G.; Meyer, T. J.; Conrad, D. *Inorg. Chem.* **1983**, *22*, 1617 c) Sahai, R.; Morgan, L.; Rillema, D, P. *Inorg. Chem.* **1988**, *27*, 3495
12. Krejcik, M.; Vlcek, A. A. *Inorg. Chem.* **1992**, *31*, 2390
13. Pavinato, R. A.; Walk, J. A.; McGuire, M. E. *Inorg. Chem.* **1993**, *32*, 4982

14. Nallas, G. N. A.; Jones, S. W.; Brewer, K. J. *Inorg. Chem.* **1996**, *35*, 6974
15. Winkler, J. R.; Netzel, T.L.; Creutz, C.; Sutin, N. *J. Amer. Chem. Soc.* **1987**, *109*, 2381
16. Van Houten, J.; Watts, R. *J. Amer. Chem. Soc.* **1975**, *97*, 3843
17. Kirchhoff, J. R.; McMillin, D. R.; Marnot, P. A.; Sauvage, J.-P. *J. Am. Chem. Soc.* **1985**, *107*, 1138
18. Hecker, C. R.; Fanwick, P. E.; McMillin, D. R. *Inorg. Chem.* **1991**, *30*, 659
19. Bessel, C. A.; See, R. F.; Jameson, D. L.; Churchill, M. R.; Takeuchi, K. J. *J. Chem. Soc., Dalton Trans* **1992**, 3223
20. Constable, E. C.; Cargill Thompson, A. M. W.; Tocher, D. A.; Daniels, M. A. M. *New J. Chem.* **1992**, *16*, 855
21. Goodwin, H. A.; Lions, F. *J. Am. Chem. Soc.* **1959**, *81*, 6415
22. Petersen, J. D. *Supramolecular Photochemistry*, D. Reidel Publishing Co., **1987**, 135
23. Thummel, R. P.; Chirayil, S. *Inorg. Chim. Acta* **1988**, *154*, 77
24. Vogler L. M.; Scott, B.; Brewer, K. J. *Inorg. Chem.* **1993**, *32*, 898
25. Harrison, J.; Brewer, K. J. unpublished work.
26. a) Caspar, J. V.; Meyer, T. J. *Inorg. Chem.* **1983**, *22*, 2444 b) Caspar, J. V.; Meyer, T. J. *J. Amer. Chem. Soc.* **1983**, *105*, 5583
27. a) Vogler, L. M.; Brewer, K. J. *Inorg. Chem.* **1996**, *35*, 818 b) Vogler, L. M.; Jones, S. W.; Jensen, G. E.; Brewer, R. G.; Brewer, K. J. *Inorg. Chim. Acta* **1996**, *250*, 155 c) Jones, S. W.; Vrana, L. M.; Brewer, K. J. *J. Organomet. Chem.* **1998**, *551*, 29.
28. Berger, R. M. *Inorg. Chem.* **1990**, *29*, 1920
29. Cooper, J. B.; MacQueen, D. B.; Petersen, J. D.; Wertz, D. *Inorg. Chem.* **1990**, *29*, 3701
30. a) Donohoe, R. J.; Tait, C. D.; DeArmond, M. K.; Wertz, D. W. *J. Phys. Chem.* **1986**, 3923 b) Donohoe, R. J.; Tait, C. D.; DeArmond, M. K.; Wertz, D. W. *J. Phys. Chem.* **1986**, 3927
31. Bugnon, P.; Hester, R. E. *Chem. Phys. Lett.* **1983**, *102*, 537

32. Brewer, K. J.; Calvin, M.; Lumpkin, R. S.; Otvos, J. W.; Spreer, L. O. *Inorg. Chem.* **1989**, *28*, 4446

33. Heath, G. A.; Yellowlees, L. J. *J. Chem. Soc., Chem. Comm.* **1981**, 287

34. a) Richter, M. M.; Jensen, G. E.; Brewer, K. J. *Inorg. Chim. Acta* **1995**, *230*, 35 b) Richter, M. M.; Brewer, K. J. *Inorg. Chem.* **1992**, *31*, 1594

35. Allen, G. C.; Hush, N. S. *Prog. Inorg. Chem.* **1967**, *8*, 357

36. Creutz, C. *Prog. Inorg. Chem.* **1983**, *30*, 1

37. Robin, M. B.; Day, P. *Adv. Inorg Chem. Radiochem.* **1967**, *10*, 247

38. Constable, E. C.; Ward, M. D. *J. Chem. Soc., Dalton Trans.* **1990**, 1405

39. a) Collin, J.-P.; Laine, P.; Launay, J.-P.; Sauvage, J.-P.; Sour, A. *J. Chem. Soc., Chem. Commun.* **1993**, 434 b) Barigelletti, F.; Flamigni, L.; Balzani, V.; Collin, J.-P.; Sauvage, J.-P.; Sour, A.; Constable, E. C.; Cargill Thompson, A. M. W. *J. Amer. Chem. Soc.* **1994**, *116*, 7692 c) Barigelletti, F.; Flamigni, L.; Balzani, V.; Collin, J.-P.; Sauvage, J.-P.; Sour, A.; Constable, E. C.; Cargill Thompson, A. M. W. *Coord. Chem. Rev.* **1994**, *132*, 209 d) Barigelletti, F.; Flamigni, L.; Balzani, V.; Collin, J.-P.; Sauvage, J.-P.; Sour, A.; *New J. Chem.* **1995**, *19*, 793 e) Indelli, M.T.; Scandola, F.; Collin, J.-P.; Sauvage, J.-P.; Sour, A. *Inorg. Chem.* **1996**, *35*, 303 f) Barigelletti, F.; Flamigni, L.; Collin, J.-P.; Sauvage, J.-P. *Chem. Commun.* **1997**, 333 g) Indelli, M.T.; Scandola, F.; Flamigni, L.; Collin, J.-P.; Sauvage, J.-P.; Sour, A. *Inorg. Chem.* **1997**, *36*, 4247 h) Beley, M.; Collin, J.-P.; Sauvage, J.-P. Sugihara, H.; Heisel, F.; Miehe, A. *J. Chem. Soc., Dalton Trans.* **1991**, 3157 i) Beley, M.; Chodorowski, S.; Collin, J.-P.; Sauvage, J.-P.; Flamigni, L.; Barigelletti, F. *Inorg. Chem.* **1994**, *33*, 2543 j) Hammarstrom, L.; Barigelletti, F.; Flamigni, L.; Indelli, M.T.; Armaroli, N.; Calogero, G.; Guardigli, M.; Sour, A.; Collin, J.-P.; Sauvage, J.-P.; *J. Phys. Chem.* **1998**, in press.

40. Constable, E. C.; Cargill Thompson, A.M.W. *J. Chem. Soc., Dalton Trans.* **1995**, 615

41. De Cola, L.; Balzani, V.; Barigelletti, F.; Flamigni, L.; Belser, P.; von Zelewsky, A.; Frank, M.; Vogtle, F. *Inorg. Chem.* **1993**, *32*, 5228

42. Hammarstrom, L.; Barigelletti, F.; Flamigni, L.; Armaroli, N.; Sour, A.; Collin, J.-P.; Sauvage, J.-P.; *J. Amer. Chem. Soc.* **1996**, *118*, 11972

43. a) Benniston, A. C.; Grosshenny, V.; Harriman, A.; Ziessel, R. *Angew. Chem. Int. Ed., Engl.* **1994**, *33*, 1884 b) Grosshenny, V.; Harriman, A.; Ziessel, R. *Angew. Chem. Int. Ed. Engl.* **1995**, *34*, 2705 c) Grosshenny, V.; Ziessel, R. *J. Organomet. Chem.* **1993**, *453*, C-19 d) Ziessel, R.; Suffert, J.; Youinou, M.-T. *J. Org. Chem.* **1996**, *61*, 6535 e) Ziessel, R. *J. Chem. Educ.* **1997**, *74*, 673 f) Grosshenny, V.; Harriman, A.; Ziessel, R. *Angew. Chem. Int. Ed. Engl.* **1995**, *34*, 1100 g) Harriman, A.; Ziessel, R. *Chem. Comm.* **1996**, 1707 h) Grosshenny, V.; Harriman, A.; Hissler, M.; Ziessel, R. *J. Chem. Soc., Faraday Trans.* **1996**, *92*, 2223

44. a) Beley, M.; Collin, J.-P.; Louis, R.; Metz, B.; Sauvage, J.-P. *J. Amer. Chem. Soc.* **1991**, *113*, 8521 b) Beley, M.; Collin, J.-P.; Sauvage, J.-P. *Inorg. Chem.* **1993**, *32*, 4539 c) Beley, M.; Chodorowski-Kimmes, S.; Collin, J.-P.; Laine, P.; Launay, J.-P.; Sauvage, J.-P. *Angew. Chem. Int. Ed., Eng.* **1994**, *33*, 1775 d) Barigelletti, F.; Flamigni, L.; Guardigli, M.; Juris, A.; Beley, M.; Chodorowski-Kimmes, S.; Collin, J.-P.; Sauvage, J.-P. *Inorg. Chem.* **1996**, *35*, 136

45. Hasenknopf, B.; Hall, J.; Lehn, J.-M.; Balzani, V.; Credi, A.; Campagna, S. *New J. Chem.* **1996**, *20*, 725

46. Constable, E. C.; Cargill Thompson, A. M. W.; Tocher, D. A. *Supramolecular Chemistry* **1992**, Kluwer Academic Publishers, Netherlands, 219

47. a) Odobel, F.; Sauvage, J.-P. *New J. Chem.* **1994**, *18*, 1139 b) Harriman, A.; Odobel, F.; Sauvage, J.-P. *J. Amer. Chem. Soc.* **1994**, *116*, 5481

48. Sullivan, B. P.; Salmon, D. J.; Meyer, T. J. *Inorg. Chem.* **1978**, *17*, 3334

49. Sullivan, B. P.; Calvert, J. M.; Meyer, T. J. *Inorg. Chem.* **1980**, *19*, 1404

50. Buckingham, D. A.; Dweyer, F. P.; Sargeson, A. M. *Aust. J. Chem.* **1961**, *14*, 250

51. Arana, C. R.; Abruna, H. D. *Inorg. Chem.* **1993**, *32*, 194

52. Bard, A. J.; Faulkner, L. R. *Electrochemical Methods, Fundamentals and Applications* **1980,** John Wiley and Sons, New York, 701
53. Brewer, R. G.; Jensen, G. E.; Brewer, K. J.; *Inorg. Chem.* **1994**, *33*, 124
54. Rasmussem, S. C.; Richter, M. M.; Yi, E.; Place, H.; Brewer, K. J. *Inorg. Chem.* **1990**, *29*, 3926
55. Ferrier, B. M.; Campbell, H. *J. Chem. Soc.* **1960**, 3513
56. Paudler, W. W.; Cornrich, S. J. *J. Heterocyclic Chem.* **1970**, *7*, 419
57. Sauvage, J.-P.; Collin, J.-P.; Chambron, J.-C.; Guillerez, S.; Coudret, C. *Chem. Rev.* **1994**, *94*, 993
58. Lytle, F. E.; Hercules, D. M. *J. Amer. Chem. Soc.* **1969**, *91*, 253

Vitae

Sumner Weston Jones was born December 3, 1969 to Charlotte and Del Jones in Seattle, Washington. In December of 1982 Sumner's family moved to Singapore for three and a half years where he gained a world view and a love for travel. Upon returning to Seattle, he attended Garfield High School and graduated in May of 1987.

After taking a year off to gut fish in Alaska and build skyscrapers in Seattle, Sumner enrolled in Washington State University in Pullman, Washington. In December of 1992 he received a B.S. in Chemistry.

Four months of selling time-share condominiums in Williamsburg, VA convinced Sumner to further his education and he plunged back into the world of academia at Virginia Polytechnic Institute and State University in July of 1993 with Professor Karen Brewer as his major professor. During graduate school, in addition to his graduate research, he was able to take a summer internship at OakRidge National Laboratories and a three week visit to The Agency of Industrial Science and Technology, Japan, as a visiting foreign scientist. In May of 1998 he received a Ph.D. in Chemistry.